

## NUMERICAL METHODS FOR BOUNDARY-LAYER TYPE EQUATIONS

### 7.1 INTRODUCTION

It was pointed out in Chapter 5 that the equations that result from the boundary-layer (or thin-shear-layer) approximation provide a useful mathematical model for several important flows occurring in engineering applications. Among these are many jet and wake flows, two-dimensional or axisymmetric flows in channels and tubes, as well as the classical wall boundary layer. Certain three-dimensional flows can also be economically treated through the boundary-layer approximation. In addition, methods have been developed to extend the boundary-layer approximation to flows containing small regions of recirculation. Often, a small region exists near the streamwise starting plane of these flows in which the thin-shear-layer approximation is a poor one, but for moderate to large Reynolds numbers, this region is very (and usually negligibly) small.

In this chapter, methods and numerical considerations related to the numerical solution of these equations will be presented. The emphasis will be on the application of methods and principles covered in Chapters 3 and 4 rather than on the exposition of a single general-numerical procedure. Several finite-difference/finite-volume methods for these equations are described in detail elsewhere. Except as an aid in illustrating key principles, those details will not be repeated here.

The history of numerical methods for boundary-layer equations goes back to the 1930s and 1940s. Finite-difference methods in a form very similar to those

now in use began emerging in the 1950s (Friedrich and Forstall, 1953; Rouleau and Osterle, 1955). We can think of numerical schemes for the boundary-layer equations as being well developed and tested as compared to methods for some other classes of flows. Despite this, new developments in the numerical treatment of these equations continue to appear regularly.

## 7.2 BRIEF COMPARISON OF PREDICTION METHODS

Before proceeding with a discussion of numerical methods for boundary-layer flows, it is well to remember that over the years, useful solutions have been obtained by other methods and for some simple flows, engineering results are available as simple formulas. These results are presented in standard textbooks on fluid mechanics, aerodynamics, and heat transfer. The books by Schlichting (1979) and White (1991) are especially valuable references for viscous flows.

Except for a few isolated papers based on similarity methods, the calculation methods for boundary-layer type problems that appear in the current literature can generally be categorized as (1) integral methods, (2) finite-difference/finite-volume methods, or (3) finite-element methods.

Integral methods can be applied to a wide range of both laminar and turbulent flows and, in fact, any problem that can be solved by a finite-difference/finite-volume method can also be solved by an integral method. Prior to the 1960s, integral methods were the primary "advanced" calculation method for solving complex problems in fluid mechanics and heat transfer. Loosely speaking, the method transforms the partial differential equations (PDEs) into one or more ordinary differential equations (ODEs) by integrating out the dependence of one independent variable (usually the normal coordinate) in advance by making assumptions about the general form of the velocity and temperature profiles (often functions of " $N$ " parameters). Many of these procedures can be grouped as weighted residual methods. It can be shown that the solution by the method of weighted residuals approaches the exact solution of the PDE as  $N$  becomes very large. Modern versions of integral methods for complex problems make use of digital computers. In practice, it appears that implementing integral methods is not as straightforward (requiring more "intuition" about the problem) as for finite-difference/finite-volume methods. The integral methods are not as flexible or general in that more changes are generally required as boundary or other problem conditions are changed. In the 1970s the preference of the scientific community shifted in favor of using finite-difference/finite-volume methods over integral methods for computing the more complex boundary-layer flows. However, integral methods have at least a few strong advocates and can be used to solve important current problems.

Finite-element methodology has been applied to boundary-layer equations. Comments on this approach for boundary layers can be found in the work by Chung (1978). The objective of all three of these methods is to transform the

problem posed through PDEs to one having an algebraic representation. The methods differ in the procedures used to implement this discretization.

## 7.3 FINITE-DIFFERENCE METHODS FOR TWO-DIMENSIONAL OR AXISYMMETRIC STEADY EXTERNAL FLOWS

### 7.3.1 Generalized Form of the Equations

The preferred form for the boundary-layer equations will vary from problem to problem. In the case of laminar flows, coordinate transformations are especially useful for maintaining a nearly constant number of grid points across the flow. The energy equation is usually written differently for compressible flow than it is for incompressible flow. In practice, it is frequently necessary to extend or alter a difference scheme established for one PDE to accommodate one that is similar but different in some detail. Optimizing the representation often requires a trial-and-error procedure.

The boundary-layer equations were given in Chapter 5 [Eqs. (5.116)–(5.119)] in physical coordinates. Here, we will utilize the Boussinesq approximation to evaluate the Reynolds shear-stress and heat flux quantities in terms of a turbulent viscosity  $\mu_T$  and the turbulent Prandtl number  $\text{Pr}_T$ . Specifically, we will let

$$-\overline{\rho u'v'} = \mu_T \frac{\partial u}{\partial y}$$

and

$$-\rho c_p \overline{v'T'} = \frac{c_p \mu_T}{\text{Pr}_T} \frac{\partial T}{\partial y}$$

To solve the energy equation numerically using  $H$  as the primary thermal variable, it will be helpful to eliminate  $T$  in the expression for the Reynolds heat flux by using the definition of total enthalpy,  $H = c_p T + u^2/2 + v^2/2$ . The  $v^2/2$  term can be neglected in keeping with the boundary-layer approximation. These substitutions permit the boundary-layer equations for a steady compressible 2-D or axisymmetric flow to be written as follows:

$x$  momentum:

$$\rho u \frac{\partial u}{\partial x} + \rho \bar{v} \frac{\partial u}{\partial y} = \rho_e u_e \frac{du_e}{dx} + \frac{1}{r^m} \frac{\partial}{\partial y} \left[ r^m (\mu + \mu_T) \frac{\partial u}{\partial y} \right] \quad (7.1)$$

energy:

$$\rho u \frac{\partial H}{\partial x} + \rho \bar{v} \frac{\partial H}{\partial y} = \frac{1}{r^m} \frac{\partial}{\partial y} \left( r^m \left\{ \left( \frac{\mu}{\text{Pr}} + \frac{\mu_T}{\text{Pr}_T} \right) \frac{\partial H}{\partial y} + \left[ \mu \left( 1 - \frac{1}{\text{Pr}} \right) + \mu_T \left( 1 - \frac{1}{\text{Pr}_T} \right) \right] u \frac{\partial u}{\partial y} \right\} \right) \quad (7.2)$$

continuity:

$$\frac{\partial}{\partial x}(r^m \rho u) + \frac{\partial}{\partial y}(r^m \rho \bar{v}) = 0 \tag{7.3}$$

state:

$$\rho = \rho(T, p) \tag{7.4}$$

Property relationships are also needed to evaluate  $\mu, k, c_p$  as a function (usually) of temperature.

As indicated in Chapter 5,  $m$  is a flow index equal to unity for axisymmetric flow and equal to zero for 2-D flow, and  $\bar{v} = (\bar{\rho} \bar{v} + \overline{\rho'v'})/\bar{\rho}$ . When  $m = 0$ ,  $r^m = 1$  and the equations are in appropriate form for 2-D flows.

The primary dependent variable in the momentum equation is  $u$ , and it is useful to think of Eq. (7.1) as a “transport” equation for  $u$ , in which terms representing convection, diffusion, and “sources” of  $u$  can be recognized. Likewise, the energy equation can be viewed as a transport equation for  $H$  with similar categories of terms. This interpretation can also be extended to include the unsteady form of the boundary-layer momentum and energy equations.

Within the transport equation context, both Eqs. (7.1) and (7.2) can usually [an exception may occur with the use of some turbulence models, Bradshaw et al. (1967)] be cast into the general form

$$\underbrace{\rho u \frac{\partial \phi}{\partial x} + \rho \bar{v} \frac{\partial \phi}{\partial y}}_{\text{Convection of } \phi} = \underbrace{\frac{1}{r^m} \frac{\partial}{\partial y} \left( r^m \lambda \frac{\partial \phi}{\partial y} \right)}_{\text{Diffusion of } \phi} + \underbrace{S}_{\text{Source terms}} \tag{7.5}$$

In Eq. (7.5),  $\phi$  is a generalized variable, which would be  $u$  for the boundary-layer momentum equation and  $H$  for the boundary-layer energy equation;  $\lambda$  is a generalized diffusion coefficient and  $S$  represents the source terms. Source terms are those terms in the PDE that do not involve a derivative of  $\phi$ . The term  $\rho_e u_e du_e/dx$  in Eq. (7.1) and the term involving  $u \partial u/\partial y$  in Eq. (7.2) are examples of source terms. Most of the transport equations for turbulence model parameters given in Chapter 5 also fit the form of Eq. (7.5).

The momentum and energy equations that can be cast into the general form of Eq. (7.5) are parabolic with  $x$  as the marching coordinate. By making appropriate assumptions regarding the evaluation of coefficients, it is possible to decouple the finite-difference representation of the equations, permitting the momentum, continuity, and energy equations to be marched one step in the  $x$  direction independently to provide new values of  $u_j, H_j$ , and  $\bar{v}_j$ . This strategy is illustrated below:

<i>Equation</i>	<i>Marched to obtain</i>
$x$ momentum	$u_j^{n+1}$
energy	$H_j^{n+1}$
equation of state + continuity	$\bar{v}_j^{n+1}$

After each marching step, the coefficients in the equations are reevaluated (updated), so that the solutions of the three equations are in fact interdependent—the decoupling is in the algebraic system for one marching step at a time. In some solution schemes, the coupling is maintained so that at each marching step, a larger system of algebraic equations must be solved simultaneously for new values of  $u_j, H_j, \tilde{v}_j$ . Uncoupling the algebraic system is conceptually the simplest procedure and can usually be made to work satisfactorily for most flow problems.

### 7.3.2 Example of a Simple Explicit Procedure

Although the simplest explicit method is no longer widely used for boundary layers owing to the restrictive stability constraint associated with it, it will be used here for pedagogical purposes to demonstrate the general solution algorithm for boundary-layer flows (Wu, 1961). Consider a 2-D laminar incompressible flow without heat transfer. The governing equations in partial differential form are given as Eqs. (5.104) and (5.105).

The difference equations can be written as follows:

$x$  momentum:

$$\begin{aligned}
 u_j^n \frac{(u_j^{n+1} - u_j^n)}{\Delta x} + \boxed{v_j^n \frac{(u_{j+1}^n - u_{j-1}^n)}{2 \Delta y}} \\
 = u_e^n \frac{(u_e^{n+1} - u_e^n)}{\Delta x} + \frac{\nu}{(\Delta y)^2} (u_{j+1}^n - 2u_j^n + u_{j-1}^n) + O(\Delta x) + O[(\Delta y)^2]
 \end{aligned} \quad (7.6)$$

continuity:

$$\frac{v_j^{n+1} - v_{j-1}^{n+1}}{\Delta y} + \frac{u_j^{n+1} + u_{j-1}^{n+1} - u_j^n - u_{j-1}^n}{2 \Delta x} = 0 + O(\Delta x) + O[(\Delta y)^2] \quad (7.7)$$

For flow over a flat plate (see Fig. 7.1), the computation is usually started by assuming that  $u_j^n = u_\infty$  at the leading edge and  $v_j^n = 0$ . The value  $v_j^n$  is required in the explicit algorithm in order to advance the solution to the  $n + 1$  level. However, in the formal mathematical formulation of the PDE problem, it is not necessary to specify an initial distribution of  $v_j^n$ . A compatible initial distribution can be obtained for  $v_j^n$  (Ting, 1965) by first using the continuity equation to eliminate  $\partial u / \partial x$  from the boundary-layer momentum equation. For a laminar, incompressible flow, this gives

$$-u \frac{\partial v}{\partial y} + v \frac{\partial u}{\partial y} = u_e \frac{du_e}{dx} + \nu \frac{\partial^2 u}{\partial y^2}$$

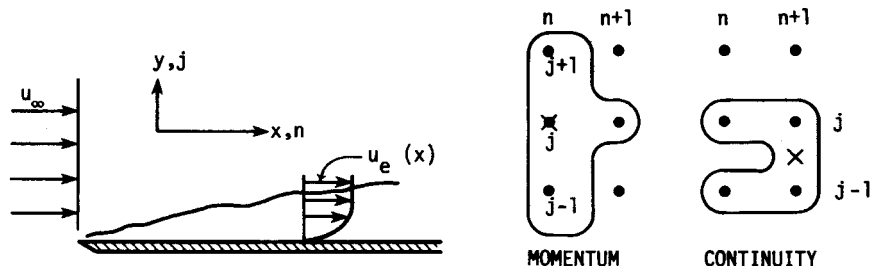


Figure 7.1 Simple explicit procedure.

We can observe that

$$-u \frac{\partial v}{\partial y} + v \frac{\partial u}{\partial y} = -u^2 \frac{\partial}{\partial y} \left( \frac{v}{u} \right)$$

Thus

$$\frac{\partial}{\partial y} \left( \frac{v}{u} \right) = -\frac{1}{u^2} \left( u_e \frac{du_e}{dx} + v \frac{\partial^2 u}{\partial y^2} \right)$$

and using  $v = 0$  at  $y = 0$ , we find

$$v(y) = -u \int_0^y \frac{1}{u^2} \left( u_e \frac{du_e}{dx} + v \frac{\partial^2 u}{\partial y^2} \right) dy \tag{7.8}$$

For the flat plate problem at hand, we would assume that  $u_j^n = u_\infty$  at  $x = 0$  (the leading edge) except at the wall, where  $u_1^n = 0$ . We can use a numerical evaluation of the integral in Eq. (7.8) to obtain an estimate of a compatible initial distribution of  $v_j^n$  to use in the explicit difference procedure. Employing the usual central-difference representation for  $\partial^2 u / \partial y^2$  gives  $v_j^n = 2v / \Delta y$  at all points except the point on the wall where  $v_1^n = 0$  and the point adjacent to the wall where  $v_2^n = v / \Delta y$ . In practice, letting  $v_j^n = 0$  initially throughout is also found to work satisfactorily.

Having initial values for  $u_j^n$ , the momentum equation, Eq. (7.6), can be solved for  $u_j^{n+1}$  explicitly, usually by starting from the wall and working outward until  $u_j^{n+1} / u_e^{n+1} = 1 - \epsilon \approx 0.9995$ ; that is, owing to the asymptotic boundary condition, we find the location of the outer boundary as the solution proceeds. The values of  $v_j^{n+1}$  can now be computed from Eq. (7.7), starting with the point next to the lower boundary and computing outward. The difference formulation of the continuity equation and the solution procedure described is equivalent to integrating the continuity equation by the trapezoidal rule for  $v_j^{n+1}$ .

The *stability constraints* for this method are

$$\frac{2\nu \Delta x}{u_j^n (\Delta y)^2} \leq 1 \text{ and } \frac{(v_j^n)^2 \Delta x}{u_j^n \nu} \leq 2$$

The second term in the momentum equation, Eq. (7.6), has been enclosed by a dashed box for two reasons. First, we should be aware that the presence of this term is mainly responsible for any difference between the stability constraints of Eq. (7.6) and the heat equation, and second, we will suggest an alternative treatment for this term below.

**Alternative formulation for explicit method.** In order to control the stability of the explicit method by checking only a single inequality, the boxed term in Eq. (7.6), can be expressed as

$$v_j^n \frac{u_j^n - u_{j-1}^n}{\Delta y}$$

when

$$v_j^n > 0$$

and

$$v_j^n \frac{u_{j+1}^n - u_j^n}{\Delta y}$$

when  $v_j^n < 0$ , whereby the stability constraint becomes

$$\Delta x \leq \frac{1}{2\nu / [u_j^n (\Delta y)^2] + |v_j^n| / (u_j^n \Delta y)}$$

The truncation error (T.E.) deteriorates to only  $O(\Delta x) + O(\Delta y)$  when this treatment of  $\nu \partial u / \partial y$  is used.

Note that the stability constraints for both methods depend upon the local values of  $u$  and  $v$ . This is typical for equations with variable coefficients. The von Neumann stability analysis has proven to be a reliable guide to stability for boundary-layer equations if the coefficients  $u$  and  $v$  that appear in the equations are treated as being locally constant. Treatment of  $\mu_T$  for turbulent flow in the stability analysis requires further consideration. For some models,  $\mu_T$  will contain derivatives whose difference representation could contribute to numerical instabilities. In the stability analysis, one can treat  $\mu_T$  as simply a specified variable property and then by trial and error develop a stable difference representation for  $\mu_T$  or one can express  $\mu_T$  in terms of the dependent flow variables and attempt to determine the appropriate stability constraints by the usual methods.

### 7.3.3 Crank-Nicolson and Fully Implicit Methods

The characteristics of most implicit methods can be visualized by considering the following representation of the compressible laminar boundary-layer equations in physical coordinates on a mesh for which  $\Delta y = \text{const.}$

momentum:

$$\begin{aligned} & \frac{[\theta(\rho_j^{n+1}u_j^{n+1}) + (1 - \theta)(\rho_j^n u_j^n)](u_j^{n+1} - u_j^n)}{\Delta x} \\ & + \frac{\theta(\rho_j^{n+1}v_j^{n+1})(u_{j+1}^{n+1} - u_{j-1}^{n+1}) + (1 - \theta)(\rho_j^n v_j^n)(u_{j+1}^n - u_{j-1}^n)}{2 \Delta y} \\ & = \frac{[\theta(\rho_e^{n+1}u_e^{n+1}) + (1 - \theta)(\rho_e^n u_e^n)](u_e^{n+1} - u_e^n)}{\Delta x} \\ & + \frac{1}{(\Delta y)^2} \left\{ \theta [\mu_{j+1/2}^{n+1}(u_{j+1}^{n+1} - u_j^{n+1}) - \mu_{j-1/2}^{n+1}(u_j^{n+1} - u_{j-1}^{n+1})] \right. \\ & \left. + (1 - \theta) [\mu_{j+1/2}^n(u_{j+1}^n - u_j^n) - \mu_{j-1/2}^n(u_j^n - u_{j-1}^n)] \right\} \quad (7.9) \end{aligned}$$

In the above,  $\theta$  is a weighting factor. If

- $\theta = 0$  Method is explicit, most convenient expansion point is  $(n, j)$ , truncation error is  $O(\Delta x) + O[(\Delta y)^2]$ ; the von Neumann stability constraint, given previously, presents a severe limitation on the marching step size.
- $\theta = \frac{1}{2}$  Crank-Nicolson implicit; the most convenient expansion point is  $(n + \frac{1}{2}, j)$ ; the T.E. is  $O[(\Delta x)^2] + O[(\Delta y)^2]$  if coefficients (and properties) are evaluated at  $(n + \frac{1}{2}, j)$ . No stability constraint arises from the von Neumann analysis, but difficulties can arise if diagonal dominance is not maintained for the tridiagonal algorithm (Hirsh and Rudy, 1974).
- $\theta = 1$  Fully implicit, expansion point  $(n + 1, j)$ , T.E. is  $O(\Delta x) + O[(\Delta y)^2]$  [if properties and coefficients are evaluated at  $(n + 1, j)$ ]. No stability constraint by the von Neumann method, but same comment as for  $\theta = \frac{1}{2}$  applies for diagonal dominance.

We note that the above scheme becomes implicit if  $\theta > 0$ , and inherently stable if  $\theta \geq \frac{1}{2}$ . Values of  $\theta$  between  $\frac{1}{2}$  and 1 have been used successfully. The same form of the continuity equation can be used for both the fully implicit and the explicit methods.

continuity:

$$\frac{\rho_j^{n+1}v_j^{n+1} - \rho_{j-1}^{n+1}v_{j-1}^{n+1}}{\Delta y} + \frac{\rho_j^{n+1}u_j^{n+1} - \rho_j^n u_j^n + \rho_{j-1}^{n+1}u_{j-1}^{n+1} - \rho_{j-1}^n u_{j-1}^n}{2 \Delta x} = 0 \quad (7.10)$$

When  $\theta = \frac{1}{2}$ , we can consider  $\rho$  and  $v$  in the first term to be at the  $n + \frac{1}{2}$  level and rewrite Eq. (7.10) accordingly. This results in a T.E. of  $O[(\Delta x)^2] + O[(\Delta y)^2]$  for the continuity equation. Differencing of the energy equation follows the same general pattern as used for the momentum equation. Choosing  $T$  as the primary thermal variable as we might for low speed flow, we can write

the energy equation as

energy:

$$\rho u c_p \frac{\partial T}{\partial x} + \rho v c_p \frac{\partial T}{\partial y} = \frac{\partial}{\partial y} \left( k \frac{\partial T}{\partial y} \right) + \beta T u \frac{dp}{dx} + \mu \left( \frac{\partial u}{\partial y} \right)^2 \quad (7.11)$$

which, utilizing the  $\theta$  notation, can be written in difference form as

$$\begin{aligned} & \left[ \theta (\rho_j^{n+1} u_j^{n+1} c_{p_j}^{n+1}) + (1 - \theta) (\rho_j^n u_j^n c_{p_j}^n) \right] \frac{T_j^{n+1} - T_j^n}{\Delta x} \\ & + \frac{\theta (\rho_j^{n+1} v_j^{n+1} c_{p_j}^{n+1}) (T_{j+1}^{n+1} - T_{j-1}^{n+1}) + (1 - \theta) (\rho_j^n v_j^n c_{p_j}^n) (T_{j+1}^n - T_{j-1}^n)}{2 \Delta y} \\ & = \frac{1}{(\Delta y)^2} \left\{ \theta [k_{j+1/2}^{n+1} (T_{j+1}^{n+1} - T_j^{n+1}) - k_{j-1/2}^{n+1} (T_j^{n+1} - T_{j-1}^{n+1})] \right. \\ & \quad \left. + (1 - \theta) [k_{j+1/2}^n (T_{j+1}^n - T_j^n) - k_{j-1/2}^n (T_j^n - T_{j-1}^n)] \right\} \\ & + \frac{[\theta (\beta_j^{n+1} T_j^{n+1} u_j^{n+1}) + (1 - \theta) (\beta_j^n T_j^n u_j^n)] (p_j^{n+1} - p_j^n)}{\Delta x} \\ & + \theta \mu_j^{n+1} \left( \frac{u_{j+1}^{n+1} - u_{j-1}^{n+1}}{2 \Delta y} \right)^2 + (1 - \theta) \mu_j^n \left( \frac{u_{j+1}^n - u_{j-1}^n}{2 \Delta y} \right)^2 \quad (7.12) \end{aligned}$$

The T.E. for the energy equation is identical to that stated for the momentum equation for  $\theta = 0, \frac{1}{2}, 1$ .

The fully implicit ( $\theta = 1$ ) scheme can be elevated to formal second-order accuracy by representing streamwise derivatives by three-level ( $n - 1, n, n + 1$ ) second-order accurate differences, such as can be found in Chapter 3. Davis (1963) and Harris (1971) have demonstrated the feasibility of such a procedure.

For any implicit method ( $\theta \neq 0$ ) the finite-difference forms of the momentum and energy equations [Eqs. (7.9) and (7.12)] are algebraically nonlinear in the unknowns owing to the appearance of quantities unknown at the  $n + 1$  level in the coefficients. Linearizing procedures that can and have been utilized are described in the following sections.

**Lagging the coefficients.** The simplest and most common strategy is to linearize the difference equations by evaluating all coefficients at the  $n$  level. This is known as “lagging” the coefficients. The procedure provides a consistent representation, since for a general function  $\phi(x, y)$ ,  $\phi(x_0 + \Delta x, y_0) = \phi(x_0, y_0) + O(\Delta x)$ . This procedure causes the difference scheme to be no better than first-order accurate in the marching coordinate. Using the generalized form [Eq. (7.5)] for a transport equation, the linearized difference representation obtained

by lagging the coefficients can be written

$$\begin{aligned} & \rho_j^n u_j^n \frac{\phi_j^{n+1} - \phi_j^n}{\Delta x} + \frac{\rho_j^n v_j^n}{2 \Delta y} \left[ \theta (\phi_{j+1}^{n+1} - \phi_{j-1}^{n+1}) + (1 - \theta) (\phi_{j+1}^n - \phi_{j-1}^n) \right] \\ &= \frac{1}{(\Delta y)^2} \left\{ \lambda_{j+1/2}^n \left[ \theta (\phi_{j+1}^{n+1} - \phi_j^{n+1}) + (1 - \theta) (\phi_{j+1}^n - \phi_j^n) \right] \right. \\ & \quad \left. - \lambda_{j-1/2}^n \left[ \theta (\phi_j^{n+1} - \phi_{j-1}^{n+1}) + (1 - \theta) (\phi_j^n - \phi_{j-1}^n) \right] \right\} \\ & \quad + \theta S_j^{n+1} + (1 - \theta) S_j^n \end{aligned} \quad (7.13)$$

The three conservation equations in difference form can now be solved in an uncoupled manner. The momentum equation can be solved for  $u_j^{n+1}$ , the energy equation for  $T_j^{n+1}$ , and an equation of state used to obtain  $\rho_j^{n+1}$ . Finally, the continuity equation can be solved for  $v_j^{n+1}$ . The matrix of unknowns in each equation (for momentum and energy) is tridiagonal, and the Thomas algorithm can be employed.

**Simple iterative update of coefficients.** The coefficients can be ultimately evaluated at the  $n + 1$  level as required in Eqs. (7.9), (7.10), and (7.12) by use of a simple iterative updating procedure. To do this, the coefficients are first evaluated at the  $n$  level (lagged) and the system solved for new values of  $u, T, v$  at the  $n + 1$  level. The coefficients can then be updated by utilizing the solution just obtained at the  $n + 1$  level and the calculation repeated to obtain “better” predictions at  $n + 1$ .

This procedure can be repeated iteratively until changes are small. Usually only two or three iterations are used, although Blottner (1975a) points out that up to 19 iterations were required in a sample calculation with the Crank-Nicolson procedure before the solution obtained behaved like a second-order accurate scheme under grid refinement (see Section 3.2). Although the programming changes involved in advancing from the lagged procedure to the simple iterative update are minimal, the use of Newton linearization, to be described next, is more efficient and is recommended for that reason.

**Use of Newton linearization to iteratively update coefficients.** Newton linearization is another linearization procedure that can be used to iteratively update coefficients and, in fact, to provide a useful representation for most nonlinear expressions arising in computational fluid dynamics (CFD). The Newton procedure is actually more efficient (converges in fewer iterations) than the simple iterative update procedure described above. To be general, suppose we wish to linearize a function of several dependent variables in a conservation equation such as  $u, v,$  and  $p$ . These variables may, in turn, depend upon independent variables such as position and time. With an iteration sequence in mind, we may think of  $u, v,$  and  $p$  as being functions of a time-like parameter (pseudo-time) that is incremented as the iterative sequence proceeds. We let

$\Delta u$ ,  $\Delta v$ , and  $\Delta p$  equal the change in  $u$ ,  $v$ , and  $p$ , respectively, between two iterative solutions to the difference equations. Thus  $u_j^{n+1} = \hat{u}_j^{n+1} + \Delta u_j$ ,  $v_j^{n+1} = \hat{v}_j^{n+1} + \Delta v_j$ ,  $p_j^{n+1} = \hat{p}_j^{n+1} + \Delta p_j$ , where the circumflex denotes an evaluation of the variable from a previous iteration level. For the first iteration with the steady boundary-layer equations, the variables with circumflexes will be assigned values from the previous marching station. We may expand the nonlinear function  $F^{n+1}(u, v, p)$  in a Taylor series in the iteration parameter  $\tau$  about the present state  $\hat{F}^{n+1}$ :

$$F^{n+1} = \hat{F}^{n+1} + \frac{\partial \hat{F}}{\partial \tau} \Delta \tau + \dots \tag{7.14}$$

Linearization is enabled by truncating the series after the first-derivative term. Using the chain rule, we can represent the derivative on the right-hand side in terms of  $u, v, p$ :

$$\frac{\partial \hat{F}}{\partial \tau} = \frac{\partial \hat{F}}{\partial u} \frac{\partial u}{\partial \tau} + \frac{\partial \hat{F}}{\partial v} \frac{\partial v}{\partial \tau} + \frac{\partial \hat{F}}{\partial p} \frac{\partial p}{\partial \tau}$$

Substituting this result into Eq. (7.14) gives

$$F^{n+1} \cong \hat{F}^{n+1} + \frac{\partial \hat{F}}{\partial u} \Delta u + \frac{\partial \hat{F}}{\partial v} \Delta v + \frac{\partial \hat{F}}{\partial p} \Delta p \tag{7.15}$$

Note that the iteration parameter  $\tau$  does not appear in this final working form of Newton linearization.

As an example, let the function to be linearized be  $uv/p$ . Applying the results indicated by Eq. (7.15), we obtain

$$F^{n+1} = \left(\frac{\hat{u}\hat{v}}{\hat{p}}\right)^{n+1} + \left(\frac{\hat{v}}{\hat{p}}\right)^{n+1} \Delta u + \left(\frac{\hat{u}}{\hat{p}}\right)^{n+1} \Delta v - \left(\frac{\hat{u}\hat{v}}{\hat{p}^2}\right)^{n+1} \Delta p$$

When solving the boundary-layer equations with an implicit scheme, we need to linearize  $(u_j^{n+1})^2$ . Here  $F^{n+1} = F^{n+1}(u) = (u_j^{n+1})^2$  and  $\partial \hat{F} / \partial u = 2\hat{u}^{n+1}$ . Our representation after linearization is

$$(u_j^{n+1})^2 \cong (\hat{u}_j^{n+1})^2 + 2\Delta u_j \hat{u}_j^{n+1} \tag{7.16}$$

in which  $\Delta u_j$  is the only unknown. Alternatively, we can substitute for  $\Delta u_j$  according to  $\Delta u_j = u_j^{n+1} - \hat{u}_j^{n+1}$  and rewrite Eq. (7.16) as

$$(u_j^{n+1})^2 \cong 2u_j^{n+1} \hat{u}_j^{n+1} - (\hat{u}_j^{n+1})^2 \tag{7.17}$$

This latter procedure will be employed in this chapter. However, both procedures, the one in which the delta quantities are treated as the unknowns [as in Eq. (7.16)] and the other in which the deltas are eliminated by substitution [as in Eq. (7.17)] are widely used in CFD. Note that upon iterative convergence, both representations are exact.

For a more specific example of the use of this procedure, consider a fully implicit ( $\theta = 1$ ) application in which the conservation equations are to be solved in an uncoupled manner for an incompressible flow. The most obvious nonlinearity appears in the representation for the  $\rho u \partial u / \partial x$  term. Applying Newton linearization to the fully implicit finite-difference representation of this term gives

$$\frac{\rho \left[ 2 \hat{u}_j^{n+1} u_j^{n+1} - (\hat{u}_j^{n+1})^2 - u_j^n u_j^{n+1} \right]}{\Delta x} \tag{7.18}$$

in which  $u_j^{n+1}$  is the only unknown. For the first iteration,  $\hat{u}_j^{n+1}$  is evaluated as  $u_j^n$ . A slightly different final result is obtained if we apply the linearization procedure to this term in the mathematically equivalent form,  $\rho \partial(u^2/2) / \partial x$ .

If the conservation equations are to be solved in an uncoupled manner, i.e., one unknown is to be determined independently from each conservation equation, the other nonlinear terms

$$\rho v \frac{\partial u}{\partial y} \quad \frac{\partial}{\partial y} \left( \mu \frac{\partial u}{\partial y} \right)$$

are usually evaluated by the simple iterative updating procedure described above.

Evaluating  $\rho u \partial u / \partial x$  by the Newton linearization as indicated in Eq. (7.18) and using simple updating on other nonlinear terms results in a tridiagonal coefficient matrix, which permits use of the Thomas algorithm with no special modifications. The calculation is repeated two or more times at each streamwise location, updating variables as indicated.

**Newton linearization with coupling.** Several investigators have observed that convergence of the iterations to update coefficients at each streamwise step in the boundary-layer momentum equation can be accelerated greatly by solving the momentum and continuity equations in a coupled manner. Second-order accuracy for the Crank-Nicolson procedure has been observed using only one iteration at each streamwise station when the equations are solved in a coupled manner (Blottner, 1975a). According to Blottner (1975a), coupling was first suggested by R. T. Davis and used by Werle and co-workers (Werle and Bertke, 1972; Werle and Dwoyer, 1972). An example of the coupled procedure for a fully implicit formulation for incompressible, constant property flow follows.

The  $u \partial u / \partial x$  term is treated as in Eq. (7.18). The  $v \partial u / \partial y$  term is linearized by using  $v_j^{n+1} = \hat{v}_j^{n+1} + \Delta v_j$  and  $u_j^{n+1} = \hat{u}_j^{n+1} + \Delta u_j$ . For the first iteration,  $\hat{v}_j^{n+1}$  and  $\hat{u}_j^{n+1}$  are most conveniently evaluated as  $v_j^n$  and  $u_j^n$ , respectively. Here we are considering  $F$  in Eq. (7.15) to be  $F(u, v)$ . After replacing the delta quantities by differences in variables at two iteration levels,

the term  $v \partial u / \partial y$  becomes

$$\left( v \frac{\partial u}{\partial y} \right)^{n+1} \approx \hat{v}^{n+1} \left( \frac{\partial u}{\partial y} \right)^{n+1} + v^{n+1} \left( \frac{\partial \hat{u}}{\partial y} \right)^{n+1} - \hat{v}^{n-1} \left( \frac{\partial \hat{u}}{\partial y} \right)^{n+1} \quad (7.19)$$

The continuity and momentum equations can then be written in difference form as

$$\begin{aligned} & \frac{u_j^{n+1} - u_j^n + u_{j-1}^{n+1} - u_{j-1}^n}{2 \Delta x} + \frac{v_j^{n+1} - v_{j-1}^{n+1}}{\Delta y} = 0 \quad (7.20) \\ & \frac{2\hat{u}_j^{n+1}u_j^{n+1} - (\hat{u}_j^{n+1})^2 - u_j^n u_j^{n+1}}{\Delta x} + \frac{\hat{v}_j^{n+1}(u_{j+1}^{n+1} - \hat{u}_{j+1}^{n+1} - u_{j-1}^{n+1} + \hat{u}_{j-1}^{n+1})}{2 \Delta y} \\ & + \frac{v_j^{n+1}(\hat{u}_{j+1}^{n+1} - \hat{u}_{j-1}^{n+1})}{2 \Delta y} \\ & = \frac{\nu}{(\Delta y)^2} (u_{j+1}^{n+1} - 2u_j^{n+1} + u_{j-1}^{n+1}) + \frac{(u_e^{n+1})^2 - u_e^{n+1}u_e^n}{\Delta x} \quad (7.21) \end{aligned}$$

To clarify the algebraic formulation of the problem, the momentum equation can be written as

$$B_j u_{j-1}^{n+1} + D_j u_j^{n+1} + A_j u_{j+1}^{n+1} + a_j v_j^{n+1} + b_j v_{j-1}^{n+1} = C_j \quad (7.22)$$

where

$$\begin{aligned} B_j &= -\frac{\hat{v}_j^{n+1}}{2 \Delta y} - \frac{\nu}{(\Delta y)^2} & D_j &= \frac{2\hat{u}_j^{n+1} - u_j^n}{\Delta x} + \frac{2\nu}{(\Delta y)^2} \\ A_j &= \frac{\hat{v}_j^{n+1}}{2 \Delta y} - \frac{\nu}{(\Delta y)^2} & a_j &= \frac{\hat{u}_{j+1}^{n+1} - \hat{u}_{j-1}^{n+1}}{2 \Delta y} & b_j &= 0 \\ C_j &= \frac{(\hat{u}_j^{n+1})^2}{\Delta x} + \hat{v}_j^{n+1} \frac{\hat{u}_{j+1}^{n+1} - \hat{u}_{j-1}^{n+1}}{2 \Delta y} + \frac{(u_e^{n+1})^2 - u_e^{n+1}u_e^n}{\Delta x} \end{aligned}$$

In this example,  $b_j$  could be dropped, since it is equal to zero. We will continue to develop the solution algorithm including  $b_j$  because the result will be useful to us for solving other difference equations in this chapter.

For any  $j$  value, *four* unknowns (five if  $b_j \neq 0$ ) appear on the left-hand side of Eq. (7.22),  $u_{j-1}^{n+1}$ ,  $u_j^{n+1}$ ,  $u_{j+1}^{n+1}$ , and  $v_j^{n+1}$ . It is obvious that the matrix of coefficients is no longer tridiagonal. However, the continuity equation can be written as

$$v_j^{n+1} = v_{j-1}^{n+1} - e_j (u_{j-1}^{n+1} + u_j^{n+1}) + d_j \quad (7.23)$$

where

$$e_j = \frac{\Delta y}{2 \Delta x} \quad d_j = \frac{(u_{j-1}^n + u_j^n) \Delta y}{2 \Delta x}$$

and Eqs. (7.22) and (7.23) together form a coupled system, which can be written in "block-tridiagonal" form (see Appendix B) with  $2 \times 2$  blocks as

$$\begin{bmatrix} B_j & b_j \\ e_j & -1 \end{bmatrix} \begin{bmatrix} u_{j-1}^{n+1} \\ v_{j-1}^{n+1} \end{bmatrix} + \begin{bmatrix} D_j & a_j \\ e_j & 1 \end{bmatrix} \begin{bmatrix} u_j^{n+1} \\ v_j^{n+1} \end{bmatrix} + \begin{bmatrix} A_j & 0 \\ 0 & 0 \end{bmatrix} \begin{bmatrix} u_{j+1}^{n+1} \\ v_{j+1}^{n+1} \end{bmatrix} = \begin{bmatrix} C_j \\ d_j \end{bmatrix}$$

A solution algorithm has been developed (see also Werle et al., 1973, or Blottner, 1975a) for solving this coupled system of equations. In this procedure (often called the modified tridiagonal algorithm), the blocks above the main diagonal are first eliminated. This permits the velocities,  $u_j^{n+1}$ , to be calculated from the recursion formula  $u_j^{n+1} = E_j u_{j-1}^{n+1} + F_j + G_j v_{j-1}^{n+1}$  after  $E_j$ ,  $F_j$ ,  $G_j$ , and  $v_{j-1}^{n+1}$  are computed as indicated below. At the upper boundary, corresponding to  $j = J$ , conditions are specified as

$$E_J = 0$$

$$F_J = u_J^{n-1} \quad (\text{specified boundary value})$$

$$G_J = 0$$

Then for  $j = J - 1, J - 2, \dots, 2$  we compute

$$\bar{D}_j = D_j + A_j E_{j+1} - e_j (A_j G_{j+1} + a_j)$$

$$E_j = - \left( \frac{B_j - e_j (A_j G_{j+1} + a_j)}{\bar{D}_j} \right)$$

$$F_j = \frac{C_j - A_j F_{j+1} - d_j (A_j G_{j+1} + a_j)}{\bar{D}_j}$$

$$G_j = - \left( \frac{A_j G_{j+1} + a_j + b_j}{\bar{D}_j} \right)$$

Then the lower boundary conditions are utilized to compute  $v_1^{n+1} = 0$ ,  $u_1^{n+1} = 0$ , after which the velocities can be computed for  $j = 2, \dots, J$  by utilizing  $u_j^{n+1} = E_j u_{j-1}^{n+1} + F_j + G_j v_{j-1}^{n+1}$  and  $v_j^{n+1} = v_{j-1}^{n+1} - e_j (u_{j-1}^{n+1} + u_j^{n+1}) + d_j$ . The above procedure reduces to the Thomas algorithm (but with elements above the main diagonal being eliminated) for a scalar tridiagonal system whenever  $a_j$ ,  $b_j$ ,  $e_j$ , and  $d_j$  are all set to zero. This system of equations can also be solved by the general algorithm for a block tridiagonal system given in Appendix B. However, the algorithm given above is more efficient because it is specialized to systems exactly of the form given by Eqs. (7.22) and (7.23).

The procedure can be extended readily to compressible variable property flows (see Blottner, 1975a). The energy equation is nearly always solved in an uncoupled manner in this case.

**Extrapolating the coefficients.** Values of the coefficients can be obtained at the  $n + 1$  level by extrapolation based on values already obtained from previous  $n$  levels. Formally, the T.E. of this procedure can be made as small as we wish. For example, we can write

$$u_j^{n+1} = u_j^n + \left. \frac{\partial u}{\partial x} \right)_j^n \Delta x_+ + O[(\Delta x)^2]$$

Approximating  $(\partial u / \partial x)_j^n$  by only a first-order accurate representation such as

$$\left. \frac{\partial u}{\partial x} \right)_j^n = \frac{u_j^n - u_j^{n-1}}{\Delta x_-} + O(\Delta x)$$

gives the following representation for  $u_j^{n+1}$ , which formally has a T.E. of  $O[(\Delta x)^2]$ :

$$u_j^{n+1} = u_j^n + \frac{u_j^n - u_j^{n-1}}{\Delta x_-} \Delta x_+ + O[(\Delta x)^2]$$

A similar procedure can be used for other coefficients needed at the  $n + 1$  level. This approach has been used satisfactorily for boundary-layer flows by Harris (1971).

**A recommendation.** For many calculations, the linearization introduced by simply lagging the coefficients  $u$  and  $v$  and the fluid properties (in cases with temperature variations) will cause no serious deterioration of accuracy. Errors associated with linearization of coefficients are simply truncation errors, which can be controlled by adjustment of the marching step size. Many investigators have used this procedure satisfactorily. For any problem in which this linearization causes special difficulties, extrapolation of coefficients or Newton linearization with coupling is recommended. The former procedure requires no iterations to update the coefficients and for that reason should be more economical in terms of computation time. Clearly, it is desirable to use a method that is consistent, so that the numerical errors can be reduced to any level required. For turbulent flow calculations in particular, the uncertainties in the experimental data that are used to guide and verify the calculations and the uncertainties introduced by turbulence modeling add up to several (at least three to five) percent, making extreme accuracy in the numerical procedures unrewarding. In this situation the merits of using a higher-order method (highly accurate in terms of order of truncation error) should be determined on the basis of computer time that can be saved through the use of the coarser grids permitted by the more accurate schemes.

**A warning on stability.** Implicit schemes are touted as being unconditionally stable (in the von Neumann sense) if  $\theta \geq \frac{1}{2}$ . The Crank-Nicolson scheme just

barely satisfies the formal stability requirement in term of  $\theta$ , and this requirement was based on a heuristic extension of von Neumann's analysis for linear equations to nonlinear ones.

For turbulent flows in particular, the Crank-Nicolson procedure has occasionally been found to become unstable. For this reason, the fully implicit scheme has become more widely used. Formal second-order accuracy can be achieved by use of a three-point representation of the streamwise derivative and extrapolation of the coefficients. As an example, for uniform grid spacing, the convective terms

$$u \frac{\partial u}{\partial x} + v \frac{\partial u}{\partial y}$$

can be represented by

$$\begin{aligned} u \frac{\partial u}{\partial x} + v \frac{\partial u}{\partial y} = & \frac{(2u_j^n - u_j^{n-1})(3u_j^{n+1} - 4u_j^n + u_j^{n-1})}{2 \Delta x} \\ & + \frac{(2v_j^n - v_j^{n-1})(u_{j+1}^{n+1} - u_{j-1}^{n+1})}{2 \Delta y} + O[(\Delta x)^2] + O[(\Delta y)^2] \end{aligned} \quad (7.24)$$

With a slight increase in algebraic complexity, these representations can be generalized to also provide second-order accurate representations when the mesh increments  $\Delta x$  and  $\Delta y$  are not constant (Harris, 1971).

There is still one very real constraint on the use of the implicit schemes given for boundary-layer flows. Though not detected by the von Neumann stability analysis, a behavior very much characteristic of numerical instability can occur if the choice of grid spacing permits the convective transport (of momentum or energy) to dominate the diffusive transport. Two sources of this difficulty can be identified. First, errors can grow out of hand in the tridiagonal elimination scheme if diagonal dominance is not maintained, that is, in terms of the notation being used for the Thomas algorithm, if  $|D_j|$  is not greater than  $|B_j| + |A_j|$ . A second and equally important cause of these unacceptable solutions can be related to a physical implausibility that arises when the choice of grid size permits the algebraic model to be an inaccurate representation for a viscous flow. The same difficulty for the viscous Burgers equation was discussed in Chapter 4. It can be shown that satisfying the conditions required to keep the algebraic representation a physically valid one provides a sufficient condition for diagonal dominance in the elimination scheme.

To illustrate the basis for these difficulties, consider the fully implicit procedure applied to the boundary-layer momentum equation for constant property flow with the coefficients lagged. The finite-difference equation can be written as

$$B_j u_{j-1}^{n+1} + D_j u_j^{n+1} + A_j u_{j+1}^{n+1} = C_j \quad (7.25)$$

with

$$\begin{aligned}
 B_j &= -\frac{v_j^n}{2 \Delta y} - \frac{\nu}{(\Delta y)^2} \\
 D_j &= \frac{u_j^n}{\Delta x} + \frac{2\nu}{(\Delta y)^2} \\
 A_j &= \frac{v_j^n}{2 \Delta y} - \frac{\nu}{(\Delta y)^2} \\
 C_j &= \frac{(u_j^n)^2}{\Delta x} + u_e^n \frac{(u_e^{n+1} - u_e^n)}{\Delta x}
 \end{aligned}$$

By reflecting on the implications of Eq. (7.25) in terms of the predicted behavior of  $u_j^{n+1}$  relative to changes in  $u_{j-1}^{n+1}$  and  $u_{j+1}^{n+1}$ , we would expect both  $A_j$  and  $B_j$  to be negative to properly imply the expected behavior of a viscous fluid. The expected behavior would be such that a decrease in the velocity of the fluid below or above the point  $n + 1, j$  would contribute toward a decrease in the velocity at point  $n + 1, j$  through the effects of viscosity. We should be able to see that such would not be the case if either  $A_j$  or  $B_j$  would become positive. To keep  $A_j$  and  $B_j$  negative in value requires

$$\frac{|v_j^n|}{2 \Delta y} - \frac{\nu}{(\Delta y)^2} < 0$$

or

$$\frac{|v_j^n| \Delta y}{\nu} \leq 2 \tag{7.26}$$

Equation (7.26) confirms our suspicion that the “correct” representation is one that permits viscous-like behavior, in that the inequality can be satisfied for a sufficiently fine mesh, which of course, is achieved at convergence. The term  $|v_j^n| \Delta y / \nu$  can be identified as a mesh Reynolds number. Mesh Peclet number, a more general terminology, is also frequently used for this term.

Maintaining the inequality of Eq. (7.26) provides a sufficient (but not the necessary) condition for diagonal dominance of the algebraic system. It appears that keeping the coefficients  $A_j$  and  $B_j$  negative to provide correct simulation of viscous behavior should be the major concern.

For some flows the constraint of Eq. (7.26) tends to require the use of an excessively large number of grid points. This has motivated several investigators to consider ways of altering the difference scheme to eliminate the mesh Reynolds number constraint. Most of the studies on this problem have focused on the more complex Navier-Stokes equations where the motivation for computational economy is stronger. The simplest remedy to the problem of the mesh Reynolds number constraint is to replace the central-difference represen-

tation for  $v \partial u / \partial y$  by an upstream (one-way) difference:

$$v \frac{\partial u}{\partial y} \cong \frac{v_j^n (u_j^{n+1} - u_{j-1}^{n+1})}{\Delta y}$$

when

$$v_j^n > 0$$

and

$$\frac{v_j^n (u_{j+1}^{n+1} - u_j^{n+1})}{\Delta y}$$

when

$$v_j^n < 0$$

The T.E. associated with the upstream (also called “upwind”) scheme creates an “artificial viscosity,” which tends to enhance viscous-like behavior, causing a deterioration in accuracy in some cases.

It is clearly possible to devise upstream weighted schemes having a more favorable T.E. (using two or more upstream grid points), but these can lead to coefficient matrices that are not tridiagonal in form—a distinct disadvantage. Most of the example calculations illustrating the detrimental effects of upstream differencing have been for the Navier-Stokes equations. Less specific information appears to be available for the boundary-layer equations. The tentative conclusion is that the use of upstream differencing for  $v \partial u / \partial y$  (when mandated by the mesh Reynolds number) is a sufficient solution to the constraint of Eq. (7.26). Use of central differencing for this term is, of course, recommended whenever feasible.

Rather than switching abruptly from the central to the upwind scheme as the mesh Reynolds number exceeds 2, the use of a combination (hybrid) of central and upwind schemes is recommended. This concept was originally suggested by Allen and Southwell (1955). Others, apparently not aware of this early work, have proposed similar or identical forms (Spalding, 1972; Raithby and Torrance, 1974). To illustrate this principle, we let  $R_{\Delta y} = |v_j^n| \Delta y / \nu$  and  $R_c$  equal the desired critical mesh Reynolds number for initiating the hybrid scheme,  $R_c \leq 2$ . Then for  $R_{\Delta y} \geq R_c$  we represent  $v \partial u / \partial y$  by

$$v \frac{\partial u}{\partial y} \cong \underbrace{\left( \frac{R_c}{R_{\Delta y}} \right) v_j^n \frac{(u_{j+1}^{n+1} - u_{j-1}^{n+1})}{2 \Delta y}}_{\text{Central-difference component}} + \underbrace{\left( 1 - \frac{R_c}{R_{\Delta y}} \right) \left( \frac{(v_j^n + |v_j^n|)}{2} \frac{(u_j^{n+1} - u_{j-1}^{n+1})}{\Delta y} + \frac{(v_j^n - |v_j^n|)}{2} \frac{(u_{j+1}^{n+1} - u_j^{n+1})}{\Delta y} \right)}_{\text{Upwind component}}$$

(7.27)

We observe that as  $R_{\Delta y}$  increases, the weighting shifts toward the upwind representation. As  $R_{\Delta y} \rightarrow \infty$ , the representation is entirely upwind. The hybrid scheme maintains negative values for  $A_j$  and  $B_j$  in Eq. (7.25) while permitting the maximum utilization of the central-difference representation.

The reader is referred to the work of Raithby (1976), Leonard (1979a, 1979b), and Chow and Tien (1978) for an introduction to the literature on the mesh Reynolds number problem.

It is interesting that nothing has been noted in the technical literature about the mesh Reynolds number constraint for boundary-layer equations when the equations are solved in a coupled manner, as with the Davis coupled scheme discussed in this section or the modified box method discussed in Section 7.3.5. When coupling is used, the  $v$  in  $v \partial u / \partial y$  is treated algebraically as an unknown and not merely as a coefficient for the unknown  $u$ 's. It is possible that the coupling eliminates the "wiggles" and nonphysical behavior observed when central differencing is used for large mesh Reynolds numbers.

**Closing comment on Crank-Nicolson and fully implicit methods.** The difference schemes presented in this section have been purposely applied to equations in physical coordinates and have been written assuming  $\Delta x$  and  $\Delta y$  were both constant. This has been done primarily to keep the equations as simple as possible as the fundamental characteristics of the schemes were being discussed. As familiarity is gained with the basic concepts involved with differencing the boundary-layer equations, ways of extending schemes to a nonuniform grid will be pointed out.

### 7.3.4 DuFort-Frankel Method

Another finite-difference procedure that has worked well for both laminar and turbulent boundary layers is an extension of the method proposed by DuFort and Frankel (1953) for the heat equation. The difference representation will be written in a form that will accommodate variable grid spacing. We let  $\Delta x_+ = x^{n+1} - x^n$ ,  $\Delta x_- = x^n - x^{n-1}$ ,  $\Delta y_+ = y_{j+1} - y_j$ ,  $\Delta y_- = y_j - y_{j-1}$ . The implicit methods of the previous section can be extended in applicability to a nonuniform grid by following a similar procedure.

In presenting the DuFort-Frankel procedure for the momentum and energy equations, the generalized transport PDE, Eq. (7.5), will be employed with the dependent variable  $\phi$  denoting velocity components, a turbulence model parameter, or a thermal variable such as temperature or enthalpy. In the DuFort-Frankel differencing, stability is promoted by eliminating the appearance of  $\phi_j^n$  in the diffusion term through the use of an average of  $\phi$  at the  $n + 1$  and  $n - 1$  levels. With unequal spacing, however, Dancey and Pletcher (1974) observed that accuracy was improved by use of a linearly interpolated value of  $\phi$  between  $n - 1$  and  $n + 1$  levels instead of a simple average. Here we define the linearly interpolated value as  $\bar{\phi}_j^n$  according to  $\bar{\phi}_j^n = (\Delta x_+ \phi_j^{n-1} + \Delta x_- \phi_j^{n+1}) /$

$(\Delta x_+ + \Delta x_-)$ . As before, for turbulent flows it is understood that  $u$  and  $v$  are time-mean quantities. For a compressible flow,  $v = \bar{v}$ . For generality, let  $\bar{\lambda} = \lambda_T + \lambda$ , where  $\lambda_T$  is a turbulent diffusion coefficient. The DuFort-Frankel representation of the generalized transport equation becomes

$$\frac{\rho_j^n u_j^n (\phi_j^{n+1} - \phi_j^{n-1})}{\Delta x_+ + \Delta x_-} + \frac{\rho_j^n v_j^n (\phi_{j+1}^n - \phi_{j-1}^n)}{\Delta y_+ + \Delta y_-} = \frac{2}{\Delta y_+ + \Delta y_-} \left[ \frac{\bar{\lambda}_{j+1/2}^n (\phi_{j+1}^n - \bar{\phi}_j^n)}{\Delta y_+} - \frac{\bar{\lambda}_{j-1/2}^n (\bar{\phi}_j^n - \phi_{j-1}^n)}{\Delta y_-} \right] + S_j^n \quad (7.28)$$

In the above,  $S_j^n$  denotes the source terms. Examples of source terms that frequently occur include the pressure gradient  $dp/dx$  in the  $x$ -momentum equation, where

$$S_j^n = \frac{p_j^{n+1} - p_j^{n-1}}{\Delta x_+ + \Delta x_-}$$

a viscous dissipation term  $\bar{\mu}(\partial u/\partial y)^2$  in the energy equation when  $T$  is used as the thermal variable,

$$S_j^n = \bar{\mu}_j^n \left( \frac{u_{j+1}^n - u_{j-1}^n}{\Delta y_+ + \Delta y_-} \right)^2$$

and a dissipation term  $C_D \rho(\bar{k})^{3/2}/l$  in the modeled form of the turbulence kinetic energy equation

$$S_j^n = C_D \rho_j^n \left( \frac{\Delta y_+ (\bar{k})_{j-1}^n + \Delta y_- (\bar{k})_{j+1}^n}{\Delta y_+ + \Delta y_-} \right)^{1/2} \left( \frac{\Delta x_+ (\bar{k})_j^{n-1} + \Delta x_- (\bar{k})_j^{n+1}}{\Delta x_+ + \Delta x_-} \right) / l_j^n$$

Note that this latter representation avoids using the dependent variable  $\bar{k}$  at  $(n, j)$ . This is required by stability (see Malik and Pletcher, 1978), as might be expected in light of the special treatment required for the diffusion term noted above.

We recall (Chapter 4) that the DuFort-Frankel representation is explicit. Although  $\phi_j^{n+1}$  appears in both the left and right sides (within  $\bar{\phi}_j^n$ ) of the equation, the equation can be rearranged to isolate  $\phi_j^{n+1}$ , so that we can write  $\phi_j^{n+1} =$  (all known quantities at the  $n$  and  $n - 1$  levels). The formal T.E. for the equation with  $\Delta x_+ = \Delta x_-$  and  $\Delta y_+ = \Delta y_-$  is  $O[(\Delta x)^2] + O[(\Delta y)^2] + O[(\Delta x/\Delta y)^2]$ . However, the leading term in the T.E. represented by  $O[(\Delta x/\Delta y)^2]$  is actually  $(\Delta x/\Delta y)^2 (\partial^2 \phi/\partial x^2)$ , and  $\partial^2 \phi/\partial x^2$  is presumed to be very small for boundary-layer flows. One can show that a deterioration in the formal T.E. is generally expected as the grid spacing becomes unequal, although a paper by Blottner (1974) points out exceptions. This deterioration would be observed in all methods presented thus far in this chapter. In practice, the increase in actual error due to the use of unequal spacing may be negligible. In

nearly all cases, remedies can be found that will restore the original formal T.E. at the expense of algebraic operations. For example, Hong (1974) demonstrated that the streamwise derivative  $\partial\phi/\partial x$  in the DuFort-Frankel method can be written as

$$\frac{(\Delta x_-)^2 \phi_j^{n+1} - (\Delta x_+)^2 \phi_j^{n-1} + [(\Delta x_+)^2 - (\Delta x_-)^2] \phi_j^n}{\Delta x_- (\Delta x_+)^2 + \Delta x_+ (\Delta x_-)^2}$$

with second-order accuracy even when  $\Delta x_+ \neq \Delta x_-$ .

A consistent treatment of the continuity equation is given by

$$\frac{\rho_j^{n+1} v_j^{n+1} - \rho_{j-1}^{n+1} v_{j-1}^{n+1}}{\Delta y_-} + \frac{\rho_j^{n+1} u_j^{n+1} - \rho_j^{n-1} u_j^{n-1} + \rho_{j-1}^{n+1} u_{j-1}^{n+1} - \rho_{j-1}^{n-1} u_{j-1}^{n-1}}{2(\Delta x_+ + \Delta x_-)} = 0 \tag{7.29}$$

with T.E. of  $O(\Delta x) + O[(\Delta y)^2]$ .

A stability analysis for  $\Delta y = \text{const}$  (Madni and Pletcher, 1975a, 1975b) suggests that

$$\Delta x_+ \leq \frac{\rho_j^n u_j^n \Delta y}{\left| \rho_j^n v_j^n + (\bar{\lambda}_{j-1}^n - \bar{\lambda}_{j+1}^n) / 2 \Delta y \right|} \tag{7.30}$$

It would appear that this constraint could also be used to provide a rough guide under variable  $\Delta y$  conditions. In practice, this condition has not proven to be especially restrictive on the marching step size, probably because  $v/u$  is generally very small and the other term in the denominator involves differences in the diffusion coefficient rather than the coefficient itself.

It is interesting to note that Eq. (7.30) follows essentially from the Courant-Friedrichs-Lewy (CFL) condition rather than the diffusion stability limit for the boundary-layer momentum equation. This becomes evident when the diffusion term  $\partial/\partial y(\bar{\lambda} \partial\phi/\partial y)$  is expanded to two terms and the boundary-layer equation is rearranged as

$$\frac{\partial\phi}{\partial x} + \frac{1}{\rho u} \left( \rho v - \frac{\partial\bar{\lambda}}{\partial y} \right) \frac{\partial\phi}{\partial y} = \frac{\bar{\lambda}}{\rho u} \frac{\partial^2\phi}{\partial y^2} + \frac{S}{\rho u}$$

Now simply applying the CFL condition gives Eq. (7.30).

The boundary-layer calculation begins by utilizing an initial distribution for the  $\phi$  variables. Since the DuFort-Frankel procedure requires information at *two* streamwise levels in order to advance the calculation, some other method must be used to obtain a solution for at least one streamwise station before the DuFort-Frankel scheme can be employed. A simple explicit scheme is most frequently used to provide these starting values. A typical calculation would require the solution to the momentum, continuity, and energy equations. The equations can be solved sequentially starting with the momentum equation in an uncoupled manner. The usual procedure is to solve first for the unknown streamwise velocities from the momentum equation starting with the point

nearest the wall and working outward to the outer edge of the boundary layer. The outer edge of the boundary layer is located when the velocity from the solution is within a prescribed tolerance of the velocity specified as the outer boundary condition. The energy equation can be solved in a like manner for the thermal variable. The density at the new station can be evaluated from an equation of state. Finally, the continuity equation is used to obtain the normal component of velocity at the  $n + 1$  level starting from the point adjacent to the wall and working outward.

The explicit nature of the DuFort-Frankel procedure is probably its most attractive feature. Those inexperienced in numerical methods are likely to feel more comfortable programming an explicit procedure than they are in applying an implicit scheme. A second significant feature of the scheme is that no additional linearizations, iterations, or assumptions are needed to evaluate coefficients in the equation, since these all appear at the  $n$ -level, where they are known values. Further details on the application of the DuFort-Frankel type schemes to wall boundary layers can be found in the work by Pletcher (1969, 1970, 1971).

### 7.3.5 Box Method

Keller and Cebeci (1972) applied the box-difference scheme (introduced in Section 4.2.8) to the boundary-layer momentum and continuity equations after they had first been transformed to a single third-order PDE using the Mangler and Levy-Lees transformations (see Cebeci and Smith, 1974). The third-order PDE is written as a system of three first-order PDEs using newly defined variables in a manner that parallels the procedure commonly employed in the numerical solution of third-order ODEs. The box-differencing scheme with Newton linearization is then applied to the three first-order PDEs, giving rise to a block tridiagonal system having  $3 \times 3$  blocks, which is solved by a block elimination scheme. The corresponding treatment for the energy equation gives rise to a block tridiagonal system with  $2 \times 2$  blocks.

The details of the Keller-Cebeci box method for the boundary-layer equations will not be given here but can be found in the work by Cebeci and Smith (1974). Instead, we will indicate how a modified box scheme can be developed that only requires the use of the same modified tridiagonal elimination scheme presented in Section 7.3.3 for the Davis coupled scheme. From reports in the literature (Blottner, 1975a; Wornom, 1977), the modified box scheme appears to require only on the order of one-half as much computer time as the standard box scheme for the boundary-layer equations.

The momentum and energy equations for a compressible flow can be written in the generalized form given by Eq. (7.5). For rectangular coordinates, this becomes

$$\rho u \frac{\partial \phi}{\partial x} + \rho \tilde{v} \frac{\partial \phi}{\partial y} = \frac{\partial}{\partial y} \left( \bar{\lambda} \frac{\partial \phi}{\partial y} \right) + S \quad (7.31)$$

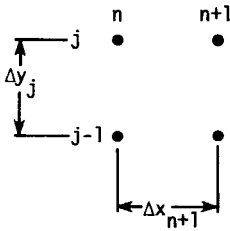


Figure 7.2 Grid arrangement for the modified box scheme.

where

$$\bar{\lambda} = \lambda_T + \lambda$$

The continuity equation can be written as

$$\frac{\partial \rho u}{\partial x} + \frac{\partial \rho \tilde{v}}{\partial y} = 0 \tag{7.32}$$

The grid nomenclature is given in Fig. 7.2. If we let

$$\begin{aligned} \bar{\lambda} \frac{\partial \phi}{\partial y} &= q \\ D &= S + \frac{\partial q}{\partial y} - \rho \tilde{v} \frac{\partial \phi}{\partial y} \end{aligned}$$

Equation (7.31) can then be written as

$$\rho u \frac{\partial \phi}{\partial x} = D \tag{7.33}$$

Centering on the box grid gives

$$\begin{aligned} & \frac{(\rho u)_{j-1/2}^{n+1} + (\rho u)_{j-1/2}^n}{2} \frac{\phi_{j-1/2}^{n+1} - \phi_{j-1/2}^n}{\Delta x_{n+1}} \\ &= S_{j-1/2}^{n+1/2} - \frac{(\rho \tilde{v})_{j-1/2}^{n+1/2} (\phi_j^{n+1/2} - \phi_{j-1}^{n+1/2})}{\Delta y_j} + \frac{q_j^{n+1/2} - q_{j-1}^{n+1/2}}{\Delta y_j} \end{aligned} \tag{7.34}$$

Utilizing the definition of  $q_{j-1/2}^{n+1/2}$ ,

$$\bar{\lambda}_{j-1/2}^{n+1/2} \frac{\phi_j^{n+1/2} - \phi_{j-1}^{n+1/2}}{\Delta y_j} = \frac{q_j^{n+1/2} + q_{j-1}^{n+1/2}}{2} \tag{7.35}$$

we can eliminate  $q_{j-1}^{n+1/2}$  from Eq. (7.34). This gives

$$\begin{aligned}
 & \frac{(\rho u)_{j-1/2}^{n+1} + (\rho u)_{j-1/2}^n}{2} \frac{\phi_{j-1/2}^{n+1} - \phi_{j-1/2}^n}{\Delta x_{n+1}} \\
 &= S_{j-1/2}^{n+1/2} - (\rho \tilde{v})_{j-1/2}^{n+1/2} \frac{\phi_j^{n+1/2} - \phi_{j-1}^{n+1/2}}{\Delta y_j} \\
 & \quad + \frac{2q_j^{n+1/2}}{\Delta y_j} - 2\bar{\lambda}_{j-1/2}^{n+1/2} \frac{\phi_j^{n+1/2} - \phi_{j-1}^{n+1/2}}{(\Delta y_j)^2} \quad (7.36)
 \end{aligned}$$

In a similar manner, the momentum equation can be put into difference form centering about the point  $(n + \frac{1}{2}, j + \frac{1}{2})$ , and  $q_{j+1}^{n+1/2}$  can be eliminated from that equation using the definition of  $q_{j+1}^{n+1/2}$ . The result is

$$\begin{aligned}
 & \frac{(\rho u)_{j-1/2}^{n+1} + (\rho u)_{j+1/2}^n}{2} \frac{\phi_{j+1/2}^{n+1} - \phi_{j+1/2}^n}{\Delta x_{n+1}} \\
 &= S_{j-1/2}^{n-1/2} - (\rho \bar{v})_{j+1/2}^{n+1/2} \frac{\phi_{j+1}^{n+1/2} - \phi_j^{n+1/2}}{\Delta y_{j+1}} \\
 & \quad + 2\bar{\lambda}_{j-1/2}^{n-1/2} \frac{\phi_{j+1}^{n+1/2} - \phi_j^{n+1/2}}{(\Delta y_{j+1})^2} - \frac{2q_j^{n+1/2}}{\Delta y_{j+1}} \quad (7.37)
 \end{aligned}$$

Equations (7.36) and (7.37) can be combined to eliminate  $q_j^{n+1/2}$ . This is accomplished by multiplying Eq. (7.36) by  $\Delta y_j$ , and Eq. (7.37) by  $\Delta y_{j+1}$  and adding the two products. After replacing quantities specified for evaluation at grid midpoints by averages from adjacent grid points, the results can be written as

$$\begin{aligned}
 & \frac{\Delta y_j}{2 \Delta x_{n+1}} \left[ (\rho u)_j^{n+1} + (\rho u)_{j-1}^{n+1} + (\rho u)_j^n + (\rho u)_{j-1}^n \right] \\
 & \quad \times (\phi_j^{n+1} + \phi_{j-1}^{n+1} - \phi_j^n - \phi_{j-1}^n) \\
 & + \frac{\Delta y_{j+1}}{2 \Delta x_{n+1}} \left[ (\rho u)_{j+1}^{n+1} + (\rho u)_j^{n+1} + (\rho u)_{j+1}^n + (\rho u)_j^n \right] \\
 & \quad \times (\phi_{j+1}^{n+1} + \phi_j^{n+1} - \phi_{j+1}^n - \phi_j^n) \\
 & + \frac{1}{2} \left[ (\rho \tilde{v})_j^{n+1} + (\rho \tilde{v})_{j-1}^{n+1} + (\rho \tilde{v})_j^n + (\rho \tilde{v})_{j-1}^n \right] \\
 & \quad \times (\phi_j^{n+1} + \phi_j^n - \phi_{j-1}^{n+1} - \phi_{j-1}^n) \\
 & + \frac{1}{2} \left[ (\rho \bar{v})_{j+1}^{n+1} + (\rho \bar{v})_j^{n+1} + (\rho \bar{v})_{j+1}^n + (\rho \bar{v})_j^n \right]
 \end{aligned}$$

$$\begin{aligned}
 & \times (\phi_{j+1}^{n+1} + \phi_{j+1}^n - \phi_j^{n+1} - \phi_j^n) \\
 & = \Delta y_j (S_j^{n+1} + S_{j-1}^{n+1} + S_j^n + S_{j-1}^n) + \Delta y_{j+1} (S_{j+1}^{n+1} + S_j^{n+1} + S_{j-1}^n + S_{j-1}^n) \\
 & \quad + \frac{(\bar{\lambda}_{j+1}^{n+1} + \bar{\lambda}_j^{n+1} + \bar{\lambda}_{j+1}^n + \bar{\lambda}_j^n)(\phi_{j+1}^{n+1} + \phi_{j+1}^n - \phi_j^{n+1} - \phi_j^n)}{\Delta y_{j+1}} \\
 & \quad - \frac{(\bar{\lambda}_j^{n+1} + \bar{\lambda}_{j-1}^{n+1} + \bar{\lambda}_j^n + \bar{\lambda}_{j-1}^n)(\phi_j^{n+1} + \phi_j^n - \phi_{j-1}^{n+1} - \phi_{j-1}^n)}{\Delta y_j} \quad (7.38)
 \end{aligned}$$

Equation (7.38) can be expressed in the tridiagonal format for the unknown  $\phi$ 's, but as for all implicit methods, some scheme must be devised for treating the algebraic nonlinearities arising through the coefficients. Conceptually, any of the procedures presented in Section 7.3.3 can be employed. The most suitable representation of the continuity equation may depend upon the procedure used to accomplish the linearization of the momentum equation. To date, Newton linearization with coupling (Blottner, 1975a) has been the most commonly used procedure. For this, the continuity equation can be written as

$$\begin{aligned}
 & \frac{(\rho u)_j^{n+1} + (\rho u)_{j-1}^{n+1} - (\rho u)_j^n - (\rho u)_{j-1}^n}{2 \Delta x_{n+1}} \\
 & + \frac{(\rho \bar{v})_j^{n+1} + (\rho \bar{v})_j^n - (\rho \bar{v})_{j-1}^{n+1} - (\rho \bar{v})_{j-1}^n}{2 \Delta y_j} = 0 \quad (7.39)
 \end{aligned}$$

The momentum equation involves  $(\rho \bar{v})_{j+1}^{n+1}$ ,  $(\rho \bar{v})_j^{n+1}$ , and  $(\rho \bar{v})_{j-1}^{n+1}$ . To employ the modified tridiagonal elimination scheme, the continuity equation (Eq. 7.39) can be written between the  $j$  and  $j + 1$  levels and  $(\rho \bar{v})_{j+1}^{n+1}$  eliminated from the momentum equation by substitution. After employing Newton linearization in a manner that parallels the procedures illustrated in Section 7.3.3 for the fully implicit Davis coupled method, the coupled momentum and continuity equations can be solved with the modified tridiagonal elimination scheme. The energy equation is usually solved in an uncoupled manner, and properties (including the turbulent viscosity) are updated iteratively as desired or required by accuracy constraints.

With the box and modified box schemes, the wall shear stress and heat flux are usually determined by evaluating  $q$  at the wall ( $j = 1$ ). For the modified box scheme this is done after the solutions for  $\phi$ ,  $\bar{v}$ , and  $\rho$  have been determined. An expression for  $q_1^{n+1/2}$  can be obtained by writing Eqs. (7.34) and (7.35) for  $j = 2$  and eliminating  $q_2^{n+1/2}$  by a simple substitution.

### 7.3.6 Other Methods

Exploratory studies of limited scope have indicated that the Barakat and Clark ADE method can be used for solving the boundary-layer equations (R. G. Hindman, 1975, private communication; S. S. Hwang, 1975, private

communication). These results indicate that ADE methods are roughly equivalent in accuracy and computation time to the more conventional implicit methods for boundary-layer problems. Higher-order schemes (up through fourth order) have also been applied to the boundary-layer equations. A critical study of some of these schemes was reported by Wornom (1977). It is worthwhile to note that the accuracy of lower-order methods can also be improved through the use of Richardson extrapolation (Ralston, 1965; Cebeci and Smith, 1974).

It is believed that the most commonly used difference schemes for 2-D or axisymmetric boundary layers have been described in this section. No attempt has been made to cover all known methods in detail.

### 7.3.7 Coordinate Transformations for Boundary Layers

The general subject of coordinate transformations has been treated in Chapter 5. In the present chapter the focus has been on the difference schemes themselves, and to illustrate these in the simplest possible manner, the equations have been presented in rectangular Cartesian, "physical coordinates."

It is well to point out that there may be advantages to numerically solving the equations in alternative forms. Two approaches are observed. One proceeds by introducing new dependent and independent variables analytically to transform the mathematical representation of the conservation principles before the equations are discretized. We shall refer to this strategy approach as the *analytical transformation approach*. A second strategy employs an independent variable transformation very much along lines introduced in Chapter 5 and will be referred to as the *generalized coordinate approach*.

The main objective of the transformations is generally to obtain a coordinate frame for computation in which the boundary-layer thickness remains as constant as possible and to remove the singularity in the equations at the leading edge or stagnation point. Unfortunately, for complex turbulent flows, the optimum transformation leading to a constant boundary-layer thickness in the transformed plane has not been identified, although the transformation suggested by Carter et al. (1980) shows promise.

**Analytical transformation approach.** The most commonly used analytical transformation makes use of the transverse similarity variable  $\eta$  employed in the Blasius similarity solution to the laminar boundary layer. We will give an example of such a transformation applied to the constant property laminar boundary-layer equations. We start with

continuity:

$$\frac{\partial u}{\partial x} + \frac{\partial v}{\partial y} = 0 \quad (7.40)$$

momentum:

$$u \frac{\partial u}{\partial x} + v \frac{\partial u}{\partial y} = u_e \frac{du_e}{dx} + \nu \frac{\partial^2 u}{\partial y^2} \quad (7.41)$$

The crucial element of the transformation is the introduction of

$$\eta = \frac{y}{x} \left( \frac{u_e x}{\nu} \right)^{1/2}$$

From this point on, several variations are possible, but a common procedure is to let  $x = x$  (no stretching of  $x$ ) and  $F = u/u_e$ . Using the chain rule, we note that

$$\left( \frac{\partial}{\partial x} \right)_y = \left( \frac{\partial}{\partial x} \right)_\eta + \left( \frac{\partial \eta}{\partial x} \right)_y \left( \frac{\partial}{\partial \eta} \right)_x = \left( \frac{\partial}{\partial x} \right)_\eta + \left( \frac{\eta}{2u_e} \frac{du_e}{dx} - \frac{\eta}{2x} \right) \left( \frac{\partial}{\partial \eta} \right)_x$$

and

$$\left( \frac{\partial}{\partial y} \right)_x = \left( \frac{\partial x}{\partial y} \right)_x \left( \frac{\partial}{\partial x} \right)_\eta + \left( \frac{\partial \eta}{\partial y} \right)_x \left( \frac{\partial}{\partial \eta} \right)_x = \left( \frac{u_e}{x\nu} \right)^{1/2} \left( \frac{\partial}{\partial \eta} \right)_x$$

Replacing the  $x$  and  $y$  derivatives in Eqs. (7.40) and (7.41) as indicated, and utilizing  $F$ , results in the transformed momentum and continuity equations:

momentum:

$$xF \frac{\partial F}{\partial x} + V \frac{\partial F}{\partial \eta} = \beta(1 - F^2) + \frac{\partial^2 F}{\partial \eta^2} \quad (7.42)$$

continuity:

$$x \frac{\partial F}{\partial x} + \frac{\partial V}{\partial \eta} + F \frac{\beta + 1}{2} = 0 \quad (7.43)$$

where

$$V = \frac{\beta - 1}{2} F \eta + \left( \frac{x}{\nu u_e} \right)^{1/2} \nu$$

$$\beta = \frac{x}{u_e} \frac{du_e}{dx}$$

When  $x = 0$ , the streamwise derivatives vanish from the transformed equations, and a system of two ODEs remains. It is common to solve these equations with a slightly modified version of the marching technique employed for the rest of the flow domain, i.e., for  $x > 0$ , although special numerical procedures applicable to ODEs could be used.

There is no singular behavior at  $x = 0$  in the new coordinate system, since the troublesome streamwise derivatives have been eliminated. In fact, for laminar flow over a plate, the solution for  $x = 0$  is the well-known Blasius similarity solution. Naturally, for a zero pressure gradient flow, the marching solution for  $x > 0$  should reproduce essentially the same solution downstream, and the boundary-layer thickness should remain constant. When pressure gradients or wall boundary conditions force a nonsimilar laminar flow solution, the boundary-layer thickness will change somewhat along the flow. For nearly

similar laminar flows, we would expect the solution of the transformed equations to provide greater and more uniform accuracy near the leading edge than the solution in physical coordinates because of the tendency of the former procedure to divide the boundary layer into a more nearly constant number of points in the transverse direction. For turbulent flows, we observe the boundary-layer thickness growing along the surface, generally quite significantly, even with the use of the above transformed variables.

Analytical transformations have also proven useful for solving the compressible boundary-layer equations. The Levy-Lees and Mangler transformations extend the similarity variable approach to compressible 2-D and axisymmetric boundary layers and have been successfully utilized in finite-difference methods by Blottner (1975b) and Christoph and Pletcher (1983).

For external laminar boundary-layer calculations, the use of transformed coordinates of the similarity type is recommended. For turbulent flows the advantages of transformations suggested to date are less certain.

**Generalized coordinate approach.** Generalized nonorthogonal coordinates can be introduced into the boundary-layer equations if care is taken to be consistent with the boundary-layer approximation. In particular, the  $x$ -axis should align with the main flow direction; however, the axis need not be straight. A second condition is that the grid lines that intersect the  $x$  axis should be straight (negligible curvature) and should be orthogonal to the  $x$  axis. A grid system that meets these conditions will be referred to as the generalized boundary-layer grid and can be established by the intersection of lines of constant  $\xi$  and  $\eta$ , where  $\xi$  is  $\xi(x)$  and  $\eta$  is  $\eta(x, y)$ . Two examples of grids that meet the above conditions are illustrated in Fig. 7.3. The grid shown in Fig. 7.3(a) would be convenient for external flow applications, while the grid of Fig. 7.3(b) would be particularly well suited for solving a flow in a straight, symmetric, 2-D channel of varying cross-sectional area. Notice that this grid allows the spacing between lines of constant  $\eta$  to vary in the  $x$  direction, permitting grid points to be packed more closely in regions where the boundary layer is thin. Letting  $\eta = (y/x)\sqrt{\text{Re}_x}$  gives the well-known Blasius similarity variable as a special case of the generalized boundary-layer grid. The generalized boundary-layer grid can be implemented by introducing  $\xi$  and  $\eta$  into the governing equations as new independent variables using the chain rule to replace derivatives with respect to  $x$  and  $y$ :

$$\frac{\partial}{\partial x} = \xi_x \frac{\partial}{\partial \xi} + \eta_x \frac{\partial}{\partial \eta}$$

$$\frac{\partial}{\partial y} = \eta_y \frac{\partial}{\partial \eta}$$

The corresponding Jacobian is  $J = \xi_x \eta_y$ .

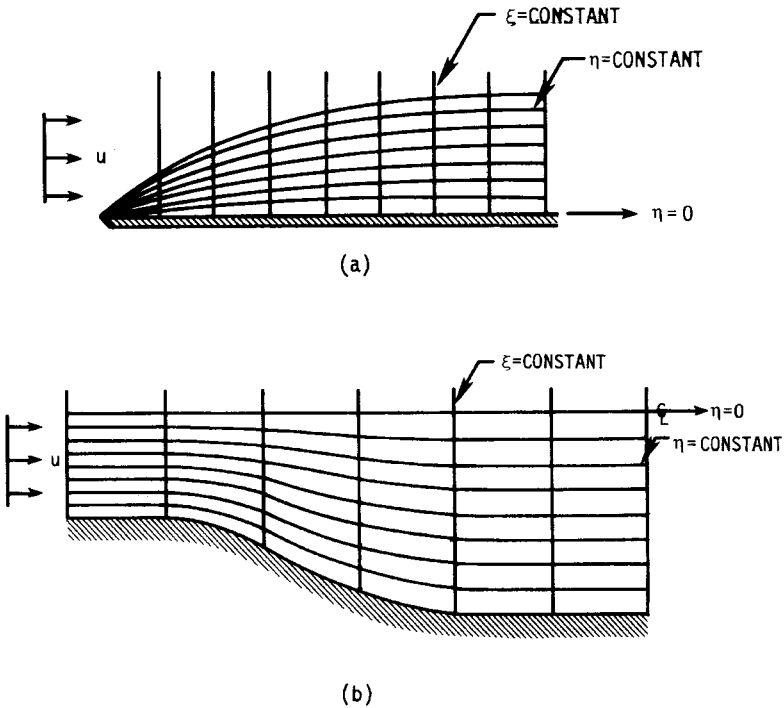


Figure 7.3 Examples of generalized boundary layer grids. (a) External flow. (b) Internal flow.

The metric terms in the equations are most conveniently represented as

$$\begin{aligned} \xi_x &= Jy_\eta = \frac{1}{x_\xi} \\ \eta_x &= -Jy_\xi \quad \eta_y = Jx_\xi = \frac{1}{y_\eta} \end{aligned} \quad (7.44)$$

After applying this independent variable transformation to the steady incompressible boundary-layer momentum and continuity equations in nondimensional form (as in Section 5.3.2), the following are obtained:

$$\begin{aligned} \frac{\partial}{\partial \xi}(x_\xi y_\eta u) + \frac{\partial}{\partial \eta}(x_\xi y_\eta V) &= 0 \\ \frac{u}{x_\xi} \frac{\partial u}{\partial \xi} + V \frac{\partial u}{\partial \eta} &= -\frac{1}{x_\xi} \frac{\partial p}{\partial \xi} + \frac{1}{y_\eta} \text{Re} \frac{\partial}{\partial \eta} \left( \frac{1}{y_\eta} \frac{\partial u}{\partial \eta} \right) \end{aligned} \quad (7.45)$$

The contravariant velocity component  $V = \eta_x u + \eta_y v$  has been introduced. The  $u$  velocity component is orthogonal to lines of constant  $\xi$  and thus also represents a contravariant velocity. Care must be taken in representing the metric quantities when discretizing the equations. When the fully implicit formulation of the finite-difference equations is used, the best results have been obtained (Ramin and Pletcher, 1993) by representing the diffusion term as

$$\frac{1}{y_\eta} \frac{\partial}{\partial \eta} \left( \frac{1}{y_\eta} \frac{\partial u}{\partial \eta} \right) \cong \frac{1}{[(y_\eta)_{i,j} + (y_\eta)_{i+1,j}]} \left[ \frac{1}{(y_\eta)_{i+1,j+1/2}} (u_{i+1,j+1} - u_{i+1,j}) - \frac{1}{(y_\eta)_{i+1,j-1/2}} (u_{i+1,j} - u_{i+1,j-1}) \right] \quad (7.46)$$

where  $(y_\eta)_{i,j}$  is to be interpreted as  $(y_{i,j+1} - y_{i,j-1})/2 \Delta \eta$ , and  $(y_\eta)_{i+1,j+1/2}$  as  $(y_{i+1,j+1} - y_{i+1,j})/\Delta \eta$ . A qualifying test for the correct representation of the metric quantities is that the scheme should reproduce the Blasius laminar boundary-layer solution exactly when the grid is specified according to  $\eta = (y/x)\sqrt{\text{Re}_x}$ .

An important advantage of using the analytical transformed coordinates discussed previously was that leading edge and stagnation point singularities could be removed. This permitted very accurate solutions to be obtained near these singular points, in contrast to what was possible when simple physical (generally Cartesian) coordinates were used. It is also possible to obtain very accurate starting solutions and to resolve regions near leading edges and stagnation points using the generalized boundary-layer grid. Since it is well known that similarity solutions are valid in such regions, it is only necessary to connect the first two marching stations by the use of a grid that is constructed from the similarity variables, such as  $\xi = x$  and  $\eta = (y/x)\sqrt{\text{Re}_x}$  for an incompressible 2-D flow. It is best to omit the points at  $x = 0$ , since the boundary layer is vanishingly thin at that location and only exists in the sense of a limit. It is sufficient to resolve the boundary layer at the first  $\Delta x$  beyond  $x = 0$ , since that is the first location where the boundary-layer thickness is finite. A characteristic of the similarity solution is that it is independent of the marching coordinate. Thus the finite-difference approximation to it can be obtained by iteratively marching from station 2 to 3. With each sweep, the solution most recently obtained at station 3 is used at station 2. The iterative sweeps from stations 2 to 3 continue until the two solutions agree. This indicates that a solution locally independent of the marching coordinate has been found.

### 7.3.8 Special Considerations for Turbulent Flows

The accurate solution of the boundary-layer equations for turbulent flow using models that evaluate the turbulent viscosity at all points within the flow requires that grid points be located within the viscous sublayer,  $y^+ \leq 4.0$  for in-

compressible flow, and perhaps  $y^+ \leq 1.0$  or  $2.0$  for flows in which a solution to the energy equation is also being obtained. The use of equal grid spacing for the transverse coordinate would require several thousand grid points across the boundary layer for a typical calculation at moderate Reynolds numbers. This at least provides motivation for considering ways to reduce the number of grid points required to span the boundary layer. The techniques that have been used successfully fall into three categories: use of wall functions, unequal grid spacing, and coordinate transformations.

**Use of wall functions.** For many turbulent wall boundary layers the inner portion of the flow appears to have a “universal” character captured by the logarithmic “law-of-the-wall” discussed previously (see Fig. 5.7). Basically, this inner region is a zone in which convective transport is relatively unimportant. The law-of-the-wall can be roughly thought of as a solution to the boundary-layer momentum equation using Prandtl’s mixing-length turbulence model when convective and pressure gradient terms are unimportant. Corresponding nearly universal behavior has been observed for the temperature distribution for many turbulent flows, and wall functions can be used to provide an inner boundary condition for solutions to the energy equation. Thus, with the wall function approach, the boundary-layer equations are solved using a turbulence model in the outer region on a relatively coarse grid, and the near-wall region is “patched in” through the use of a form of the law-of-the-wall, which in fact, represents an approximate solution for the near-wall region. In this approach, the law-of-the-wall is usually assumed to be valid in the range  $30 < y^+ < 200$ , and the first computational point away from the wall is located in this interval. Boundary conditions are developed for the dependent variables in the transport equations being solved ( $u$ ,  $T$ ,  $\bar{k}$ ,  $\epsilon$ , etc.) at this point from the wall functions. Many variations in this procedure are possible, and details depend upon the turbulence model and difference scheme being used. The procedure has been well developed for use with the  $\bar{k}$ - $\epsilon$  turbulence model, and recommended wall functions for  $u$ ,  $T$ ,  $\bar{k}$ , and  $\epsilon$  can be found in the work by Launder and Spalding (1974).

Like turbulence models themselves, wall functions need modifications to accurately treat effects such as wall blowing and suction and surface roughness. Their use does, however, circumvent the need for many closely spaced points near the wall.

**Use of unequal grid spacing.** Almost without exception, turbulent boundary-layer calculations that have applied the difference scheme right down to the wall have utilized either a variable grid scheme or what is often equivalent, a coordinate transformation. Arbitrary spacing will work. Pletcher (1969) used  $\Delta y$  corresponding to  $\Delta y^+$  [defined as  $\Delta y(\tau_w/\rho)^{1/2}/\nu_w] \cong 1.0$  for several mesh increments nearest the wall and then approximately doubled every few points until  $\Delta y^+$  reached 100 in the outer part of the flow.

Another commonly used (Cebeci and Smith, 1974) and very workable scheme maintains a constant ratio between two adjacent increments:

$$\frac{\Delta y_+}{\Delta y_-} = \frac{\Delta y_{j+1}}{\Delta y_j} = K \quad (7.47)$$

In this constant ratio scheme, each grid spacing is increased by a fixed percentage from the wall outward. This results in a geometric progression in the size of the spacing.  $K$  is usually a number between 1.0 and 2.0 for turbulent flows. For the constant ratio scheme it follows that

$$\Delta y_j = K^{j-1} \Delta y_1 \quad y_j = \Delta y_1 \frac{K^{j-1} - 1}{K - 1} \quad (7.48)$$

The accuracy (and occasionally the stability) of some schemes appears sensitive to the value of  $K$  being used. Most methods appear to give satisfactory results for  $K \leq 1.15$ . For a typical calculation using  $\Delta y_1^+ \cong 1.5$ ,  $K = 1.04$ , and  $y_e^+ \cong 3000$ , Eqs. (7.47) and (7.48) can be used to determine that about 113 grid points in the transverse direction would be required.

As a difference scheme is being generalized to accommodate variable grid spacing, the truncation error should be reevaluated, since a deterioration in the formal T.E. is common in these circumstances. For example, the treatment previously recommended for the transverse shear stress derivative is

$$\begin{aligned} \frac{\partial}{\partial y} \left( \mu \frac{\partial u}{\partial y} \right)_j^n &= \frac{2}{\Delta y_+ + \Delta y_-} \left( \mu_{j+1/2}^n \frac{u_{j+1}^n - u_j^n}{\Delta y_+} - \mu_{j-1/2}^n \frac{u_j^n - u_{j-1}^n}{\Delta y_-} \right) \\ &\quad + O(\Delta y_+ - \Delta y_-) + O[(\Delta y_+ + \Delta y_-)^2] \end{aligned}$$

which at first appears to be first order accurate unless there is a way to show that  $O(\Delta y_+ - \Delta y_-) = O[(\Delta y)^2]$  for a particular scheme. Blottner (1974) has shown that the treatment of derivatives indicated above in his Crank-Nicolson scheme using the constant ratio arrangement for mesh spacing is locally second order accurate. To prove this, Blottner interpreted the constant ratio scheme in terms of a coordinate transformation (see below) and verified his findings by calculations that indicated that his scheme behaved as though the T.E.s were second order as the mesh was refined.

**Use of coordinate transformations.** The general topic of coordinate transformations was treated in Chapter 5. Here we are considering the use of a coordinate transformation for the purpose of providing unequal grid spacing in the physical plane. Transformation 1 of Section 5.6 provides a good example of this concept (see also Fig. 5.8). Such a transformation permits the use of standard equal-increment differencing of the governing equations in terms of the transformed coordinates. Thus the clustering of points near the wall can be achieved without deterioration in the *order* of the T.E. On the other hand, the equations generally become more complex in terms of the transformed variables, and new

variable coefficients always appear. The actual *magnitude* of the T.E. will be influenced by the new coefficients.

Transformations 1 and 2 in Section 5.6 of Chapter 5 are representative of those that can be readily used with the boundary-layer equations.

### 7.3.9 Example Applications

For laminar flows in which the boundary-layer approximation is valid, finite-difference predictions can easily be made to agree with results of more exact theories to several significant figures. Even with only modest attention to mesh size, agreement to within  $\pm 1-2\%$  of some "exact" standard is relatively common. Figure 7.4 compares the velocity profile computed by a DuFort-Frankel type difference scheme (Pletcher, 1971) with the analytical results of van Driest (1952) for laminar flow at a Mach number of 4 and  $T_w/T_e = 4$ . The temperature profiles are compared for the same flow conditions in Fig. 7.5. The agreement is excellent and typical of what can be expected for laminar boundary-layer flows.

The prediction of turbulent boundary-layer flows is another matter. The issue of turbulence modeling adds complexity and uncertainty to the prediction. Turbulence models can be adjusted to give good predictions for a limited class of flows, but when applied to other flows containing conditions not accounted for by the model, poor agreement is often noted. Because of the usual level of uncertainty in both the experimental measurements and turbulence models, agreement to within  $\pm 3-4\%$  is generally considered good for turbulent flows.

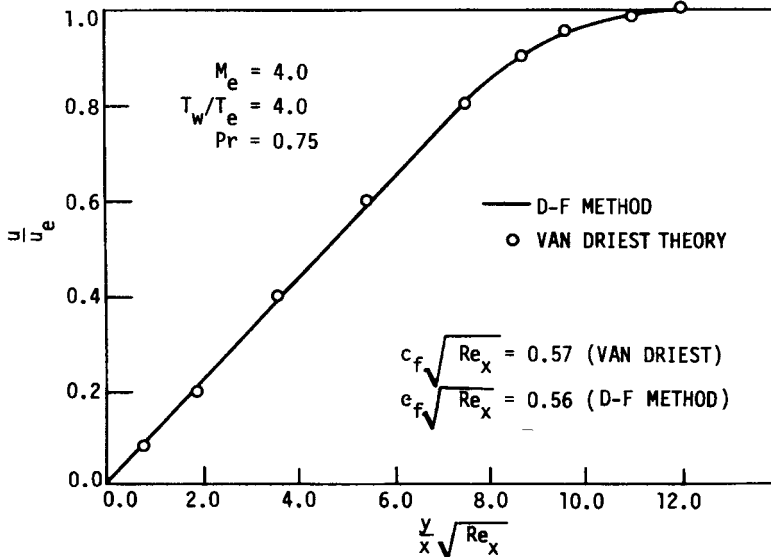


Figure 7.4 Velocity profile comparisons for a laminar compressible boundary layer. Solid line represents predictions from the DuFort-Frankel finite-difference scheme (Pletcher, 1971).

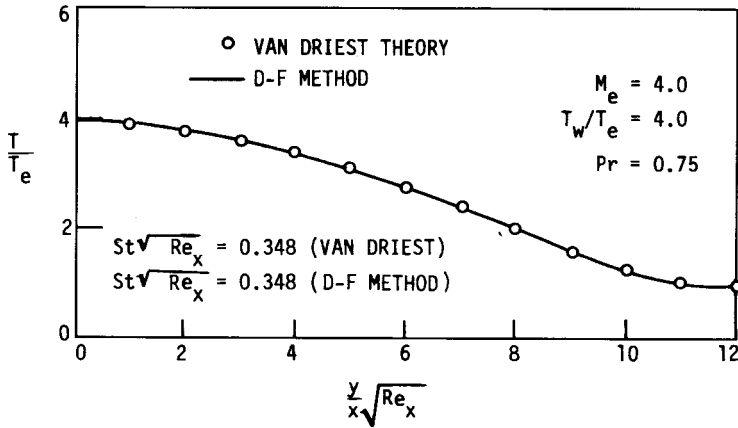


Figure 7.5 Temperature profile comparisons for a laminar compressible boundary layer. Solid line represents predictions from the DuFort-Frankel finite-difference scheme (Pletcher, 1971).

Even a simple algebraic turbulence model can give good predictions over a wide range of Mach numbers for turbulent boundary-layer flows in zero or mild pressure gradients. Figure 7.6 compares the prediction of a DuFort-Frankel finite-difference method with the measurements of Coles (1953) for a turbulent boundary layer on an adiabatic plate at a free stream Mach number of 4.554. The agreement is excellent.

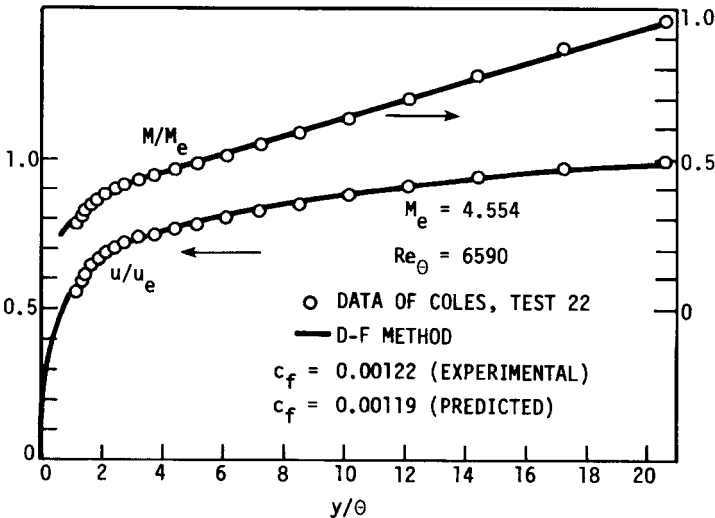


Figure 7.6 Comparison for a compressible flat plate flow measured by Coles (1953). Solid line represents predictions from the DuFort-Frankel finite-difference scheme (Pletcher, 1970).

Finite-difference methods easily accommodate step changes in boundary conditions, permitting solutions to be obtained for conditions under which simple correlations are especially unreliable. Figure 7.7 compares predictions of an algebraic mixing-length turbulence model used with a DuFort-Frankel type finite-difference procedure with the measurements of Moretti and Kays (1965) for low-speed flow over a cooled flat plate with a step change in wall temperature and a favorable pressure gradient. The Stanton number ( $St$ ) in Fig. 7.7 is defined as  $k(\partial T/\partial y)_w/[\rho_e u_e (H_{aw} - H_w)]$ , where  $H_{aw}$  is the total enthalpy of the wall under adiabatic conditions.

Examples of cases where predictions of the simplest algebraic turbulence models fail to agree with experimental data abound in the technical literature. Several effects, which are not well predicted by the simplest models, were cited in Chapter 5. One of these was flow at low  $Re$ , especially at supersonic Mach numbers. This low  $Re$  effect is demonstrated in Fig. 7.8, where it can be seen that the point at which the simplest algebraic model (Model A) begins to fail

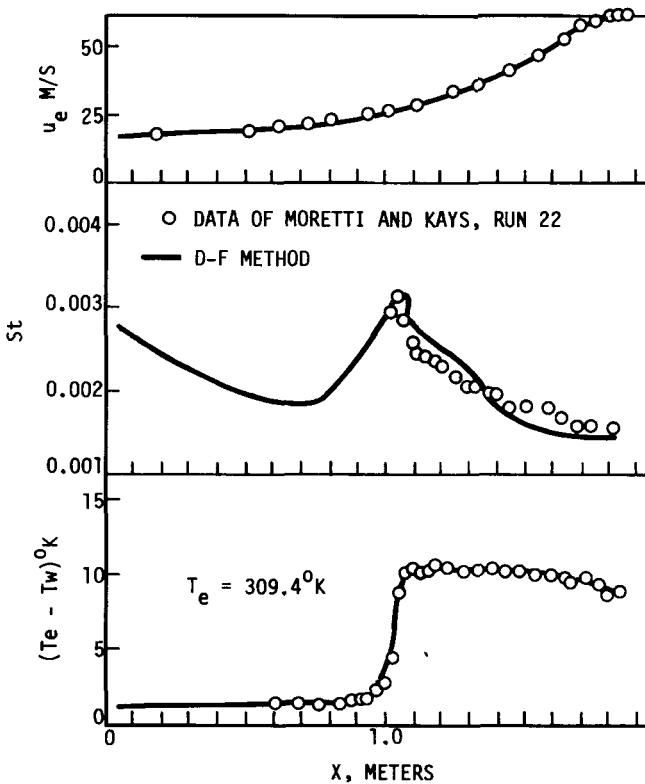
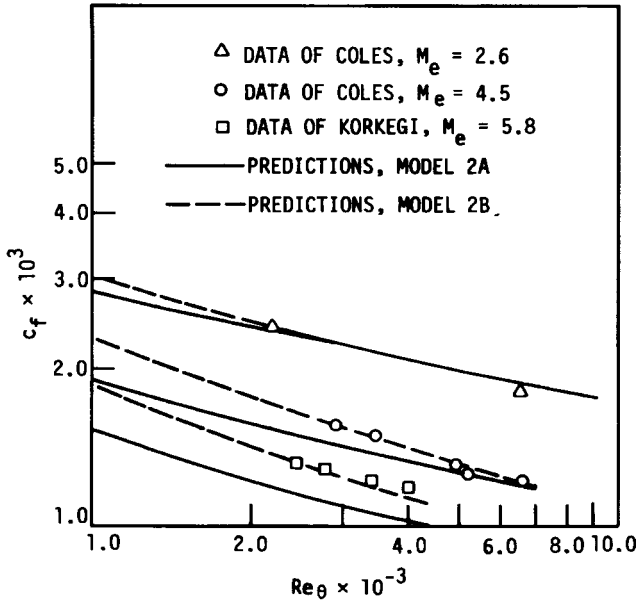


Figure 7.7 Comparison for a cooled flat plate with flow acceleration measured by Moretti and Kays (1965). Solid lines represent predictions from the DuFort-Frankel finite-difference scheme (Pletcher, 1970).



**Figure 7.8** Comparison of predicted skin-friction coefficients with the measurements of Coles (1953) and Korkegi (1956) for the compressible turbulent boundary layer on a flat plate at low Reynolds number.

shifts to higher and higher  $Re$  as the Mach number of the flow increases. Predictions of a model containing the simple modification discussed in Section 5.4.3 for low  $Re$  are included in Fig. 7.8 as Model B.

### 7.3.10 Closure

This section has discussed several topics that are important in the finite-difference solution of the boundary-layer equations for two-dimensional and axisymmetric flows. Several difference schemes have been described. In computational work, as in many endeavors, “hands on” participation or “practice” is important. Accordingly, several example problems should be solved using the schemes discussed in order to develop an appreciation of the concepts and issues involved. Just as an engineer could hardly be considered an experimentalist without running an experiment, one likewise should not be considered a computational fluid dynamicist until some computations have been completed.

Which finite-difference scheme is best for the boundary-layer equations? The question is a logical one to raise at this point, but we need to establish measures by which “best” can be identified. All consistent difference schemes should provide numerical results as accurate as needed with sufficient grid

refinement. With ultimate accuracy no longer an issue, the remaining concerns are computational costs and, to a lesser extent, ease of programming. In the present discussion it is assumed that the user insists on understanding all algebraic operations. We will include the time and effort needed to *understand* a given algorithm as part of the programming effort category. Programming effort then will measure, not the number of statements in a computer program, but the implied algebraic complexity of the steps in the algorithm and the difficulty of following the various steps for the beginner.

A review of the technical literature suggests that the schemes listed in Table 7.1 have been satisfactorily employed in the solution of the 2-D or axisymmetric boundary-layer equations for both laminar and turbulent flow and are recommended on the basis of their well-established performance.

The computation time for a typical calculation for all of the above schemes is expected to be modest (only a few seconds) on present-day computers. More details can be found in the literature cited above within the discussion of those methods. Only a few studies have been reported in which the computer times for several schemes have been compared for the boundary-layer equations. The work of Blottner (1975a) suggests that the Crank-Nicolson scheme with coupling requires about the same time as the modified box scheme for comparable accuracy. Again, for comparable accuracy, Blottner (1975a) found that the box scheme requires 2 to 3 times more computer time than the modified box scheme.

For the beginner wishing to establish a general purpose boundary-layer computer program, a reasonable way to start would be with the fully implicit scheme. The scheme is only first-order accurate in the marching direction, but second-order accuracy does not appear to be crucial for most boundary-layer calculations. This may be due partly to the fact that the  $O(\Delta x)$  term in the T.E. usually includes the second streamwise derivative, which is relatively small when the boundary-layer approximation is valid. If second-order accuracy becomes desirable in the streamwise coordinate, it can be achieved with only minor changes through the use of a three-point, second-order representation of the streamwise derivative or by switching to the Crank-Nicolson representation. In increasing order of programming complexity, the logical choices for linearizing the coefficients are lagging, extrapolation, and Newton linearization with

**Table 7.1 Recommended finite-difference schemes for the boundary-layer equations listed in estimated order of increasing programming effort**

1	DuFort-Frankel
2	Fully implicit
3	Crank-Nicolson implicit
4	Fully implicit with continuity equation coupling
5	Crank-Nicolson implicit with continuity equation coupling
6	Modified box scheme
7	Box scheme

coupling. If lagging is adopted as standard, it would be advisable to program one of the latter two more accurate (for the same mesh increment) procedures as an option to provide periodic checks.

## 7.4 INVERSE METHODS, SEPARATED FLOWS, AND VISCOUS-INVISCID INTERACTION

### 7.4.1 Introduction

Thus far we have only considered the conventional or “direct” boundary-layer solution methods for the standard equations and boundary conditions given in Section 5.3. An “inverse” calculation method for the boundary-layer equations is a scheme whereby a solution is obtained that satisfies boundary conditions that differ from the standard ones. The usual procedure in an inverse method is to replace the outer boundary condition,

$$\lim_{y \rightarrow \infty} u(x, y) = u_e(x)$$

by the specification of a displacement thickness or wall shear stress that must be satisfied by the solution. The pressure gradient [or  $u_e(x)$ ] is determined as part of the solution. It should be noted clearly that it is the *boundary conditions* that differ between the conventional direct methods and the inverse methods. It is perhaps more correct to think of the problem specification as being direct or inverse rather than the method. However, we will yield to convention and refer to the solution method as being direct or inverse.

The inverse methods are not merely an alternative way to solve the boundary-layer equations. The successful development of inverse calculation methods has permitted an expansion of the range of usefulness for the boundary-layer approximation.

Clearly, some design applications can be envisioned where it is desirable to calculate the boundary-layer pressure distribution that will accompany a specified distribution of displacement thickness or wall shear stress. This has provided some of the motivation for the development of inverse methods for the boundary-layer equations. Perhaps the most interesting applications of inverse methods have been in connection with separated flow. The computation of separated flows has long been thought to require the solution of the full Navier-Stokes equations. Thus, any suggestion that these flows, which are very important in applications, can be adequately treated with a much simpler mathematical model has been received with great interest. For this reason, the present discussion of inverse methods will emphasize applications to flows containing separated regions. The ability to remove the separation point singularity (Goldstein, 1948) is one of the most unique characteristics of the inverse methods.

### 7.4.2 Comments on Computing Separated Flows Using the Boundary-Layer Equations

Originally, it was thought that the usefulness of the boundary-layer approximation ended as the flow separation point was approached. This was because of the well-known singularity (Goldstein, 1948) of the standard boundary-layer formulation at separation and because the entire boundary-layer approximation is subject to question as the layer thickens and the normal component of velocity becomes somewhat larger (relative to  $u$ ) than in the usual high Reynolds number flow. It is now known that the inverse formulation is regular at separation (Klineberg and Steger, 1974) and the evidence suggests (Williams, 1977; Kwon and Pletcher, 1979) that the boundary-layer equations provide a useful approximation for flows containing small, confined (bubble) separated regions. In support of the validity of the boundary-layer approximation, it is noted that the formation of a separation bubble normally does not cause the thickness of the viscous region to increase by an order of magnitude; that is, the boundary-layer measure of thinness,  $\delta/L \ll 1$ , is still met. The “triple-deck theory” of Lighthill (1953) and Stewartson (1974) (see Section 7.4.4) also provides analytical support for the validity of the boundary-layer approximation for large Reynolds number flows containing small separated regions. On the other hand, large local values of  $d\delta/dx$  may occur and are expected to induce rather large values of  $v/u$ . At best, it should be conceded that the boundary-layer model is a weaker approximation for flow containing recirculation, even though it may provide estimates of flow parameters accurate enough for many purposes. The full range of applicability of the boundary-layer equations for separated flows is still under study.

Flow separation presents two obstacles to a straightforward space-marching solution procedure using conventional boundary conditions with the boundary-layer equations; these are (1) the singularity at separation and (2) the flow reversal, which prohibits marching the solution in the direction of the external flow (see Fig. 7.9) unless the convection terms in the equations are altered. When the pressure gradient is fixed near separation by the conventional boundary conditions, the normal component of the velocity and  $d\tau_w/dx$  tend

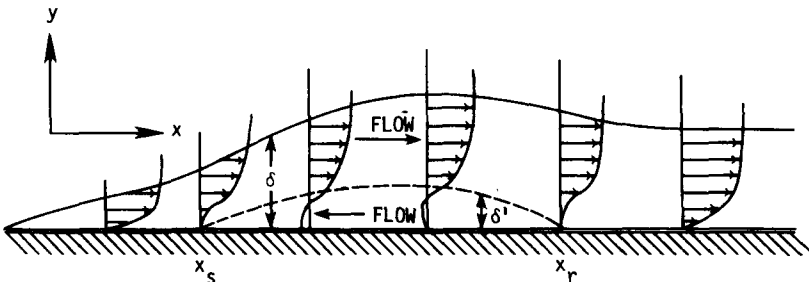
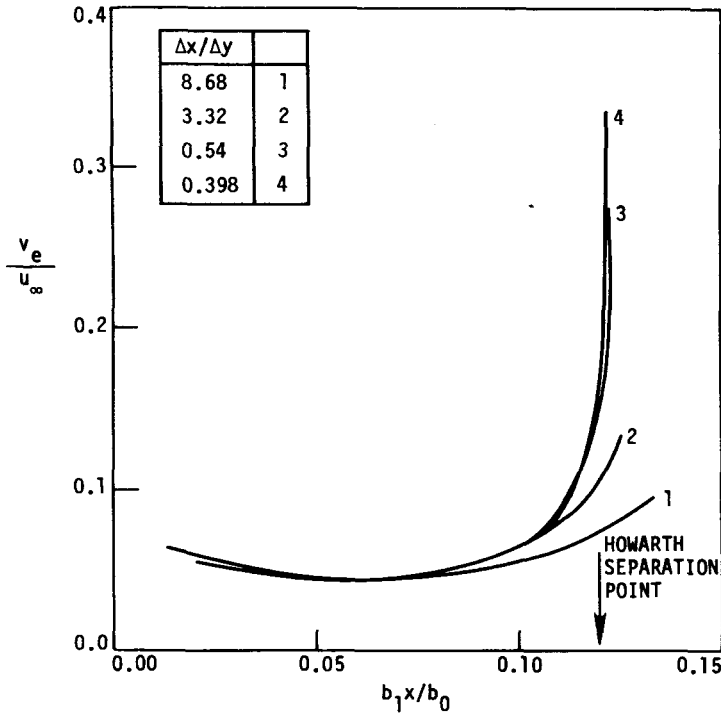


Figure 7.9 Flow containing a separation bubble.



**Figure 7.10** Effect of  $x$ -grid refinement on  $v_e$  for a direct finite-difference boundary-layer calculation (Pletcher and Dancey, 1976) near the separation point for a linearly retarded stream:  $u_e = b_0 - b_1x$ ,  $b_0 = 30.48 \text{ m/s}$ ,  $b_1 = 300 \text{ s}^{-1}$ ,  $\nu = 1.49 \times 10^{-4} \text{ m}^2/\text{s}$ .

toward infinity at the point of separation. A detailed discussion of this singularity can be found in the works of Goldstein (1948) and Brown and Stewartson (1969). This phenomenon appears in finite-difference solutions, where  $u_e(x)$  is prescribed, as the tendency for  $v$  to increase without limit as the streamwise step size is reduced. This is illustrated in Fig. 7.10 for the Howarth linearly retarded flow (Howarth, 1938). Naturally, a finite  $v$  will be obtained for a finite step size, but the solution will not be unique. This singular behavior, which is mathematical rather than physical, can be overcome by the use of an auxiliary pressure interaction relationship with direct methods (Reyhner and Flügge-Lotz, 1968; Napolitano et al., 1978) or by the use of inverse procedures. In this section we will concentrate on the inverse procedures that require no auxiliary relationships to eliminate the singular behavior.

The difficulty with the convective terms can be viewed as follows. We recall that the steady boundary-layer equations are parabolic. For  $u > 0$  the solution can be marched in the positive  $x$  direction. Physically, information is carried downstream from the initial plane by the flow. In regions of reversed flow, however, the “downstream” direction is in the negative  $x$  direction (Fig. 7.9).

Mathematically, we observe that when  $u < 0$ , the boundary-layer momentum equation remains parabolic, but the correct marching direction is in the negative  $x$  direction.

It would seem, then, that a solution procedure might be devised to overcome the problem associated with the "correct" marching direction by making initial guesses or approximations for the velocities in the reversed flow portion of a flow with a separation bubble, storing these velocities, and correcting them by successive iterative calculation sweeps over the entire flow field. To do this requires using a difference representation that honors the appropriate marching direction, forward or backward, depending on the direction of flow. To follow this iterative procedure means abandoning the once-through simplicity of the usual boundary-layer approach. Computer storage must also be provided for velocities in and near the region of reversed flow. Such multiple-pass procedures have been employed by Klineberg and Steger (1974), Carter and Wornom (1975), and Cebeci (1976). Some crucial aspects of differencing for multiple-pass procedures will become apparent from the material presented in Chapter 8.

Reyhner and Flügge-Lotz (1968) suggested a simpler alternative to the multiple-pass procedure. Noting that the reversed flow velocities are generally quite small for confined regions of recirculation, they suggested that the convective term  $u \partial u / \partial x$  in the boundary-layer momentum equation be represented in the reversed flow regions by  $C|u| \partial u / \partial x$ , where  $C$  is zero or a small positive constant. This representation has become known as the FLARE approximation and permits the boundary-layer solution to proceed through separated regions by a simple forward-marching procedure. It should be clear that the FLARE procedure introduces an additional approximation (or assumption) into the boundary-layer formation, namely, that the  $u \partial u / \partial x$  term is small relative to other terms in the momentum equation in the region of reversed flow. On the other hand, the FLARE approximation appears to give smooth and plausible solutions for many flows with separation bubbles. Example solutions are presented in Section 7.4.3. Experimental and computational evidence accumulated to date indicates that for naturally occurring separation bubbles, the  $u$  component of velocity in reversed flow regions is indeed fairly small in magnitude, usually less than about 10% of the maximum velocity found in the viscous region.

It should be noted that, although ways of satisfactorily treating the  $u \partial u / \partial x$  convective term have been presented, it still does not appear possible to obtain a unique convergent solution of the steady boundary-layer equations alone by a direct marching procedure. Direct calculation procedures reported to date have always employed an interaction relation whereby the pressure gradient specified becomes dependent upon the displacement thickness (or related parameter) of the viscous regions, usually in a time-dependent manner (Napolitano et al., 1978). This is not necessarily a disadvantage. Viscous-inviscid interaction usually needs to be considered ultimately in obtaining the solution for the complete flow field containing a separated region, if the boundary-layer equations are used for the viscous regions. Viscous-inviscid interaction is treated further in

Section 7.4.4. On the other hand, we should note that a unique convergent solution can be obtained for the steady boundary-layer equations alone using inverse methods.

### 7.4.3 Inverse Finite-Difference Methods

Two procedures will be illustrated. The first is conceptually the simplest and is especially useful for illustrating the concept of the inverse method. It appears to work very well when the flow is attached (no reversed flow region), but gives rise to small controlled oscillations in the skin friction when reversed flow is present. This oscillatory behavior is overcome by the second method, which solves the boundary-layer equations in a coupled manner. The FLARE approximation will be employed in both of these methods. For simplicity, the methods will be illustrated for incompressible flows.

**Inverse Method A.** The boundary-layer equations are written as follows.

continuity:

$$\frac{\partial u}{\partial x} + \frac{\partial v}{\partial y} = 0 \quad (7.49)$$

momentum:

$$C|u|\frac{\partial u}{\partial x} + v\frac{\partial u}{\partial y} = u_e\frac{du_e}{dx} + \frac{1}{\rho}\frac{\partial \tau}{\partial y} \quad (7.50)$$

In the above,  $C = 1.0$  when  $u > 0$ , and  $C$  is a small ( $\leq 0.2$ ) positive constant when  $u \leq 0$  and

$$\tau = \mu\frac{\partial u}{\partial y} - \overline{\rho u'v'} = (\mu + \mu_T)\frac{\partial u}{\partial y} \quad (7.51)$$

The above equations are in a form applicable to either laminar or turbulent flow. For laminar flow the primed velocities and  $\mu_T$  are zero, and for turbulent flow the unprimed velocities are time-mean quantities.

The boundary conditions for the inverse procedure are

$$u(x, 0) = v(x, 0) = 0 \quad (7.52)$$

and

$$\int_0^\infty \left(1 - \frac{u}{u_e}\right) dy = \delta^*(x) \quad (7.53)$$

where  $\delta^*$  is a prescribed function. Alternatively,  $\tau_w(x)$  can be specified as a boundary condition. Clearly Eqs. (7.49) and (7.50) can be solved by a direct method utilizing the conventional boundary condition

$$\lim_{y \rightarrow \infty} u(x, y) = u_e(x) \quad (7.54)$$

in place of Eq. (7.53) for attached portions of the flow. It is possible to start a

boundary-layer calculation in the direct mode and switch to the inverse procedure when desired.

The boundary-layer equations are cast into a fully implicit difference form, and the coefficients are lagged. Such a difference representation is discussed in Section 7.3 and will not be repeated here. The inverse treatment of boundary conditions is implemented by varying  $u_e$  in successive iterations at each streamwise calculation station until the solution satisfies the specified value of  $\delta^*(x)$ . In each of these iterations the numerical formulation and implementation of boundary conditions are the same as for a direct method. The displacement thickness is evaluated from the computed velocity distribution by numerical integration (use of either Simpson's rule or the trapezoidal rule is suggested). The appropriate value of  $u_e$  needed to satisfy the boundary condition on  $\delta^*$  ( $\delta_{BC}^*$ ) is determined by considering  $\delta^* - \delta_{BC}^*$  to be a function of  $u_e$  at each streamwise station,  $\delta^* - \delta_{BC}^* = F(u_e)$ , and seeking the value of  $u_e$  required to establish  $F = 0$  by a variable secant (Fröberg, 1969) procedure. In the above,  $\delta^*$  is the  $\delta^*$  actually obtained from the solution for a specified value of  $u_e$ . Two initial guesses are required for this procedure, which usually converges in three or four iterations (Pletcher, 1978).

The variable secant procedure can be thought of as a generalization of Newton's method (also known as the Newton-Raphson method) for finding the root of  $F(x) = 0$ . In Newton's method we expand  $F(x)$  in a Taylor series about a reference point  $x_n$ :

$$F(x_n + \Delta x) = F(x_n) + F'(x_n) \Delta x + \dots$$

We truncate the series after the first derivative term and compute the value of  $\Delta x$  required to establish  $F(x_n + \Delta x) = 0$ . For Newton's method this gives

$$x_{n+1} - x_n = \Delta x = -\frac{F(x_n)}{F'(x_n)} \quad (7.55)$$

Thus, starting with an initial guess,  $x_n$ , an improved approximation,  $x_{n+1}$ , can be computed from Eq. (7.55). The process is repeated iteratively until  $|(x_{n+1} - x_n)| < \epsilon$ .

Newton's method is a simple and effective procedure. Its use does, however, require that  $F'(x)$  be evaluated analytically. When this is not possible, the variable secant generalization of the Newton procedure represents a reasonable alternative.

In the variable secant procedure, the derivative is replaced by a secant line approximation through two points:

$$F'(x_n) \cong \frac{F(x_n) - F(x_{n-1})}{x_n - x_{n-1}}$$

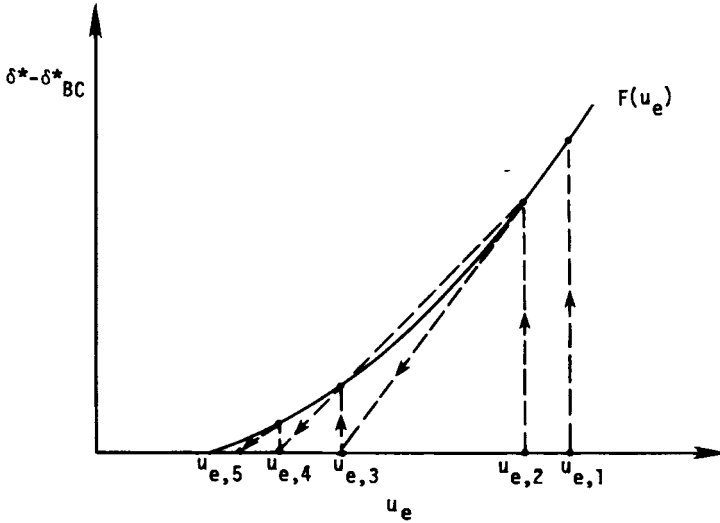


Figure 7.11 Determination of  $u_e(x)$  through the use of the variable secant procedure.

After two initial guesses for  $x$ , the third approximation to the root is obtained from

$$x_{n+1} = x_n - \frac{F(x_n)}{F(x_n) - F(x_{n-1})} (x_n - x_{n-1}) \tag{7.56}$$

In the application of the variable secant method to the inverse boundary-layer calculation,  $x_n$  becomes  $(u_e)_n$  and  $F = \delta^* - \delta_{BC}^*$ . The iterative process is illustrated in Fig. 7.11.

When the iterative search for the  $u_e(x)$  that provides the specified  $\delta^*(x)$  is completed, the solution may be advanced to another streamwise station in the usual manner for parabolic equations. The simplicity of inverse method A is obvious. Apart from small changes to implement the FLARE representation, the difference equations are solved the same as for the standard direct method for boundary layers. The method performs reasonably well (Pletcher, 1978; Kwon and Pletcher, 1979) but does predict small oscillations in the wall shear stress when separation is present. These oscillations can be eliminated by suitable coupling of the momentum and continuity equations and are not present in solutions obtained by the method described below.

**Inverse Method B.** Here we will describe the method developed by Kwon and Pletcher (1981). More recently, Truman et al. (1993) have described a similar

strategy in a more general context. The overall strategy of this method is to couple all unknowns and the boundary conditions in one simultaneous system of algebraic equations to be solved at each streamwise station. To accomplish this, it is convenient to introduce the stream function  $\psi$ . Accordingly,

$$u = \frac{\partial \psi}{\partial y}$$

$$v = -\frac{\partial \psi}{\partial x}$$

The conservation equations for mass and momentum are written as

$$u = \frac{\partial \psi}{\partial y} \quad (7.57)$$

$$Cu \frac{\partial u}{\partial x} - \frac{\partial \psi}{\partial x} \frac{\partial u}{\partial y} = u_e \frac{du_e}{dx} + \frac{1}{\rho} \frac{\partial \tau}{\partial y} \quad (7.58)$$

where

$$\tau = \bar{\mu} \frac{\partial u}{\partial y}$$

$$\bar{\mu} = \mu + \mu_T$$

The boundary conditions are

$$u(x, 0) = \psi(x, 0) = 0 \quad (7.59)$$

$$\psi_e = u_e [y_e - \delta^*(x)] \quad (7.60)$$

where  $\delta^*(x)$  is a prescribed function. The boundary condition for  $\psi_e$  follows from the definition of  $\delta^*$ :

$$\delta^* = \int_0^\infty \left( 1 - \frac{u}{u_e} \right) dy$$

The upper limit of this integral can be replaced by  $y$  at the outer edge of the boundary layer,  $y_e$ , since the integrand is equal to zero for  $y > y_e$ . Multiplying by  $u_e$  gives

$$u_e \delta^* = \tilde{u}_e y_e - \int_0^{y_e} u dy$$

Expressing  $u$  in terms of the stream function permits the integral to be evaluated as  $\psi_e$ . Rearranging gives Eq. (7.60). When the difference equations that follow are solved in a direct mode, the outer boundary condition becomes the conventional one given by Eq. (7.54) instead of that specified by Eq. (7.60).

Equations (7.57) and (7.58) are first represented in finite-difference form as

$$\frac{u_j^{n+1} + u_{j-1}^{n+1}}{2} = \frac{\psi_j^{n+1} - \psi_{j-1}^{n+1}}{\Delta y_-} \tag{7.61}$$

$$\begin{aligned} C u_j^{n+1} \frac{u_j^{n+1} - u_j^n}{\Delta x} - \frac{\psi_j^{n+1} - \psi_j^n}{\Delta x} \frac{u_{j+1}^{n+1} - u_{j-1}^{n+1}}{\Delta y_+ + \Delta y_-} \\ = \chi^{n+1} + \frac{2}{\rho(\Delta y_+ + \Delta y_-)} \\ \times \left( \bar{\mu}_{j+1/2} \frac{u_{j+1}^{n+1} - u_j^{n+1}}{\Delta y_+} - \bar{\mu}_{j-1/2} \frac{u_j^{n+1} - u_{j-1}^{n+1}}{\Delta y_-} \right) \end{aligned} \tag{7.62}$$

In the above,

$$C = 1 \quad \text{when} \quad u_j^{n+1} > 0$$

$$C = 0 \quad \text{when} \quad u_j^{n+1} < 0$$

$$\chi = -\frac{1}{\rho} \frac{dp}{dx}$$

Newton linearization is next applied to the above nonlinear convective terms following the procedures presented in Section 7.3.3. We let  $u_j^{n+1} = \hat{u}_j^{n+1} + \Delta u_j$  and  $\psi_j^{n+1} = \hat{\psi}_j^{n+1} + \Delta \psi_j$ , where the circumflexes indicate provisional values of the variables in an iterative process. The quantities  $\Delta u_j$  and  $\Delta \psi_j$  are the changes in the variables between two iterative sweeps, i.e.,  $\Delta \phi_j = \phi_j^{n+1} - \hat{\phi}_j^{n+1}$  for a general variable  $\phi$ . The resulting difference equations can be written in the form

$$\psi_{j-1}^{n+1} - \psi_j^{n+1} + b_j(u_{j-1}^{n+1} + u_j^{n+1}) = 0 \tag{7.63}$$

$$B_j u_{j-1}^{n+1} + D_j u_j^{n+1} + A_j u_{j+1}^{n+1} + E_j \psi_j^{n+1} = H_j \chi^{n+1} + C_j \tag{7.64}$$

where

$$A_j = -\frac{\hat{\psi}_j^{n+1} - \psi_j^n}{\Delta x(\Delta y_+ + \Delta y_-)} - \frac{2\bar{\mu}_{j+1/2}}{\rho \Delta y_+(\Delta y_+ + \Delta y_-)}$$

$$B_j = \frac{\hat{\psi}_j^{n+1} - \psi_j^n}{\Delta x(\Delta y_+ + \Delta y_-)} - \frac{2\bar{\mu}_{j-1/2}}{\rho \Delta y_-(\Delta y_+ + \Delta y_-)}$$

$$C_j = \frac{C(\hat{u}_j^{n+1})^2}{\Delta x} - \frac{\hat{\psi}_j^{n+1}(\hat{u}_{j+1}^{n+1} - \hat{u}_{j-1}^{n+1})}{\Delta x(\Delta y_+ + \Delta y_-)}$$

$$D_j = \frac{C(2\hat{u}_j^{n+1} - u_j^n)}{\Delta x} + \frac{2}{\rho(\Delta y_+ + \Delta y_-)} \left( \frac{\bar{\mu}_{j+1/2}}{\Delta y_+} + \frac{\bar{\mu}_{j-1/2}}{\Delta y_-} \right)$$

$$E_j = -\frac{\hat{u}_{j+1}^{n+1} - \hat{u}_{j-1}^{n+1}}{\Delta x(\Delta y_+ + \Delta y_-)}$$

$$H_j = 1$$

$$b_j = \frac{\Delta y_-}{2}$$

The above algebraic formulation is similar to that presented in Section 7.3 in connection with the Davis coupled scheme and solved by the modified Thomas algorithm. Equations (7.63) and (7.64) form a block-tridiagonal system with  $2 \times 2$  blocks and require the simultaneous solution of  $2(NJ) - 2$  equations for  $2(NJ) - 2$  unknowns at each streamwise marching step. The parameter  $NJ$  is the number of grid points across the flow, including boundary points. One difference between this formulation and the algebraic equations arising from the Davis coupled scheme is the appearance of the new term,  $H_j \chi^{n+1}$ , on the right-hand side of Eq. (7.64). The pressure gradient parameter  $\chi^{n+1}$  is one of the unknowns in the inverse formulation. The outer boundary conditions are also different. These facts preclude the use of the modified tridiagonal algorithm presented in Section 7.3. However, the blocks below the main diagonal can be eliminated, and a recursion formula can be developed (Kwon and Pletcher, 1981) for the back substitution. Before the back substitution is carried out, however, the parameter  $\chi^{n+1}$  must be determined by a special procedure to be indicated subsequently.

The unknowns can be computed from

$$u_j^{n+1} = A'_j u_{j+1}^{n+1} + H'_j \chi^{n+1} + C'_j \tag{7.65}$$

$$\psi_j^{n+1} = B'_j u_{j+1}^{n+1} + D'_j \chi^{n+1} + E'_j \tag{7.66}$$

providing the coefficients  $A'_j, H'_j, C'_j, B'_j, D'_j, E'_j$  and the quantities  $u_{j+1}^{n+1}$  and  $\chi^{n+1}$  are known a priori. The coefficients are given by

$$A'_j = -\frac{A_j}{R_1}$$

$$B'_j = A'_j R_2$$

$$C'_j = \frac{C_j - B_j C'_{j-1} - E_j (b_j C'_{j-1} + E'_{j-1})}{R_1}$$

$$D'_j = b_j H'_{j-1} + D'_{j-1} + H'_j R_2$$

$$E'_j = b_j C'_{j-1} + E'_{j-1} + C'_j R_2$$

$$H'_j = \frac{H_j - B_j H'_{j-1} - E_j (b_j H'_{j-1} + D'_{j-1})}{R_1}$$

$$R_1 = D_j + (B_j + E_j b_j) A'_{j-1} + E_j (B'_{j-1} + b_j)$$

$$R_2 = b_j (1 + A'_{j-1}) + B'_{j-1}$$

Since the inner ( $j = 1$ ) boundary conditions on  $u_j^{n+1}$  and  $\psi_j^{n+1}$  are zero, the coefficients  $A'_1, B'_1, C'_1, D'_1, E'_1, H'_1$ , are also zero and the coefficients above can be computed starting from  $j = 2$  and continuing to the outer boundary ( $j = NJ$ ).

The pressure gradient parameter  $\chi^{n+1}$  is evaluated by simultaneously solving the equations obtained from Eqs. (7.65) and (7.66) by replacing  $j$  with  $NJ - 1$  and the boundary conditions in the following manner. At  $j = NJ - 1$ , Eqs. (7.65) and (7.66) become

$$u_{NJ-1}^{n+1} = A'_{NJ-1} u_{NJ}^{n+1} + H'_{NJ-1} \chi^{n+1} + C'_{NJ-1} \quad (7.67)$$

$$\psi_{NJ-1}^{n+1} = B'_{NJ-1} u_{NJ}^{n+1} + D'_{NJ-1} \chi^{n+1} + E'_{NJ-1} \quad (7.68)$$

The boundary conditions are written as

$$\psi_{NJ}^{n+1} = u_{NJ}^{n+1} (y_{NJ} - \delta^{*n+1}) \quad (7.69)$$

and

$$\chi^{n+1} = \frac{1}{\Delta x} \left[ (2\hat{u}_{NJ}^{n+1} - u_{NJ}^n) u_{NJ}^{n+1} - (\hat{u}_{NJ}^{n+1})^2 \right] \quad (7.70)$$

Equation (7.61) is written as

$$\psi_{NJ}^{n-1} = \psi_{NJ-1}^{n+1} + \frac{\Delta y_-}{2} (u_{NJ}^{n+1} + u_{NJ-1}^{n+1}) \quad (7.71)$$

Solving Eqs. (7.67)–(7.71) for  $\chi^{n+1}$  gives

$$\chi^{n+1} = \frac{(F_3/F_1)(2\hat{u}_{NJ}^{n+1} - u_{NJ}^n) - (u_{NJ}^{n+1})^2}{\Delta x - (F_2/F_1)(2\hat{u}_{NJ}^{n+1} - u_{NJ}^n)} \quad (7.72)$$

where

$$F_1 = y_{NJ} - \delta^{*n+1} - B'_{NJ-1} - \frac{\Delta y_-}{2} (1 + A'_{NJ-1})$$

$$F_2 = D'_{NJ-1} + \frac{\Delta y_-}{2} H'_{NJ-1}$$

$$F_3 = E'_{NJ-1} + \frac{\Delta y_-}{2} C'_{NJ-1}$$

Once the pressure gradient parameter  $\chi^{n+1}$  is determined, the edge velocity  $u_{NJ}^{n+1}$  can be calculated using Eqs. (7.67)–(7.71) as

$$u_{NJ}^{n+1} = \frac{F_2}{F_1} \chi^{n+1} + \frac{F_3}{F_1} \quad (7.73)$$

Then,  $\psi_{NJ}^{n+1}$  can be computed directly from Eq. (7.69). Now the back substitution process can be initiated using Eqs. (7.65) and (7.66) to compute  $u_j^{n+1}$  and  $\psi_j^{n+1}$  from the outer edge to the wall. The Newton linearization requires that the system of equations be solved iteratively, with  $\hat{u}_j^{n+1}$  and  $\hat{\psi}_j^{n+1}$  being updated between iterations. The iterative process is continued at each streamwise

location until the maximum change, in  $u$ 's and  $\psi$ 's between two successive iterations is less than some predetermined tolerance. The calculation is initiated at each streamwise station by setting  $\hat{u}_j^{n+1} = u_j^n$  and  $\hat{\psi}_j^{n+1} = \psi_j^n$ . In previous applications of this method, only two or three iterations were generally required for the maximum fractional change in the variables, i.e.,  $\Delta\phi/\phi$ , to be reduced to  $5 \times 10^{-4}$ .

Details of other somewhat different coupled inverse boundary-layer finite-difference procedures employing the FLARE approximation can be found in the works of Cebeci (1976) and Carter (1978).

#### 7.4.4 Viscous-Inviscid Interaction

In design it is common to obtain the pressure distribution about aerodynamic bodies from an inviscid flow solution. The inviscid flow solution then provides the edge velocity distribution needed as a boundary condition for solving the boundary-layer equations to obtain the viscous drag on the body. In many cases, the presence of the viscous boundary layer only slightly modifies the flow pattern over the body. It is possible to obtain an improved inviscid flow solution by augmenting the physical thickness of the body by the boundary-layer displacement thickness. The definition of  $\delta^*$  is such that the new inviscid flow solution properly accounts for the displacement of the inviscid flow caused by the viscous flow near the body. The improved inviscid edge velocity distribution can then be used to obtain yet another viscous flow solution. In principle, this viscous-inviscid interaction procedure can be continued iteratively until changes are small. In practice, however, severe underrelaxation of the changes from one iterative cycle to another is often required for convergence.

Fortunately, for most flows involving an attached boundary layer, the changes that arise from accounting for the viscous-inviscid interaction are negligibly small, and it suffices for engineering design purposes to compute the inviscid and viscous flows independently (i.e., without considering viscous-inviscid interaction). Flows that separate or contain separation bubbles are a notable exception.

The displacement effect of the separated regions locally alters the pressure distribution in a significant manner. A rapid thickening of the boundary layer under the influence of an adverse pressure gradient even without separation can also alter the pressure distribution locally, to the extent that a reasonable flow solution cannot be obtained without accounting for the displacement effect of the viscous flow. Often under such conditions, a boundary-layer calculation obtained using the edge velocity distribution from an inviscid flow solution that neglects the displacement effect will predict separation when the real flow does not separate at all.

It is often possible to confine the region where viscous-inviscid interaction effects are important to the local neighborhood of the "bulge" in the displacement surface. Such a local interaction region is depicted in Fig. 7.12.

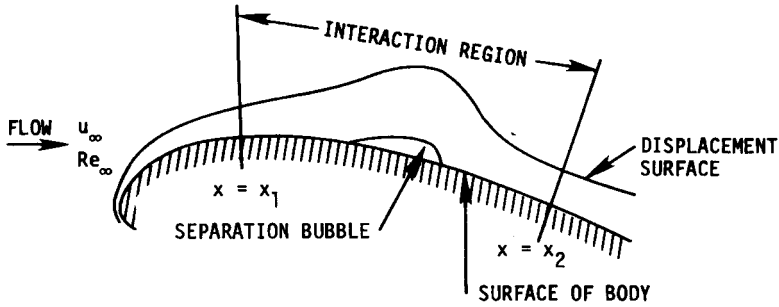


Figure 7.12 Local interaction region on a two-dimensional body.

The inverse boundary procedure described in Section 7.4.3 is particularly well suited for flows in which separation may occur.

The essential elements of a viscous-inviscid interaction calculation procedure are the following:

1. A method for obtaining an improved inviscid flow solution that provides a pressure distribution or edge velocity distribution that accounts for the viscous flow displacement effect. In principle, any inviscid flow “solver” could be used, but it is also frequently possible to employ a greatly simplified inviscid flow calculation scheme based on a small-disturbance approximation.
2. A technique for obtaining a solution to the boundary-layer equations suitable for the problem at hand. For a flow that may separate, an inverse boundary-layer procedure would be appropriate.
3. A procedure for relating the inviscid and viscous flow solutions in a manner that will drive the changes from one iterative cycle to the next toward zero.

Over the years, numerous viscous-inviscid interaction schemes have been proposed. It will not be possible to discuss all of these here. Instead, we will summarize a suitable approach for predicting the flow in the neighborhood of a separation bubble on an airfoil in incompressible flow. This configuration is illustrated in Fig. 7.12.

For this case, a good estimate of the effect of the displacement correction for the inviscid flow solution can be obtained by the use of a small-disturbance approximation. We let  $u_{e,o}$  denote the tangential component of velocity of the inviscid flow over the solid body (neglecting all effects of the viscous flow) and  $u_c$  be the velocity on the displacement surface induced only by the sources and sinks distributed on the surface of the body due to the displacement effect of the viscous flow in the interaction region. Then, the  $x$  component of velocity of a fluid particle on the displacement surface can be written as

$$u_e = u_{e,o} + u_c \quad (7.74)$$

Following Lighthill (1958), the intensity of the line source or sinks displacing a streamline at a displacement surface of the viscous flow can be evaluated as

$$q = \frac{d(u_e \delta^*)}{dx} \quad (7.75)$$

For small values of  $\delta^*$ ,  $u_c$  can be evaluated from the Hilbert integral

$$u_c(x) = \frac{1}{\pi} \int_{-\infty}^{\infty} \frac{d(u_e \delta^*)}{dx'} \frac{dx'}{x - x'} \quad (7.76)$$

In the numerical computation of  $u_c$ , it is usually assumed that strong interaction is limited to the region  $x_1 \leq x \leq x_2$  shown in Fig. 7.12. The intensity of the source or sink caused by the viscous displacement is assumed to approach zero as  $x$  approaches  $\pm\infty$ . Consequently,  $d(u_e \delta^*/dx)$  is normally only computed in the region  $x_1 < x < x_2$  using the boundary-layer solution. An arbitrary extrapolation of the form (Kwon and Pletcher, 1979)

$$q'(x) = \frac{b}{x^2} \quad (7.77)$$

is often used for the regions  $x < x_1$  and  $x > x_2$  in order to evaluate the integral in Eq. (7.76). The constant  $b$  is chosen to match the  $q$  obtained from the boundary-layer solution at  $x_1$  and  $x_2$ . Equation (7.76) can now be written as

$$u_c(x) = \frac{1}{\pi} \left[ \int_{-\infty}^{x_1} \frac{q'(x')}{x - x'} dx' + \int_{x_1}^{x_2} \frac{q(x')}{x - x'} dx' + \int_{x_2}^{\infty} \frac{q'(x')}{x - x'} dx' \right] \quad (7.78)$$

The first and third integrals can be evaluated analytically. The second integral is evaluated numerically, normally using the trapezoidal rule. The singularity at  $x = x'$  can be isolated using the procedure found in the work by Jobe (1974). Some authors have found it possible to evaluate the integral numerically with no special attention given to the singularity as long as  $(x - x')$  remained finite (Briley and McDonald, 1975).

The inviscid surface velocity on the solid body (neglecting the boundary layer),  $u_{e,o}$ , can be obtained by the methods cited in Chapter 6 [as, for example, the Hess and Smith (1967) method], or from experimental data. The Hess and Smith procedure could be used iteratively for all of the inviscid flow calculations. However, the relatively simple small-disturbance procedure requires significantly less computer time and has been found to provide sufficient accuracy for incompressible viscous-inviscid interaction calculations of a type that permits the use of the boundary-layer equations for the viscous flow.

The inverse boundary-layer procedures discussed in Section 7.4.3 are quite suitable for computing the viscous portion of the flow, which may include separated regions. The iterative updating of the solutions can be effectively carried out by the method successfully demonstrated by Carter (1978) and Kwon and Pletcher (1979).

The interaction strategy known as a semi-inverse (inviscid solution proceeds directly, the viscous, inversely) method proceeds in the following way. First,  $u_{e0}$  is obtained for the body of interest, and the viscous flow is computed up to the beginning of the interaction region by a conventional direct method. These two solutions do not change. Next, an initial  $\delta^*(x)$  distribution is chosen over the region  $x_1 < x < x_2$  (see Fig. 7.12). The initial guess is purely arbitrary but should match the  $\delta^*(x)$  of the boundary layer computed by the direct method at  $x = x_1$ . The boundary-layer solution is next obtained by an inverse procedure using this  $\delta^*(x)$  as a boundary condition. An edge velocity distribution  $u_{e,BL}(x)$  is obtained as an output.

Now the small-disturbance inviscid flow procedure, Eq. (7.78), is used to compute the correction to the inviscid flow velocity. This establishes a new distribution for the edge (surface) velocity  $u_{e,inv}(x)$ . The  $u_e(x)$  from the two calculations, boundary layer and inviscid, will not agree until convergence has been achieved. The difference between  $u_e(x)$  calculated both ways can be used as a potential to calculate an improved distribution for  $\delta^*(x)$ . To do this formally, one would seek to determine the way in which a change in  $u_e$  would influence  $\delta^*$ . A suitable scheme has been developed for subsonic flows by noting that a response to small excursions in local  $u_e$  tends to preserve the volume flow rate per unit width in the boundary layer, i.e.,  $u_e \delta^* \cong \text{const}$ . This implies that a local decrease in  $u_e(x)$  (associated with a more adverse pressure gradient) causes an increase in  $\delta^*(x)$  and a local increase in  $u_e(x)$  (associated with a more favorable pressure gradient) causes a decrease in  $\delta^*(x)$ . This concept is put into practice by computing the appropriate new distribution of  $\delta^*$  (Carter, 1978) to use for a new pass through the boundary-layer calculation by

$$\delta_{k+1}^* = \delta_k^* \left( \frac{u_{e,BLk}}{u_{e,invk}} \right) \quad (7.79)$$

where  $k$  denotes iteration level. It is important to note that Eq. (7.79) only serves as a basis for correcting  $\delta^*$  between iterative passes so that no formal justification for its use is required so long as the iterative process converges. At convergence  $u_{e,BL} = u_{e,inv}$ ; thus, Eq. (7.79) represents an identity, thereby having no effect on the final solution. In this sense, the use of Eq. (7.79) is somewhat like the use of an arbitrary overrelaxation factor in the numerical solution of an elliptic equation by successive overrelaxation (SOR). Carter (1978) has given a somewhat more formal justification of Eq. (7.79) based on the von Kármán momentum integral.

The viscous-inviscid interaction calculation is completed by making successive passes first through the inverse boundary-layer scheme, then through the inviscid flow procedure with  $\delta^*$  being computed by Eq. (7.79) prior to each boundary-layer calculation. When  $|u_{e,BL} - u_{e,inv}|$  is less than a prescribed tolerance, convergence is considered to have been achieved. In some applications of this matching procedure, overrelaxation of  $\delta^*$  in Eq. (7.79) has been observed to speed convergence. An illuminating discussion of several matching procedures can be found in the paper by Wigton and Holt (1981).

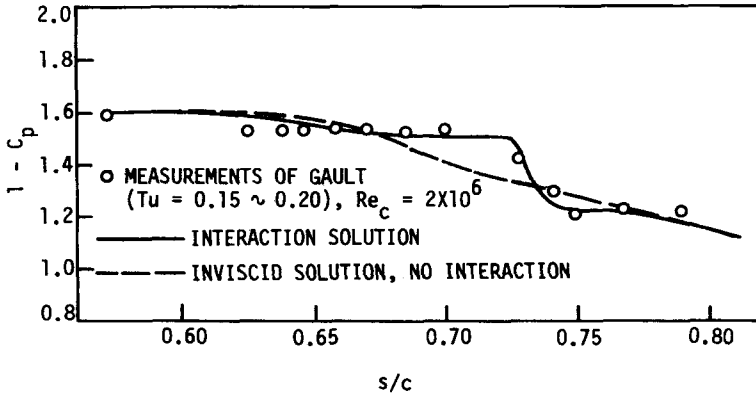


**Figure 7.13** Comparison of the predicted pressure distribution with experimental data (Gault, 1955) for a NACA 66<sub>3</sub>-0.18 airfoil at zero angle of incidence.

Some example predictions (Kwon and Pletcher, 1979) are shown in Figs. 7.13 and 7.14 for the flow in the neighborhood of a transitional separation bubble on a NACA 66<sub>3</sub>-018 airfoil. The parameter  $Tu$  in the figures is the free stream turbulence level, and  $Re_c$  is the Reynolds number based on the airfoil chord. Figure 7.13 compares the predicted pressure coefficient with measurements. The dashed line in Fig. 7.13 indicates the pressure coefficient predicted by inviscid flow theory neglecting the presence of the boundary layer. In the neighborhood of the separation bubble centered at  $s/c \approx 0.7$  ( $s$  is the distance along the airfoil surface measured from the leading edge, and  $c$  is the chord), this predicted pressure coefficient is seen to be considerably in error compared to the measurements. The solid line indicates the prediction of a viscous-inviscid interaction procedure, which is seen to follow the trend of the measurements fairly closely. Seventeen passes through the viscous-inviscid procedure were required for convergence in this case. Velocity profiles are compared in Fig. 7.14. Reversed flow is evident from the profiles in the vicinity of  $s/c \approx 0.7$ . The predicted results are quite sensitive to the model used for laminar-turbulent transition.

The same general strategy outlined above for viscous-inviscid interaction calculations has also been found to work well for compressible flows, including transonic and supersonic applications (Carter, 1981; Werle and Verdon, 1979). However, there has been some evidence that the semi-inverse coupling procedure described above becomes unstable for large separated flow regions in a supersonic stream. This has led to the development of quasi-simultaneous (Le Balleur, 1984; Houwink and Veldman, 1984; Bartels and Rothmayer, 1994) and simultaneous (Lee and Pletcher, 1988) methods for achieving the coupling between viscous and inviscid solutions. When the flow becomes compressible, the boundary-layer form of the energy equation is solved in the viscous flow region, usually with the use of the FLARE approximation. The solution

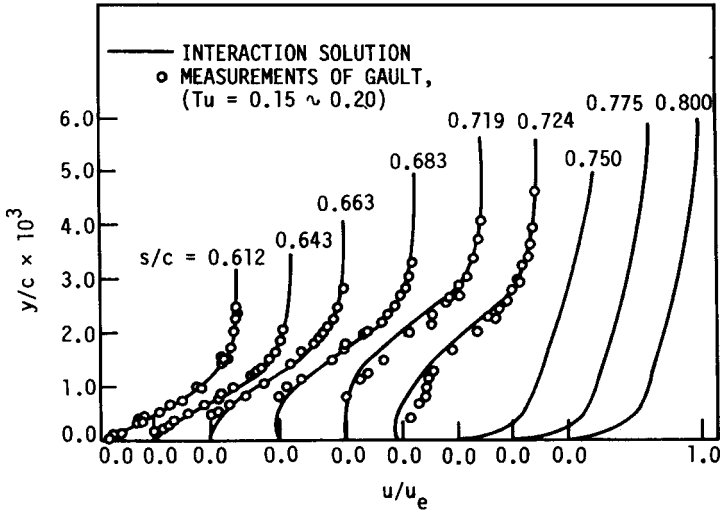


**Figure 7.14** Comparison of the predicted mean velocity profiles with experimental data (Gault, 1955) for a NACA 66<sub>3</sub>-018 airfoil at zero angle of attack.

procedure used for the inviscid flow normally varies as the flow regime changes. A relaxation solution of the full potential equation for inviscid flow was used by Carter (1981) in his transonic viscous-inviscid interaction calculations. For fully supersonic streams the concept of a small-disturbance approximation (linearized theory) is again useful, and the component of the pressure gradient attributed to viscous displacement can be related to the second derivative of the boundary-layer displacement thickness in a very simple manner. The exact form of the appropriate pressure gradient relation varies somewhat with the application considered. The reader is referred to the works of Werle and Vatsa (1974) and Burggraf et al. (1979) for specific examples. Despite the fact that the pressure gradient depends upon local quantities in the case of a supersonic external stream, a downstream condition must be imposed (usually it is on  $\delta^*$ ) in order to obtain a unique solution. Various time-dependent interaction schemes have also been successfully applied to both subsonic and supersonic flows (Briley and McDonald, 1975; Werle and Vatsa, 1974).

Mention is often made of “triple-deck theory” or “triple-deck structure” in connection with viscous-inviscid interactions. It is natural to wonder if this theory introduces something that ought to be taken into account by those applying finite-difference methods to viscous-inviscid interaction problems. The theory itself is based on a multistructured asymptotic expansion valid as  $Re \rightarrow \infty$  for laminar flow in the neighborhood of a perturbation to a boundary-layer flow such as would occur owing to small separated regions or near the trailing edge of a flat plate. We will primarily concentrate on the application of triple-deck theory to the small-separation problem.

Several individuals have contributed to the theory. Some of the early concepts were introduced by Lighthill (1958). Stewartson and co-workers have made several contributions. An excellent review of developments in the theory up through 1974 is given by Stewartson (1974).

The theory is applicable if the streamwise length of the disturbance is relatively short. Thus, the theory would be applicable to small separation bubbles, but not to catastrophic separation. The length of the perturbation region where the triple-deck analysis would be applicable is of the order of  $Re^{-3/8}$ , where  $Re$  is the Reynolds number based on the origin of the boundary layer. The "decks" in the theory are flow regions measured normal to the wall. The thickness of the lower deck is of order  $Re^{-5/8}$ . The flow in this thin lower region has very little inertia, so that it responds quite readily to disturbances transmitted by the pressure gradient. The thickness of the middle (main) deck is of the order  $Re^{-1/2}$ . The flow in this region is essentially a streamwise continuation of the upstream boundary-layer flow and is predominantly rotational and inviscid. All flow quantities in this region are only perturbed slightly from those in a conventional noninteracting boundary layer. The disturbances being transmitted by the lower deck displace the main deck boundary layer outward. The upper deck is of order  $Re^{-3/8}$  in thickness. The upper deck flow is the perturbed part of the inviscid irrotational flow.

Triple-deck theory provides the equations and boundary conditions needed to match the solutions in each of the three regions. The results are only valid for laminar flows where  $Re \rightarrow \infty$  so in a sense are of limited practical value. These equations are frequently solved numerically using viscous-inviscid interaction procedures (Jobe and Burggraf, 1974).

To the computational fluid dynamicist, the most important ideas and conclusions that come from the development of the triple-deck theory to date are as follows.

1. The equations that result from the triple-deck theory applied to flows containing small perturbations (such as small closed separated regions and trailing edge flow) contain no terms that are not present in the boundary-layer viscous-inviscid interaction model. This tends to confirm that the boundary-layer viscous-inviscid interaction model is correct in the limit as  $Re \rightarrow \infty$ . Normal pressure gradients are neglected in the triple-deck theory when applied to the class of flows being considered here.
2. Triple-deck theory identifies length scales that can prove useful in finite-difference computations for laminar flows. The theory predicts that the lower deck is of order  $Re^{-5/8}$  in thickness. Although this conclusion is only strictly valid in the limit as  $Re \rightarrow \infty$ , it would appear prudent to use a mesh near the wall sufficiently fine to resolve this lower deck region, where pressure variations can have a fairly drastic effect on the flow. The importance of honoring this scaling is confirmed by the finite-difference study made by Burggraf et al. (1979).

3. The theory provides clear evidence that the supersonic separation problem is boundary value in nature, requiring a downstream boundary condition in order to select a unique solution from the branching solutions that might otherwise be obtained. This requirement is not immediately obvious in the supersonic case because the boundary-layer equations themselves are parabolic and, according to linearized theory, the pressure depends only on the *local* slope of the displacement body. The downstream boundary condition is usually invoked as a prescribed value of the displacement thickness.

The paper by Burggraf et al. (1979) is helpful in clarifying the differences between the application of boundary-layer viscous-inviscid interaction schemes and the numerical solution of the triple-deck equations. At very large  $Re$  ( $\geq 10^9$ ) the boundary-layer viscous-inviscid interaction calculation agreed very well with the triple-deck results for separating supersonic flow past a compression ramp. As  $Re$  decreased, the predictions of the boundary-layer viscous-inviscid interaction procedure and the triple-deck results differed very noticeably.

## 7.5 METHODS FOR INTERNAL FLOWS

### 7.5.1 Introduction

The thin-shear-layer equations provide a reasonably accurate mathematical model for two-dimensional and axisymmetric internal flows. These include the developing flow in straight tubes and in the annulus formed between two concentric straight tubes. In addition, the flow in the central portion of a large aspect ratio straight rectangular channel ("parallel plate duct") is often found to be reasonably two-dimensional. These flow configurations are illustrated in Fig. 7.15. The flow cross-sectional area does not change with axial distance in these standard geometries. The boundary-layer model also provides a good approximation for some internal flows in channels having abrupt expansions in cross-sectional area, which cause regions of flow reversal. These new areas of possible applicability of the thin-shear-layer equations are discussed further in Section 7.5.3.

The finite-difference/finite-volume approach is particularly useful in analyzing the flow from the inlet to the region of fully developed flow. The flow is said to be hydrodynamically fully developed when the velocity distribution is no longer changing with the axial distance along the flow passage. The hydrodynamic fully developed idealization is generally only realized for flows in which fluid property variations in the main flow direction are negligible. The thermal development of the flow is also of interest and can be predicted for the class of flow mentioned above by solving the thin-shear-layer form of the energy equation simultaneously with the momentum and continuity equations. Under constant property assumptions and with either constant wall temperature or uniform wall heat flux thermal boundary conditions, it is possible for the nondimensional temperature distribution to become independent of the axial

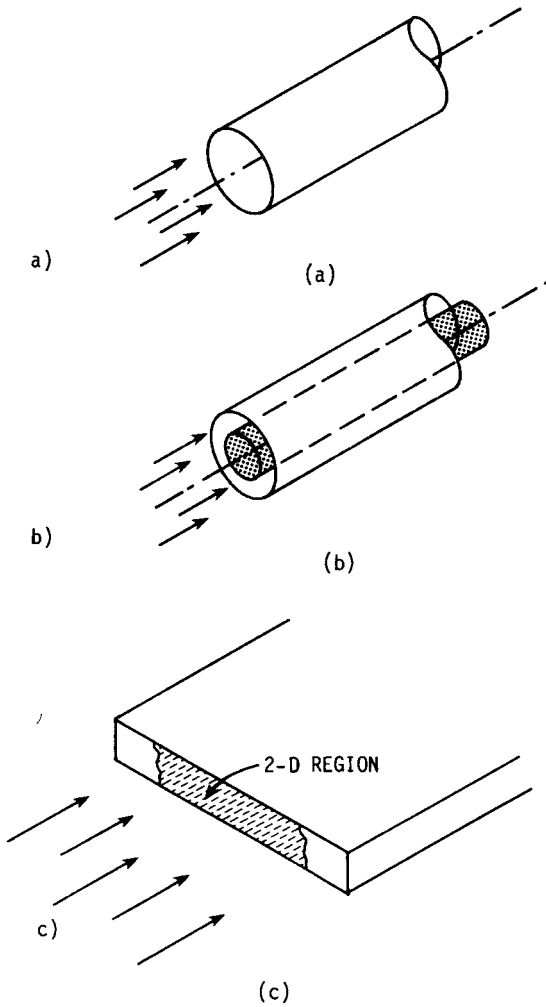


**Figure 7.15** Internal flow configurations in which the thin-shear-layer equations are applicable. (a) Circular duct. (b) Annular passage. (c) Large aspect ratio rectangular channel.

direction. Shah and London (1978) provide an excellent discussion of the thermal aspects of internal flows.

The finite-difference/finite-volume approach is of less interest for treating constant-property fully developed flow, since the governing PDEs reduce to ODEs under these conditions. Laminar fully developed flow in a tube is the well-known Hagen-Poiseuille flow (White, 1991). If a relatively simple algebraic turbulence model is used, even turbulent fully developed flow can be treated by numerical methods appropriate for ODEs. With heat transfer present, it becomes more likely that the property variations will prevent the flow from reaching a fully developed state.

The characteristic Re for internal flows makes use of the channel hydraulic diameter,  $D_H$ , as the characteristic length. The hydraulic diameter is evaluated as  $4A/P$ , where  $A$  is the flow cross-sectional area and  $P$  is the wetted perimeter. For circular ducts,  $D_H$  reduces to the duct diameter.

We expect to find a small region near the channel inlet where the boundary-layer approximation is poor. This corresponds to the low Re leading edge region in external flows. For channel Re greater than about 75, this region is negligibly small. Comparisons of various numerical models for very low Re channel inlet flows can be found in the works of McDonald et al. (1972) and Chilukuri and Pletcher (1980).

### 7.5.2 Coordinate Transformation for Internal Flows

For steady laminar two-dimensional and axisymmetric constant property flows in straight channels (including pipes of circular cross section), Re can be removed from the governing equations by a simple nondimensionalization. As a result, it becomes apparent that only one solution of the boundary-layer equations is required for each geometry. The scaling factors for this nondimensionalization are given by

$$u^* = \frac{u}{\bar{u}_i} \quad v^* = \frac{v \text{ Re}}{\bar{u}_i} \quad x^* = \frac{x}{D \text{ Re}} \quad y^* = \frac{y}{D} \quad p^* = \frac{p}{\rho \bar{u}_i^2} \quad (7.80)$$

where  $D$  is the channel diameter and Re is the Reynolds number based on the inlet average velocity  $\bar{u}_i$  and diameter  $D$ . The  $x$  axis is at the center of the straight channel. Specializing Eqs. (7.1) and (7.3) for constant property laminar flow and introducing the variables defined above yields

$$\frac{\partial u^*}{\partial x^*} + \frac{1}{r^m} \frac{\partial r^m v^*}{\partial y^*} = 0 \quad (7.81)$$

$$u^* \frac{\partial u^*}{\partial x^*} + v^* \frac{\partial u^*}{\partial y^*} = -\frac{dp^*}{dx^*} + \frac{1}{r^m} \frac{\partial}{\partial y^*} \left( r^m \frac{\partial u^*}{\partial y^*} \right) \quad (7.82)$$

where  $r$  is the distance from the center of the channel and  $m$  is a flow index equal to unity for axisymmetric flow and equal to zero for 2-D flow, as before. It should be easy to see that if one has a solution to Eqs. (7.81) and (7.82) for a developing flow, the results can be stretched (scaled) to be applicable for a flow at any specific Re by using Eqs. (7.80). Note again that this simple state of affairs is for constant-property laminar flow and, to date, an appropriate general scaling for variable-property and turbulent flows has not been identified.

### 7.5.3 Computational Strategies for Internal Flows

It is very important to observe that for steady channel flow, the flux of mass across any plane perpendicular to the channel axis is constant in the absence of wall blowing or suction. Since an initial velocity and temperature distribution

must be given as part of the problem specification for the parabolic equations, the mass flow rate can also be considered as specified. If wall blowing or suction occurs, the normal component of velocity at the walls would be required as part of the boundary conditions for the boundary-layer equations; hence the changing mass flow rate through the channel can be computed from the problem specifications. For simplicity, in the discussion to follow, we will assume that no flow passes through the channel walls. However, computation procedures can easily be modified to account for these effects. This additional information about the global or overall mass flow in the channel permits a constraint to be placed on the solution from which the pressure gradient can be determined. In a sense, this mass flow constraint serves the same purpose as the simple relation between  $u_e(x)$  and  $dp/dx$ , which can be obtained from the steady Euler momentum equation for external flows. In the usual treatment for external flows, the flow outside the boundary layer is assumed to be inviscid, and at the outer edge we specialize the Euler equation to  $dp/dx = -\rho u_e du_e/dx$ . Thus for external flows, we usually think of the pressure gradient being specified, meaning that  $dp/dx$  is either given or easily calculated from  $u_e(x)$ . When we apply the boundary-layer equations alone to calculate steady internal flows, no information is available from an inviscid flow solution, and "outer" boundary conditions on  $u$  are established from geometric considerations. In general, viscous effects may be important throughout the flow, so that the Euler momentum equations cannot be used in any manner to obtain the pressure gradient. Instead, the global mass flow constraint is used. Thus, in steady internal flows, *the pressure gradient is determined from the solution* (with the help of the global mass flow constraint) rather than being "specified" as for external flows. This is the primary difference between the numerical treatment of internal and external flows.

The thin-shear-layer equations can be written in a form applicable to 2-D internal flows as follows:

momentum:

$$\rho u \frac{\partial u}{\partial x} + \rho \tilde{v} \frac{\partial u}{\partial y} = -\frac{dp}{dx} + \frac{1}{r^m} \frac{\partial}{\partial y} (r^m \tau) \quad (7.83)$$

energy:

$$\rho u c_p \frac{\partial T}{\partial x} + \rho \tilde{v} c_p \frac{\partial T}{\partial y} = \frac{1}{r^m} \frac{\partial}{\partial y} (-r^m q_y) + \beta T u \frac{dp}{dx} + \tau \frac{\partial u}{\partial y} \quad (7.84)$$

mass:

$$\frac{\partial}{\partial x} (\rho u r^m) + \frac{\partial}{\partial y} (\rho \tilde{v} r^m) = 0 \quad (7.85)$$

global mass:

$$\dot{m} = \int_A \rho u dA = \text{const} \quad (7.86)$$

In the above,  $A$  is the cross-sectional area perpendicular to the channel axis. In addition, an equation of state is normally used to relate density to temperature and pressure. When  $m = 0$ , the above equations are applicable to 2-D flows, and when  $m = 1$ , they apply to axisymmetric flows. For turbulence models utilizing the Boussinesq assumption, we find

$$\tau = \mu \frac{\partial u}{\partial y} - \rho \overline{u'v'} = (\mu + \mu_T) \frac{\partial u}{\partial y} \quad (7.87)$$

$$q_y = -k \frac{\partial T}{\partial y} + \rho c_p \overline{v'T'} = \left( -k + \frac{c_p \mu_T}{\text{Pr}_T} \right) \frac{\partial T}{\partial y} \quad (7.88)$$

The governing equations reduce to a form applicable to laminar flows whenever the fluctuating Reynolds terms above are equal to zero.

The wall boundary conditions remain the same as for external flows. For flows in straight tubes and parallel plate channels, a symmetry line or plane exists, and outer boundary conditions of the form

$$\left. \frac{\partial u}{\partial y} \right)_{r=0} = \left. \frac{\partial T}{\partial y} \right)_{r=0} = 0 \quad (7.89)$$

are used. For tube flow, the shear-stress and heat flux terms in Eqs. (7.83) and (7.84) are singular at  $r = 0$ . A correct representation can be found from an application of L'Hospital's rule, from which we find

$$\lim_{r \rightarrow 0} \frac{1}{r} \frac{\partial}{\partial y} \left( \mu r \frac{\partial \phi}{\partial y} \right) = 2 \frac{\partial}{\partial y} \left( \mu \frac{\partial \phi}{\partial y} \right)$$

Except for the treatment of the pressure gradient, the differencing of the governing equations proceeds in the same manner as for external boundary-layer flow. The pressure gradient is treated as an unknown in the internal flow case, its value to be determined with the aid of the global mass flow constraint, as indicated previously. This can be done in several ways.

When explicit difference schemes are used, the pressure gradient can be determined as follows. The finite-difference form of the momentum equation can be written in the form

$$u_j^{n+1} = Q_j^n + \frac{dp}{dx} R_j^n \quad (7.90)$$

where  $Q_j^n$  and  $R_j^n$  contain quantities that are all known. Equation (7.90) is then multiplied by the density  $\hat{\rho}_j^{n+1}$ , and the resulting equation integrated numerically over the channel cross section by Simpson's or the trapezoidal rule. This gives

$$\int_A \hat{\rho}_j^{n+1} u_j^{n+1} dA = \dot{m} = \int_A \hat{\rho}_j^{n+1} Q_j^n dA + \frac{dp}{dx} \int_A \hat{\rho}_j^{n+1} R_j^n dA \quad (7.91)$$

The density  $\hat{\rho}_j^{n+1}$  is not known a priori at the  $n + 1$  level at the time the pressure gradient is being determined. The circumflex indicates the provisional nature of this one variable. Very good results have been obtained by simply

letting  $\hat{\rho}_j^{n+1} = \rho_j^n$ . In fact, this has been the most common procedure. An alternative is to evaluate  $\hat{\rho}_j^{n+1}$  from  $\rho_j^n$  and  $\rho_j^{n-1}$  by a second-order accurate extrapolation. Since  $\dot{m}$  is specified by the problem initial conditions and the integrals in Eq. (7.91) contain all known quantities,  $dp/dx$  can be determined as

$$\frac{dp}{dx} = \frac{\dot{m} - \int_A \hat{\rho}_j^{n+1} Q_j^n dA}{\int_A \hat{\rho}_j^{n+1} R_j^n dA} \tag{7.92}$$

Once  $dp/dx$  has been evaluated, the finite-difference form of the momentum, continuity, and energy equations can be solved just as for external flows. The most widely used explicit scheme for internal flow appears to be of the DuFort-Frankel type. The DuFort-Frankel scheme was given for the thin-shear-layer equations in Section 7.3.4. A typical comparison between the predictions of the DuFort-Frankel scheme and experimental measurements of Barbin and Jones (1963) is shown in Fig. 7.16 for the turbulent flow of air in a tube. In the figure,  $u_b$  denotes the bulk velocity in the tube and  $r_w$  is the radius of the tube. Even very near the inlet ( $x/D = 1.5$ ), the predictions are seen to be in good agreement with the measurements. A simple algebraic turbulence model was used in the predictions.

The internal flow problem is conceptually very similar to the inverse boundary-layer problem discussed in Section 7.4 for external flows. This is most evident when implicit difference schemes are used. For internal flows the “correct” pressure gradient must be determined that will give velocities that

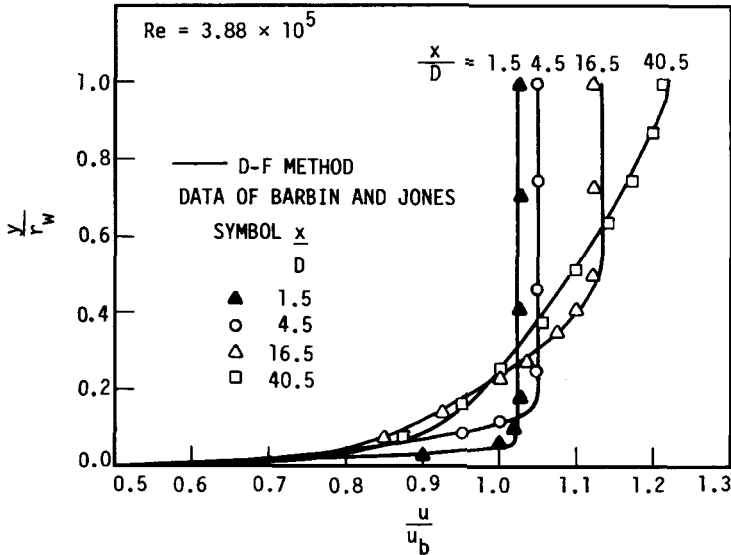


Figure 7.16 Comparison of predicted and measured turbulent velocity profiles in the entrance region of a pipe (Nelson and Pletcher, 1974). D-F denotes DuFort-Frankel method.

satisfy the global mass flow constraint. This corresponds to adjusting the pressure gradient (or edge velocity) until the velocity distribution satisfies the specified displacement thickness in inverse methods for external flows. Several different procedures have been used with implicit methods to determine the pressure gradient. A number of these are briefly discussed below.

**Variable secant iteration.** The pressure gradient can be varied iteratively at each streamwise location until the global mass flow constraint is met (Briley, 1974) by employing the variable secant procedure discussed in Section 7.4.3 in connection with imposing the  $\delta^*$  boundary condition for the inverse boundary-layer method. For fixed coefficients, velocities vary linearly with the pressure gradient, so that convergence is usually obtained with three iterations.

**Lagging the pressure adjustment.** Patankar and Spalding (1970) pointed out that iterating at each streamwise station is uneconomical and have suggested that a value for the pressure gradient be guessed to advance the solution and then let the knowledge of any resulting error in mass flow rate guide our choice of pressure gradient for the *next* step. That is, in analogy with the way an automobile is steered, adjustments are made to correct the course without going back to retrace the path. This was the common-sense approach included in the early versions of the Patankar-Spalding finite-difference method for confined flows. Although the common-sense aspect of this logic cannot be denied, the algorithm appears a bit too approximate by present-day standards and is not recommended. In concert with the trend toward lower computer costs observed over the past decade, there has been a cost-equalizing trend toward the use of algorithms that are potentially more accurate.

**Newton's method.** Raithby and Schneider (1979) proposed a scheme suitable for incompressible flows that requires one-third less effort than the minimum (three iterations) variable secant calculation. The scheme assumes that the coefficients in the difference equations will remain constant, i.e., no form of updating is employed as the pressure gradient is adjusted until the global mass flow constraint is satisfied. The idea is that once an initial guess for  $dp/dx$  is made and a provisional solution obtained for the difference equations, a correction can be obtained by employing a form of Newton's method. With "frozen" coefficients, the velocities will vary linearly with the pressure gradient, and it follows that one Newton-type correction should provide the correct pressure gradient. To illustrate, we will let  $S = dp/dx$ . We make an initial guess for  $dp/dx = (dp/dx)^*$  and calculate provisional velocities  $(u_j^{n+1})^*$  and a provisional mass flow rate  $\dot{m}^*$ . Due to the linearity of the momentum equation with frozen coefficients, we observe from an application of Newton's method (see Section 7.4.2) that the correct velocity at each point would be

$$u_j^{n+1} = (u_j^{n+1})^* + \frac{\partial u_j^{n+1}}{\partial S} \Delta S \quad (7.93)$$

where  $\Delta S$  is the change in the pressure gradient required to satisfy the global mass flow constraint. We define  $u_{p,j}^{n+1} = \partial u_j^{n+1} / \partial S$ . The difference equations are actually differentiated with respect to the pressure gradient ( $S$ ) to obtain difference equations for  $u_{p,j}^{n+1}$  that are tridiagonal in form. The coefficients for the unknowns in these equations will be the same as for the original implicit difference equations. The Thomas algorithm is used to solve the system of algebraic equations for  $u_{p,j}^{n+1}$ . The boundary conditions on  $u_{p,j}^{n+1}$  must be consistent with the velocity boundary conditions. On boundaries where the velocity is specified,  $u_{p,j}^{n+1} = 0$ , whereas on boundaries where the velocity gradient is specified,  $\partial u_{p,j}^{n+1} / \partial n = 0$  ( $n$  normal to boundary). The solution for  $u_{p,j}^{n+1}$  is then used to compute  $\Delta S$  by noting that  $u_{p,j}^{n+1} \Delta S$  is the correction in velocity at each point required to satisfy the global mass flow constraint. Thus we can write

$$\dot{m} - \dot{m}^* = \Delta S \int_A \rho u_{p,j}^{n+1} dA \quad (7.94)$$

where the integral is evaluated by numerical means. The  $\dot{m}$  in Eq. (7.94) is the known value specified by the initial conditions. The required value of  $\Delta S$  is determined from Eq. (7.94). The correct values of velocity  $u_j^{n+1}$  can then be determined from Eq. (7.93). The continuity equation is then used to determine  $v_j^{n+1}$ . The computational effort of this procedure is roughly equivalent to two iterations of the method employing the variable secant procedure.

**Treating the pressure gradient as a dependent variable.** In all of the procedures discussed above, the pressure gradient is treated as a known quantity whenever the simultaneous algebraic equations for the new velocities are solved. The standard Thomas algorithm can be used for the three methods above. Here we consider schemes in which the pressure gradient is treated as an unknown in the algebraic formulation. The coefficient matrix is no longer tridiagonal. Early methods of this type (Hornbeck, 1963) tended to employ conventional Gaussian elimination. More recent procedures (Blottner, 1977; Cebeci and Chang, 1978; Kwon and Pletcher, 1981) have used more efficient block elimination procedures. The method of Kwon and Pletcher (1981) is a modification of inverse method B presented in Section 7.4.3. The procedure employs the FLARE approximation to permit the calculation of separated regions in internal flows. The changes that must be made in inverse method B in order to treat internal incompressible flows in a 2-D channel will now be described. The flow is assumed to be symmetric about the channel centerline located at  $y = H/2$ , where  $y$  is measured from the channel wall. The channel height is  $H$ . Equations (7.57) and (7.58) apply. The outer boundary conditions become

$$\left. \frac{\partial u}{\partial y} \right|_{y=H/2} = 0 \quad \psi \left( x, \frac{H}{2} \right) = \frac{\dot{m}}{2\rho} \quad (7.95)$$

where  $\dot{m}$  is the mass flow rate per unit width for a 2-D channel. The difference equations, Eqs. (7.61)-(7.64), are applicable, and  $\chi^{n+1}$  represents the unknown

pressure gradient

$$-\frac{1}{\rho} \frac{dp}{dx}$$

as before. The procedures for internal and external flow differ in the way in which  $\chi^{n+1}$  and  $u_{NJ}^n$  are determined from the outer boundary conditions, which are different in the two cases. We express  $(\partial u / \partial y)_{H/2}$  in terms of a one-sided second-order accurate difference representation,

$$\left(\frac{\partial u}{\partial y}\right)_{NJ}^{n+1} \cong \frac{u_{NJ}^{n+1}}{2} \left(\frac{4}{\Delta y_-} - \frac{1}{\Delta y_{--}}\right) - \frac{2u_{NJ-1}^{n+1}}{\Delta y_-} + \frac{u_{NJ-2}^{n+1}}{2\Delta y_{--}} \quad (7.96)$$

where

$$\Delta y_- = y_{NJ} - y_{NJ-1}$$

$$\Delta y_{--} = y_{NJ-1} - y_{NJ-2}$$

The outer boundary conditions, Eq. (7.95) can now be written as

$$u_{NJ}^{n+1} = c_1 u_{NJ-1}^{n+1} - c_2 u_{NJ-2}^{n+1} \quad (7.97)$$

$$\psi_{NJ}^{n+1} = \frac{\dot{m}}{2\rho} \quad (7.98)$$

where

$$c_1 = \frac{4}{4 - K}$$

$$c_2 = \frac{K}{4 - K}$$

$$K = \frac{\Delta y_-}{\Delta y_{--}}$$

Equations (7.97) and (7.98) are to be solved with Eqs. (7.67), (7.68), and (7.71). However, one additional relationship is needed, since five unknowns appear ( $u_{NJ}^{n+1}$ ,  $u_{NJ-1}^{n+1}$ ,  $u_{NJ-2}^{n+1}$ ,  $\psi_{NJ-1}^{n+1}$ ,  $\chi^{n+1}$ ) and only four independent relationships among them have been identified thus far [Eqs. (7.97), (7.67), (7.68), and (7.71)]. The additional equation can be obtained by specializing Eq. (7.65) for  $u_{NJ-2}^{n+1}$  as

$$u_{NJ-2}^{n+1} = A'_{NJ-2} u_{NJ-1}^{n+1} + H'_{NJ-2} \chi^{n+1} + C'_{NJ-2} \quad (7.99)$$

This system of equations can be solved for  $\chi^{n+1}$  by defining

$$\alpha_1 = 1 - A'_{NJ-1}(c_1 - c_2 A'_{NJ-2})$$

$$\alpha_2 = (c_1 - c_2 A'_{NJ-2})H'_{NJ-1} - c_2 H'_{NJ-2}$$

$$\alpha_3 = (c_1 - c_2 A'_{NJ-2})C'_{NJ-1} - c_2 C'_{NJ-2}$$

$$\alpha_4 = 1 + \frac{2}{\Delta y_-} B'_{NJ-1} + A'_{NJ-1}$$

$$\alpha_5 = - \left( H'_{NJ-1} + \frac{2}{\Delta y_-} D'_{NJ-1} \right)$$

$$\alpha_6 = \frac{\dot{m}}{\rho \Delta y_-} - \frac{2}{\Delta y_-} E'_{NJ-1} - C'_{NJ-1}$$

Then

$$\chi^{n+1} = \frac{\alpha_1 \alpha_6 - \alpha_3 \alpha_4}{\alpha_2 \alpha_4 - \alpha_1 \alpha_5} \quad (7.100)$$

The axial component of velocity at the line of symmetry can be found from

$$u_{NJ}^{n+1} = \frac{\alpha_2}{\alpha_1} \chi^{n+1} + \frac{\alpha_3}{\alpha_1} \quad (7.101)$$

At this point the back substitution process can be initiated using Eqs. (7.65) and (7.66) to compute  $u_j^{n+1}$  and  $\psi_j^{n+1}$  from the outer boundary to the wall. The remaining portions of the algorithm are as discussed in Section 7.4.3. The only differences between inverse method B and the related procedure for internal flows are due to the minor differences in the boundary conditions for the two cases. This requires that slightly different algebraic procedures be used to evaluate  $\chi^{n+1}$  and  $u_{NJ}^{n+1}$  prior to the back substitution step in the block tridiagonal solution procedure.

An interesting application of this method has been made to laminar channel flows having a sudden symmetric expansion that creates a region of recirculation downstream of the expansion. The general pattern of such a flow is illustrated in Fig. 7.17. The predictions were obtained by the boundary-layer method described above utilizing a fully developed velocity profile at the step.  $Re_h$  is the Reynolds

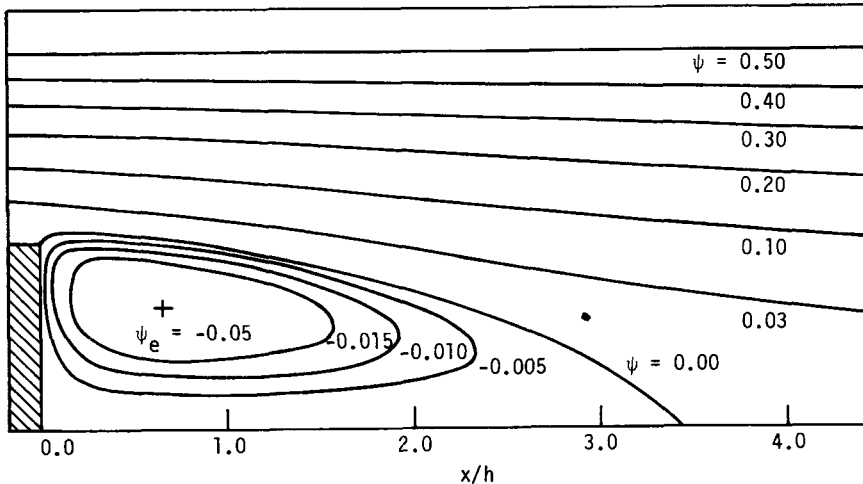
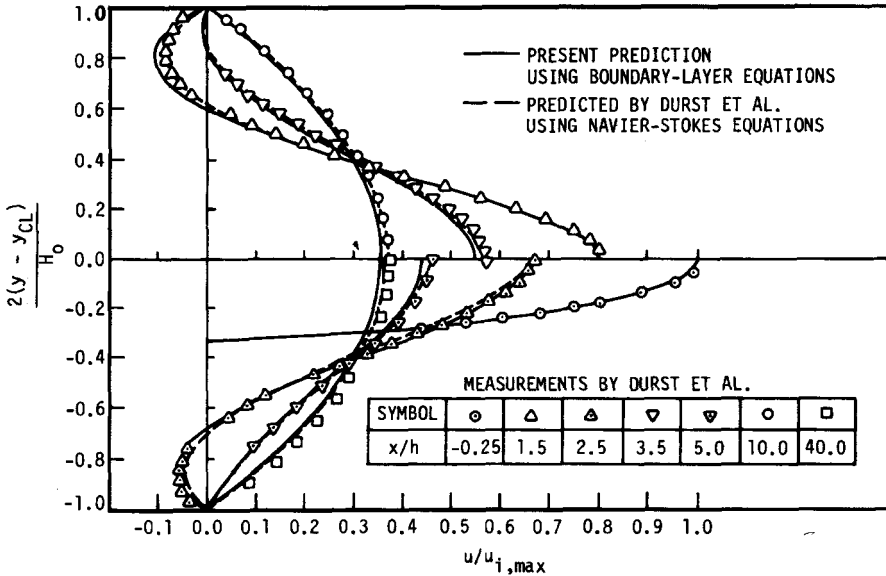


Figure 7.17 Streamline contours predicted from boundary-layer equations (Kwon et al., 1984) for a laminar flow in a channel with a symmetric sudden expansion,  $Re_h = 50$ ,  $H_1/H_2 = 0.5$ .



**Figure 7.18** Velocity profiles for a laminar flow in a channel with a symmetric sudden expansion.  $Re_h$  (based on  $u_{max}$ ) = 56,  $H_1/H_2 = \frac{1}{3}$  (Kwon et al., 1984).

number based on step height, and  $H_1/H_2$  is the ratio of the channel height before and after the expansion. Such flows have customarily been predicted by solving the full Navier-Stokes equations.

Figure 7.18 compares velocity profiles predicted by the same method with experimental data and Navier-Stokes solutions for a symmetric sudden expansion flow. In the figure,  $u_{i,max}$  denotes the maximum velocity just upstream of the expansion (step),  $H_0$  is the channel height downstream of the expansion, and  $y_{CL}$  is the distance from the wall to the channel centerline. The symbols  $h$ ,  $H_1$ ,  $H_2$  are as defined previously. The method based on boundary-layer equations requires an order of magnitude less computer time than required for the solution of the Navier-Stokes equations.

In Fig. 7.19 the reattachment length and distance to the vortex center predicted by the boundary-layer solutions (Lewis and Pletcher, 1986) are compared with the Navier-Stokes solutions and experimental data obtained by Macagno and Hung (1967) for a 1:2 pipe expansion. The Reynolds number ( $Re$ ) and  $l/d$  in the figure are based on the diameter upstream of the expansion. The agreement is quite good for  $Re$  greater than about 20. Note that the boundary-layer results yield straight lines in Fig. 7.19 due to the scaling laws of Eqs. (7.80), which are applicable even in the case of fully developed flow undergoing a sudden expansion in cross-sectional flow area. Although the solutions to the boundary-layer equations are in close agreement with experimental data and solutions to the full Navier-Stokes equations for velocity profiles and the distance to the reattachment point, some limitations exist. For example, details

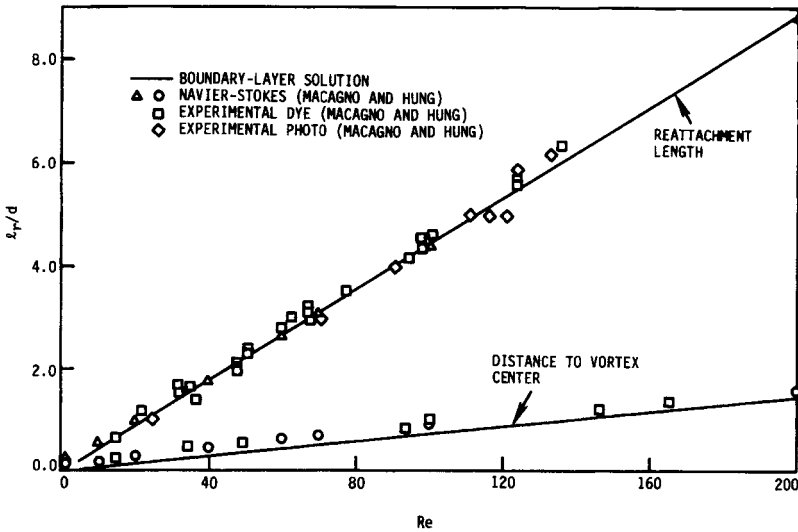


Figure 7.19 Comparison of the distances to flow reattachment and vortex center for experiments and Navier-Stokes solutions (Macagno and Hung, 1967) and solution of boundary-layer equations with FLARE (Lewis and Pletcher, 1986) for a 1:2 pipe expansion.

of the eddy structure are not well predicted at low Re, as can be seen in Fig. 7.20, where the magnitude of the minimum nondimensional stream function is plotted against Re for the 1:2 pipe and planar expansions. The minimum stream function measures the volume rate of flow in the recirculating eddy. Note that the boundary-layer values are independent of Re (indicating that the dimensional

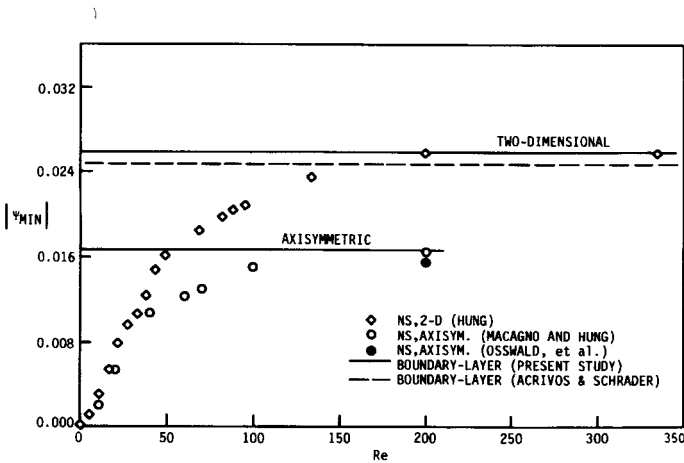


Figure 7.20 Comparison of the stream function at the center of the trapped vortex predicted by boundary-layer equations (Lewis and Pletcher, 1986; Acivos and Schrader, 1982) and the Navier-Stokes equations (Macagno and Hung, 1967; Osswald et al., 1984) for a 1:2 expansion.

volume flow reduces linearly with  $Re$ ) but are only correct for  $Re$  greater than about 200. At lower  $Re$  the volume rate of flow in the eddy actually reduces more rapidly with decreasing  $Re$  as indicated by the solutions to the full Navier-Stokes equations.

#### 7.5.4 Additional Remarks

Details of several difference schemes suitable for the thin-shear-layer equations were presented in Section 7.3 as they applied to ordinary external boundary-layer flows. As methods for confined flows have been considered in the present section, numerical details that remain the same as for external flows have not been repeated. However, an attempt has been made to clearly point out and emphasize those details that change and are unique to internal flows.

Coverage in this section has been limited to flows in straight channels. Blottner (1977) demonstrated that the thin-shear-layer approximation (also known as the "slender channel" approximation) can be extended to curved 2-D channels with varying channel height. The equations solved are the boundary-layer equations with longitudinal curvature (Van Dyke, 1969). The normal pressure gradient induced by the channel curvature is accounted for by

$$\frac{\partial p}{\partial n} = \frac{\kappa \rho u^2}{1 + \kappa n} = 0$$

where  $n$  is the coordinate normal to the channel centerline and  $\kappa$  is the curvature of the centerline.

Viscous-inviscid interaction schemes can be applied to internal flows in which an inviscid core region can be identified. The interaction effect is expected to be negligibly small except very near the inlet for low Reynolds number flows and under conditions in which the channel cross-sectional area changes abruptly. Viscous-inviscid interaction permits information to be transmitted upstream and can give improved predictions for flows in which the pressure field at a point is expected to be influenced by conditions farther downstream. The incompressible inviscid flow in channels is conveniently determined through a numerical solution of Laplace's equation for the stream function. Inverse method B discussed in Section 7.4.3 can be used for the viscous portion of the flow. Such a combination has been employed interactively to predict the flow over a rearward facing step in a channel (Kwon and Pletcher, 1986a, 1986b).

### 7.6 APPLICATION TO FREE-SHEAR FLOWS

The thin-shear-layer equations provide a fairly accurate mathematical model for a number of free-shear flows. These include the plane or axisymmetric jet discharging to a quiescent or co-flowing ambient, the planar mixing layer, and simple wake flows. The majority of free-shear layers encountered in engineering

applications are turbulent. To date, turbulence models for free-shear flows have not exhibited nearly the degree of generality as those used for wall boundary layers. It is still a major challenge to find models that can provide accurate predictions for the development of both the planar and axisymmetric jet without requiring adjustments in the model parameters.

A complete treatise on the subject of the numerical prediction of free-shear flows might devote 60% of its content to turbulence modeling, 25% to coverage of the physics of various categories of free-shear flows, and 15% to numerical procedures. The numerical procedures, which are our main concern here, are the least troublesome aspect of the problem of obtaining accurate predictions for turbulent free-shear flows.

The round jet has been studied extensively both experimentally and analytically and provides a representative example of a free-shear flow. The thin-shear-layer equations will provide a good mathematical model for the round jet following a straight trajectory if pressure in the interior of the jet can be assumed to be equal to that of the surrounding medium. This requires that the surface tension of the jet be negligible and that the jet be fully expanded, i.e., the pressure at the discharge plane equals the pressure in the surrounding medium. A subsonic jet discharging from a tube can always be considered as fully expanded. For the jet cross section to remain round and the trajectory to remain straight, it is necessary that no forces act on the jet in the lateral direction. This requires that the medium into which the jet is injected be at rest or flowing in the same direction as the discharging jet (co-flowing) and that body forces (such as buoyancy) be negligible. Under these conditions, the form of the thin-shear-layer equations given by Eqs. (5.116)-(5.119) are applicable. These equations are specialized further below for the steady incompressible flow of a round jet in the absence of a pressure gradient:

continuity:

$$\frac{\partial(yu)}{\partial x} + \frac{\partial(yv)}{\partial y} = 0 \tag{7.102}$$

momentum:

$$u \frac{\partial u}{\partial x} + v \frac{\partial u}{\partial y} = \frac{1}{y} \frac{\partial}{\partial y} \left[ y \left( v \frac{\partial u}{\partial y} - \overline{u'v'} \right) \right] \tag{7.103}$$

Numerically, the primary difference between the wall boundary layer and the round jet is in the specification of the boundary conditions. Figure 7.21 illustrates the round jet flow configuration. Due to the symmetry that exists about the jet centerline, the appropriate boundary conditions at  $y = 0$  are  $(\partial u / \partial y)_{y=0} = 0$  and  $v(x, 0) = 0$ . The outer boundary condition is identical to that for a wall boundary layer,

$$\lim_{y \rightarrow \infty} u(x, y) = u_e$$

Initial conditions are also needed for the finite-difference/finite-volume

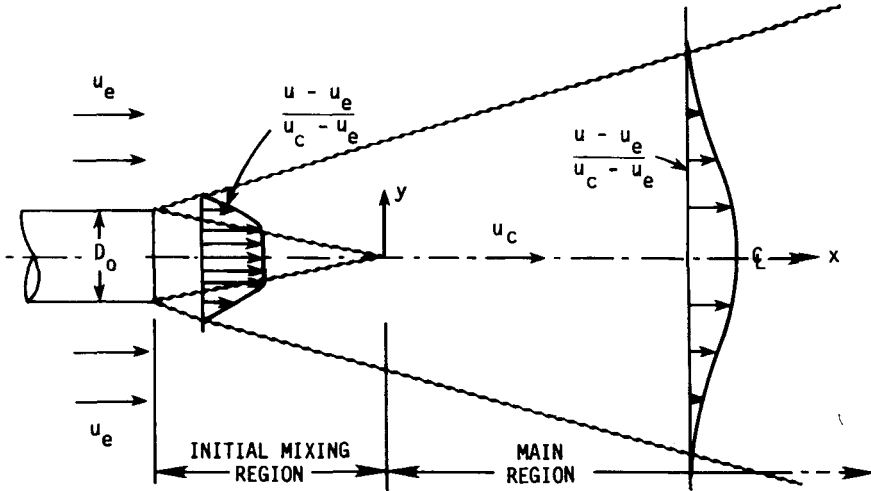


Figure 7.21 Round jet configuration.

calculation. For turbulent jets especially, the initial streamwise velocity distribution is usually taken as a uniform stream at the discharge velocity,  $u_0$ . Naturally, this cannot be completely correct, in that the velocities in a small region must exhibit the retarding effects of the tube walls. On the other hand, the boundary-layer equations are not expected to provide an extremely accurate solution very near the discharge plane, i.e., for  $x/D_0$  less than about one, where  $D_0$  is the diameter of the jet at discharge. Using a uniform velocity distribution at discharge for the turbulent jet appears to provide fairly accurate results for  $x/D_0 > 1$ , which includes the region of most interest in engineering applications. Some finite-difference schemes applied to the jet problem in the Cartesian coordinate system will also require an initial distribution for  $v$ . As was mentioned in Section 7.3 for wall boundary layers, this is a requirement of the numerical procedure and not a requirement in the mathematical specification of the problem. When an initial distribution for  $v$  is required, using  $v(0, y) = 0$  is recommended. Taking several very small streamwise steps near the starting plane helps confine the effects of the starting singularity (which is due to the very large values of  $\partial u / \partial x$  associated with the vanishingly small initial mixing zone) to a small region. This starting singularity is similar to that observed at the leading edge of a flat plate for the wall boundary layer when the equations are solved in the Cartesian coordinate system.

For a turbulent jet discharging to a quiescent ambient, the initial mixing region, indicated in Fig. 7.21, extends to an  $x/D$  of about 5. For jets discharging to a co-flowing stream, the initial mixing region is even longer. This initial mixing region is characterized by the fact that the fluid at the centerline is moving at the jet discharge velocity. Beyond the initial mixing region, the

velocities throughout the jet are influenced by the ambient stream velocity,  $u_e$ . The growth properties of the jet differ in the two regions, initial and main, and when algebraic turbulence models are used, it is expected that somewhat different models (or values for the constants in the models) will be required in the two regions.

Most of the finite-difference schemes discussed in Section 7.3 have been observed to work well for jets. Several methods are described in the *Proceedings of the Langley Working Conference on Free Turbulent Shear Flows* (NASA, 1972). This reference should provide a good starting point for obtaining a background on the special problems associated with achieving accurate predictions for several types of turbulent free-shear flows. Many numerical details can also be found in the works of Hornbeck (1973), Madni and Pletcher (1975a, 1975b, 1977a), and Hwang and Pletcher (1978). This latter work gives the difference equations used in evaluating the fully implicit, Crank-Nicolson implicit, DuFort-Frankel, Larkin alternating direction explicit (ADE), Saul'yev ADE, and Barakat and Clark ADE methods for the round jet. A useful evaluation of available experimental data on uniform-density turbulent free-shear layers has been provided by Rodi (1975).

The boundary-layer form of the energy equation is also applicable to free-shear flows. For a heated jet discharging vertically into a quiescent ambient, with or without thermal stratification, the trajectory of the jet is straight, and no special difficulties arise with the boundary-layer model. For the heated jet discharging at other angles or discharging at any angle with a cross flow, the jet is expected to follow a curved trajectory. Such flows have been treated by solving the fully 3-D Navier-Stokes equations by Patankar et al. (1977) and others and by more approximate parabolic finite-difference models that assume the flow remains axisymmetric (Madni and Pletcher, 1977b; Hwang and Pletcher, 1978). In these latter axisymmetric models, the momentum equation in the transverse direction is treated in a lumped manner, which yields an ODE for the angle between the tangent to the trajectory of the jet centerline and the horizontal direction. This approach requires only slightly more computational effort than solving the axisymmetric boundary-layer equations and gives surprisingly good agreement with experimental measurements, especially with regard to the trajectory of the jet.

No finite-difference algorithms will be provided in this section, since the procedures discussed in Section 7.3 can be adapted to free-shear flows in a straightforward manner. However, one numerical anomaly that sometimes occurs in the prediction of jets discharging to an ambient at rest is worth mentioning. For this case, some schemes are unable to correctly predict  $u$  to asymptotically approach the free stream velocity of zero. The problem is thought to be related to the treatment of the coefficients of the convective terms and the procedures used to locate the outer boundary. The difficulty is most evident if the coefficients are lagged. It is commonplace to overcome this problem in a practical manner by letting  $u_e$  be a small positive velocity of the order of 1-3% of the jet centerline velocity. Reports in the literature claim that this approximation does

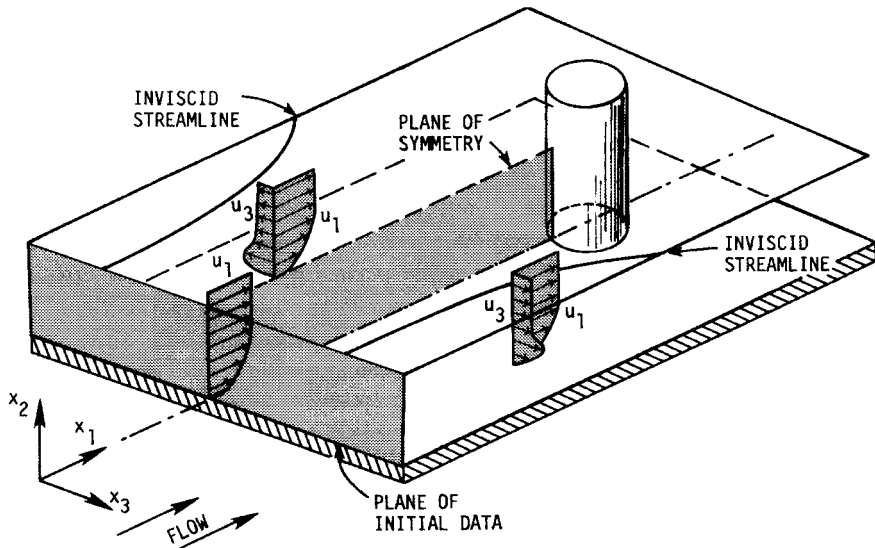


Figure 7.22 Example of subsonic three-dimensional boundary-layer flow.

not seriously degrade the accuracy of the calculations. Hornbeck (1973) shows that a satisfactory solution for  $u_e = 0$  can be obtained with implicit methods by iteratively updating the coefficients.

## 7.7 THREE-DIMENSIONAL BOUNDARY LAYERS

### 7.7.1 Introduction

The majority of the flows that occur in engineering applications are 3-D. In this section we will consider finite-difference methods for those 3-D flows that are “thin” (i.e., with large velocity gradients) in only one coordinate direction. Such flows are sometimes referred to as “boundary sheets.” Many flows occurring in applications are of this type. These are predominantly external flows. Examples include much of the viscous portion of the flow over wings and general aerodynamic bodies.

An example of a 3-D boundary-layer flow is illustrated in Fig. 7.22. The presence of the cylinder alters the pressure field, causing the inviscid flow streamlines to turn as indicated qualitatively in the figure. In accordance with the equations of motion, a component of the pressure gradient (responsible for the turning) is directed away from the center of curvature of the inviscid flow streamlines. Because the viscous layer is thin, this pressure gradient does not change in the direction normal to the surface. As a result, the velocity vector rotates toward the center of curvature of the inviscid streamlines as we move down within the boundary layer. This occurs because the pressure gradient

remains fixed but the inertia of the fluid decreases as we move nearer the wall. This requires that the radius of streamline curvature decrease as we move in the normal direction toward the wall in the boundary layer. Thus the crossflow component of velocity will generally reach a maximum at some point within the boundary layer, as indicated in Fig. 7.22. This pressure-induced "cross flow" is referred to as a secondary flow in some applications and is responsible for such phenomena as the transport of sand toward the inside bank of a curved riverbed and the migration of tea leaves toward the center (near the bottom) of a stirred cup of tea.

Another interesting example of 3-D boundary-layer flow occurs on bodies of revolution at incidence. Such flows on a prolate spheroid, for example, have been studied extensively by several investigators, including Wang (1974, 1975), Blottner and Ellis (1973), Patel and Choi (1979), and Cebeci et al. (1979a).

The 3-D boundary-layer equations are not applicable to flows near the intersection of two surfaces (for example, near wing-body junctions and corners in channels) because stress gradients in two directions are important in those regions. Other reduced forms of the Navier-Stokes equations can be used to treat the flow near corners. These are discussed in Chapter 8.

The subject of 3-D boundary layers will not be covered in great detail here. Instead, we will outline the general numerical strategy required for the solution of the problem posed by these equations, making use of the material developed in earlier sections for the 2-D boundary-layer equations. Several new considerations arise with the 3-D problem, and these will be emphasized.

### 7.7.2 The Equations

The 3-D boundary-layer equations were presented in Chapter 5 in Cartesian coordinates [Eqs. (5.120)-(5.123)] and in body intrinsic orthogonal curvilinear coordinates [Eqs. (5.124)-(5.128)]. For certain special conditions (the laminar supersonic flow over a cone at incidence being one of them), the number of independent variables can be reduced from three to two. Special cases of this sort will not be discussed here.

The Cartesian coordinate system can be used for flows over developable surfaces (those that can be formed by bending a plane without stretching or shrinking), including of course, the special case of a flat surface. Curvilinear systems are required for flows over more general bodies. A few studies have been made using a curvilinear coordinate system coinciding with the inviscid streamlines (see Cebeci et al., 1973). However, most 3-D boundary-layer computations have been made with coordinate systems related to the geometry of the surface. Even with a body-oriented coordinate system, choices remain in the selection of the coordinate axes. Blottner (1975b) provides a review of the coordinate systems that have been used for 3-D flows.

The 3-D boundary-layer equations presented in Chapter 5 are singular at the origin at the  $x_1$  coordinate. This singularity is of the same type as found at the leading edge of a flat plate in 2-D flow (see Section 7.3.7). Several

investigators have satisfactorily used the equations in this form both for flows in the Cartesian coordinate system (Klinksiek and Pierce, 1973) and for more complex flows over axisymmetric bodies (Wang, 1972; Patel and Choi, 1979). These authors have generally used a separate procedure to generate a satisfactory stagnation point solution before utilizing their 3-D solution scheme.

It is also quite common to eliminate the singular behavior of the equations by use of a suitable dependent variable transformation. No single transformation has proven optimum for all flows. Blottner (1975b) discusses several that have been used for specific problems. An example transformation will be presented here that will remove the singularity at the origin of  $x_1$  and will permit the stagnation point profiles to be obtained from the solution of the ODEs that remain when  $x_1 = 0$ . The transformed equations will permit the solution to be advanced from the stagnation point in a smooth and systematic manner. For laminar flows the boundary layer will tend to have a nearly uniform thickness in the transformed coordinates.

We first note that the boundary-layer equations revert to the Euler equations at the outer edge of the boundary layer, where the viscous terms vanish and  $\partial u_1/\partial x_2$  and  $\partial u_3/\partial x_2 \rightarrow 0$ . This permits the components of the pressure gradient in Eqs. (5.126) and (5.127) to be written as

$$-\frac{1}{h_1} \frac{\partial p}{\partial x_1} = \frac{\rho u_{1,e}}{h_1} \frac{\partial u_{1,e}}{\partial x_1} + \frac{\rho u_{3,e}}{h_3} \frac{\partial u_{1,e}}{\partial x_3} + u_{1,e} u_{3,e} K_1 - \rho u_{3,e}^2 K_3 \quad (7.104)$$

$$-\frac{1}{h_3} \frac{\partial p}{\partial x_3} = \frac{\rho u_{1,e}}{h_1} \frac{\partial u_{3,e}}{\partial x_1} + \frac{\rho u_{3,e}}{h_3} \frac{\partial u_{3,e}}{\partial x_3} - u_{1,e}^2 K_1 + \rho u_{1,e} u_{3,e} K_3 \quad (7.105)$$

where  $u_{1,e}(x_1, x_3)$  and  $u_{3,e}(x_1, x_3)$  are given by the inviscid flow solution over the body. The subscript  $e$  denotes quantities evaluated at the outer edge of the boundary layer.

Let us assume that the Reynolds stresses for a turbulent flow will be evaluated by a viscosity model. That is, let

$$-\overline{\rho u_1' u_2'} = \mu_T \frac{\partial u_1}{\partial x_2} \quad -\overline{\rho u_3' u_2'} = \mu_T \frac{\partial u_3}{\partial x_2}$$

$$-\rho c_p \overline{u_2' T'} = k_T \frac{\partial T}{\partial x_2} \quad \frac{\mu_T c_p}{k_T} = \text{Pr}_T$$

$$\bar{\mu} = \mu_T + \mu$$

The model for  $\mu_T$  may be simple or complex; no assumption about the complexity of  $\mu_T$  is made at this time. The equations remain valid for laminar flow where  $\bar{\mu} = \mu$ .

It is convenient to introduce nondimensional variables for velocity components defined by

$$F = \frac{u_1}{u_{1,e}} \quad G = \frac{u_3}{W_e} \quad I = \frac{H}{H_e}$$

where  $W_e$  will be designated below as either  $u_{1,e}$  or  $u_{3,e}$ .

We now let  $x = x_1, z = x_3,$  and

$$\eta = \left[ \frac{u_{1,e}}{x(\rho\mu)_e} \right]^{1/2} \int_0^{x_2} \rho dx_2$$

Using the chain rule for differentiation, derivatives with respect to the original independent variables can be replaced according to

$$\begin{aligned} \frac{\partial}{\partial x_1} &= \frac{\partial}{\partial x} + \frac{\partial \eta}{\partial x} \frac{\partial}{\partial \eta} \\ \frac{\partial}{\partial x_2} &= \frac{\partial \eta}{\partial x_2} \frac{\partial}{\partial \eta} = \left[ \frac{u_{1,e}}{x(\rho\mu)_e} \right]^{1/2} \rho \frac{\partial}{\partial \eta} \\ \frac{\partial}{\partial x_3} &= \frac{\partial}{\partial z} + \frac{\partial \eta}{\partial z} \frac{\partial}{\partial \eta} \end{aligned}$$

Making the indicated substitutions permits Eqs. (5.125)-(5.128) to be written as follows:

continuity:

$$\begin{aligned} \frac{x}{h_1 h_3} \frac{\partial(h_3 F)}{\partial x} + \frac{F}{2h_1} (1 + \beta_1) + \frac{\partial V}{\partial \eta} + \frac{1}{h_1 h_3 [(\rho\mu)_e u_{1,e}/x]^{1/2}} \\ \times \frac{\partial}{\partial z} \left\{ \frac{h_1 W_e G}{u_{1,e}} [x u_{1,e} (\rho\mu)_e]^{1/2} \right\} = 0 \end{aligned} \tag{7.106}$$

x momentum:

$$\begin{aligned} \frac{x F}{h_1} \frac{\partial F}{\partial x} + V \frac{\partial F}{\partial \eta} + \underbrace{\frac{x G}{h_3} \frac{\partial F}{\partial z}}_{(1)} + \underbrace{FGxK_1}_{(2)} - \underbrace{xG^2K_3}_{(3)} \\ = \beta_1 \left( \theta - \underbrace{F^2}_{(4)} \right) + \beta_2 \left( \frac{\theta u_{3,e}}{u_{1,e}} - \underbrace{FG}_{(5)} \right) \\ + \theta \left( \frac{xu_{3,e}K_1}{u_{1,e}} - \frac{xu_{3,e}^2K_3}{u_{1,e}^2} \right) + \frac{\partial}{\partial \eta} \left[ \frac{\rho\bar{\mu}}{(\rho\mu)_e} \frac{\partial F}{\partial \eta} \right] \end{aligned} \tag{7.107}$$

z momentum:

$$\begin{aligned} \frac{x F}{h_1} \frac{\partial G}{\partial x} + V \frac{\partial G}{\partial \eta} + \frac{x G}{h_3} \frac{\partial G}{\partial z} + xFGK_3 - xF^2K_1 \\ = \theta \left( \beta_3 + \beta_4 + \frac{xK_3 u_{3,e}}{u_{1,e}} - xK_1 \right) - \beta_5 GF - \beta_6 G^2 + \frac{\partial}{\partial \eta} \left[ \frac{\rho\bar{\mu}}{(\rho\mu)_e} \frac{\partial G}{\partial \eta} \right] \end{aligned} \tag{7.108}$$

energy:

$$\begin{aligned} \frac{xF}{h_1} \frac{\partial I}{\partial x} + V \frac{\partial I}{\partial \eta} + \frac{xGW_e}{h_3 u_{1,e}} \frac{\partial I}{\partial z} \\ = -\beta_7 FI - \frac{\beta_8 GW_e I}{u_{1,e}} + \frac{\partial}{\partial \eta} \left\{ \left( \frac{\mu}{Pr} + \frac{\mu_T}{Pr_T} \right) \frac{\rho}{(\rho\mu)_e} \frac{\partial I}{\partial \eta} \right. \\ \left. + \frac{\rho u_{1,e}^2 F}{H_e (\rho\mu)_e} \left[ \mu \left( 1 - \frac{1}{Pr} \right) + \mu_T \left( 1 - \frac{1}{Pr_T} \right) \right] \frac{\partial F}{\partial \eta} \right. \\ \left. + \frac{\rho W_e^2 G}{H_e (\rho\mu)_e} \left[ \mu \left( 1 - \frac{1}{Pr} \right) + \mu_T \left( 1 - \frac{1}{Pr_T} \right) \right] \frac{\partial G}{\partial \eta} \right\} \quad (7.109) \end{aligned}$$

where

$$\begin{aligned} V &= \rho \tilde{u}_2 \left[ \frac{x}{u_{1,e} (\rho\mu)_e} \right]^{1/2} + \frac{xF}{h_1} \frac{\partial \eta}{\partial x} + \frac{xGW_e}{h_3 u_{1,e}} \frac{\partial \eta}{\partial z} \\ \theta &= \frac{\rho_e}{\rho} & \beta_1 &= \frac{x}{h_1 u_{1,e}} \frac{\partial u_{1,e}}{\partial x} \\ \beta_2 &= \frac{x}{h_3 u_{1,e}} \frac{\partial u_{1,e}}{\partial z} & \beta_3 &= \frac{x}{h_1 W_e} \frac{\partial u_{3,e}}{\partial x} \\ \beta_4 &= \frac{x u_{3,e}}{W_e h_3 u_{1,e}} \frac{\partial u_{3,e}}{\partial z} & \beta_5 &= \frac{x}{W_e h_1} \frac{\partial W_e}{\partial x} \end{aligned}$$

The metrics and geodesic curvatures of the surface coordinate lines are as defined in Chapter 5.

$$\beta_6 = \frac{x}{h_3 u_{1,e}} \frac{\partial W_e}{\partial z} \quad \beta_7 = \frac{x}{h_1 H_e} \frac{\partial H_e}{\partial x} \quad \beta_8 = \frac{x}{h_3 H_e} \frac{\partial H_e}{\partial z}$$

An equation of state,  $\rho = \rho(p, T)$ , is needed to close the system of equations for a compressible flow. Several terms in Eq. (7.107) have been numbered for future reference.

The usual boundary conditions are

$$\eta = 0:$$

$$V = F = G = 0 \quad I = I(x, 0, z)$$

or

$$\left. \frac{\partial I}{\partial \eta} \right)_{\eta=0} = Q(x, 0, z)$$

$$\eta \rightarrow \infty:$$

$$F = G = 1 \quad G = \frac{u_{3,e}}{W_e}$$

where  $Q(x, 0, z)$  is a specified function related to the wall heat flux. In addition, initial distributions of  $F$ ,  $G$ , and  $I$  must be provided. Distributions of  $u_{1,e}$ ,  $u_{3,e}$ , and  $H_e$  are also required.

The question of initial conditions requires careful consideration. Examination of the 3-D boundary-layer equations in the original orthogonal curvilinear coordinates prior to the transformation indicated above (or for that matter, in Cartesian coordinates) indicates that the roles of the  $x_1$  and  $x_3$  coordinates are interchangeable; that is, the equations are symmetric with respect to the interchange of  $x_1$  and  $x_3$  coordinates. As long as both  $u_1$  and  $u_3$  are positive, no single coordinate direction emerges as the obvious "marching" direction from considering the equations alone. Since first derivatives of  $u_1$ ,  $u_3$ , and  $H$  appear with respect to both  $x_1$  and  $x_3$ , it is expected that initial data should be provided in two intersecting planes to permit marching the dependent variables in both the  $x_1$  and  $x_3$  directions. The correct (permissible) marching direction is dictated by the zone-of-dependence principle, which will be discussed later. For now, we will proceed under the assumption that it is possible to march the solution in either the  $x_1$  or  $x_3$  directions and that initial data are needed on two intersecting planes. It is generally easy to determine a "main" flow direction from considerations of the body geometry and the direction of the oncoming stream. In defining  $\eta$  above, we have already assumed that the  $x$  or  $x_1$  coordinates are in this main flow direction and the  $x_3$  or  $z$  coordinates are in the crossflow direction. We will first discuss the determination of initial distributions of  $F$ ,  $G$ , and  $I$  in the  $z, \eta$  plane, which will provide information appropriate for marching the solution in the  $x$  direction.

If the origin of the  $x$  coordinate is taken at the stagnation point (or line in some flows), the momentum and energy equations reduce to ODEs, which can be solved with the continuity equation to provide the necessary initial conditions in one plane. For the flow illustrated in Fig. 7.22, the appropriate form of the equations is obtained by simply neglecting all terms multiplied by  $x$  (which becomes equal to zero). This starting condition is similar to the flow at the leading edge of a sharp flat plate. On blunt bodies having a true stagnation point,  $u_{1,e}$  and  $u_{3,e}$  are known (Howarth, 1951) to vary linearly with  $x$  in the stagnation region. Thus, some of the terms that vanish for the sharp leading edge starting condition now have a nonzero limiting value as  $x \rightarrow 0$  for blunt bodies. Blottner and Ellis (1973) discuss the stagnation point formulation in detail for incompressible flow.

In most 3-D boundary-layer flows, it is possible to compute initial distributions of  $F$ ,  $G$ , and  $I$  (and  $u_1$ ,  $u_3$ , and  $H$  when the untransformed curvilinear system is used) on a second intersecting plane by solving the PDEs on a *plane of symmetry*. The formulation of the plane-of-symmetry problem will be discussed below, but first, it is worth mentioning that in a few problems it is not possible to identify a plane of symmetry. An example of this is the sharp spinning cone considered by Dwyer (1971) and Dwyer and Sanders (1975). Controversy erupted over the question as to whether this flow can be treated as an initial value problem with the boundary-layer equations (Lin and Rubin,

1973a). It appears that use of difference schemes that lag the representation of the crossflow derivatives (Dwyer and Sanders, 1975; Kitchens et al., 1975) permits the solution to be marched away from a single initial data plane into those regions not forbidden by the zone-of-dependence principle. Such difference representations as well as the zone-of-dependence principle are discussed in Section 7.7.3.

The plane of symmetry is indicated in Fig. 7.22 for the flow over a flat plate with an attached cylinder. Flows over nonspinning bodies of revolution at incidence typically have both a windward and a leeward plane of symmetry, the former being most commonly used to develop the required second plane of initial data. Along the plane of symmetry,

$$G = \frac{\partial F}{\partial z} = \frac{\partial V}{\partial z} = \frac{\partial^2 G}{\partial z^2} = 0 \quad (7.110)$$

The inviscid flow and fluid properties are also symmetric about the plane of symmetry. Using Eq. (7.110), the  $x$ -momentum and energy equations reduce to 2-D form. The problem remains 3-D, however, because the cross-derivative term in the continuity equation does *not* vanish on the plane of symmetry. Expanding out the cross-derivative term in Eq. (7.106) and invoking the symmetry conditions, Eq. (7.110), permits the continuity equation to be written as

$$\frac{x}{h_1 h_3} \frac{\partial(h_3 F)}{\partial x} + \frac{F}{2h_1} (1 + \beta_1) + \frac{\partial V}{\partial \eta} + \frac{x G_z}{h_3 u_{1,e}} \frac{\partial u_{3,e}}{\partial z} = 0 \quad (7.111)$$

where

$$G_z = \frac{\partial u_3 / \partial z}{\partial u_{3,e} / \partial z}$$

The  $z$ -momentum equation in the form given by Eq. (7.108) provides no useful information because  $G = 0$  everywhere in the plane of symmetry. However, differentiating the  $z$ -momentum equation with respect to  $z$  and again invoking the symmetry conditions provides an equation that can be solved for the required values of  $G_z$ :

$$\begin{aligned} \frac{x F}{h_1} \frac{\partial G_z}{\partial x} + V \frac{\partial G_z}{\partial \eta} + x F G_z K_3 = \beta_9 (\theta - F G_z) + \beta_{10} (\theta - G_z^2) + x \theta K_3 \\ + \frac{\partial}{\partial \eta} \left[ \frac{\rho \bar{\mu}}{(\rho \mu)_e} \frac{\partial G_z}{\partial \eta} \right] \end{aligned} \quad (7.112)$$

Defining  $W_{e,z} = \partial u_{3,e} / \partial z$ , we can express the parameters  $\beta_9$  and  $\beta_{10}$  as

$$\beta_9 = \frac{x}{h_1 W_{e,z}} \frac{\partial W_{e,z}}{\partial x} \quad \beta_{10} = \frac{x W_{e,z}}{h_3 u_{1,e}}$$

$W_{e,z}$  is to be obtained from the inviscid flow solution. Equation (7.112) for  $G_z$  has the same general form as the original  $z$ -momentum equation and can be solved by marching in the  $x$  direction along the plane of symmetry.

The arbitrary parameter  $W_e$  used in nondimensionalizing the crossflow velocity component is chosen to avoid singular behavior. We take  $W_e = u_{3,e}$  at the stagnation point and along the plane of symmetry, and  $W_e = u_{1,e}$  elsewhere.

### 7.7.3 Comments on Solution Methods for Three-Dimensional Flows

The 3-D boundary-layer problem involves several complicating features and considerations not present in the 2-D flows treated thus far. The inviscid flow solution required to provide the pressure gradient input for the boundary-layer solution is often considerably more difficult to obtain than for 2-D flows. Generation of the metrics and other information needed to establish the curvilinear-body-oriented coordinate system can also be a significant task for complex bodies. Turbulence models need to be extended to provide representation for the new apparent stress. In addition, the following features require special attention in the difference formulation: (1) implementation of the zone-of-dependence principle, and (2) representation of the crossflow convective derivatives in a manner to permit a stable solution for both positive and negative crossflow velocity components.

The 3-D boundary-layer equations have a hyperbolic character in the  $x$ - $z$  plane, and the mathematical constraint that results is very much like the Courant-Friedrichs-Lewy condition discussed in connection with the wave equation. Major contributions to the formulation and interpretation of the zone of dependence principle for 3-D boundary layers can be found in the work of Raetz (1957), Der and Raetz (1962), Wang (1971), and Kitchens et al. (1975). The principle actually addresses both a zone of dependence and a zone of influence and is sometimes just referred to as the "influence" principle. The dependence part of the principle is the most relevant to the proper establishment of difference schemes and so has been given emphasis here.

If we consider the point labeled P in Fig. 7.23 within a 3-D boundary layer, the influence principle states that the influence of the solution at P is transferred instantaneously by diffusion to all points in the viscous flow on a line (labeled A-B in Fig. 7.23) normal to the surface passing through P and by convection downstream along all streamlines through that point. Normals to the body surface form the characteristic surfaces, and the speed of propagation is infinite in that direction. Disturbances anywhere along A-B are felt instantaneously along the whole line A-B and are carried downstream by *all* streamlines passing through A-B. The positions of the two outermost streamlines through A-B and extending downstream define the lateral extent of the wedge-shaped zone of influence for points on A-B. Events along A-B can influence the flow within the region bounded by the characteristics (lines normal to the wall) through these outermost streamlines. Typically, one outermost streamline is the limiting streamline at the wall and the other is the inviscid flow streamline. The flow along A-B is obviously influenced by the flow upstream, and a *zone of dependence* is defined by the characteristic lines passing through the two outermost streamlines extending upstream. Events at all points within this wedge-shaped

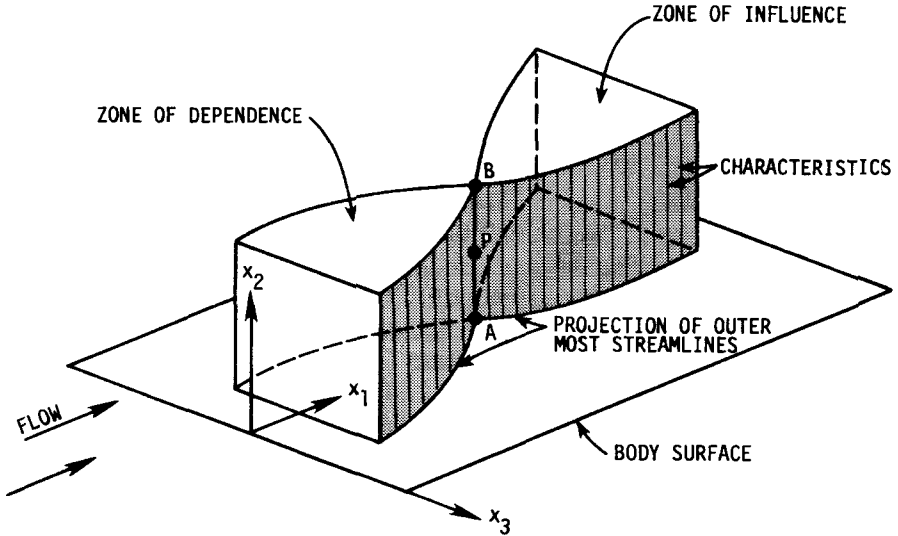


Figure 7.23 Zones of dependence and influence in three-dimensional boundary layers.

region upstream can influence events along A-B. The “outermost” streamlines are those having the maximum and minimum angular displacement from the constant  $x_3$  (or  $z$ ) surface passing through A-B. The zone of dependence then designates the minimum amount of initial data that must be supplied to determine the solution along A-B. These concepts apply to the PDEs. It is important for the difference molecule used along A-B not to exclude information in the zone of dependence; that is, the zone of dependence implied by the difference representation must be at least as large as the zone identified with the PDEs. This has also been shown previously for hyperbolic PDEs and identified as the CFL condition. The exact quantitative statement of the zone-of-dependence principle depends upon the difference molecule employed. For example, using a scheme that represents  $\partial G/\partial z$  centrally (with  $\Delta z$  constant) at the  $n$  marching level as the solution is advanced to the  $n + 1$  level, the zone-of-dependence principle would require that

$$F > 0 \quad \left| \frac{h_1 \Delta x G}{h_3 \Delta z F} \right| \leq 1 \tag{7.113}$$

Equation (7.113) indicates that the local angle made by the streamlines with the plane of constant  $z$  must be contained within the angle whose tangent is given by the mesh parameter  $h_3 \Delta z / (h_1 \Delta x)$ . We would like Eq. (7.113) to be satisfied at a given  $x$  level, with  $\Delta x$  being the increment back upstream. It would be unprofitable to iterate simply to establish the allowable step size, so the usual procedure is to utilize the most recently calculated values of  $G$  and  $F$  to establish the new step size using a safety factor to allow for anticipated

changes in  $G$  and  $F$  over a  $\Delta x$  increment. In using Eq. (7.113) to establish the maximum allowable marching step increment, the inequality should be checked at each internal point at a given  $x$  level before  $\Delta x$  is established for the next step. With the use of certain difference schemes for flows in which  $G$  does not change sign, the zone-of-dependence constraint is automatically satisfied, as will be illustrated below for the 3-D Crank-Nicolson scheme.

Stability is also a concern in 3-D boundary-layer calculations. The presence of the additional convective derivative in the momentum equation generally influences the stability properties of the difference scheme. The stability constraint of a scheme is very likely to change as it is extended from 2-D to 3-D flow. The concept of stability is separate from the concept of the zone of dependence. This point is demonstrated very well in the work of Kitchens et al. (1975). For some schemes the constraint imposed by the zone-of-dependence principle will coincide with the stability constraint determined by the usual von Neumann analysis, but not always. Kitchens et al. (1975) show that for four difference schemes investigated, errors tend to grow whenever the zone-of-dependence principle was violated, but that for some schemes the solution remained very smooth and “stable” in appearance even though the errors were very significant. In other schemes, violation of the zone-of-dependence principle may trigger unstable behavior characterized by large oscillations even when such behavior is not predicted by a stability analysis. It is even possible to devise inherently unstable schemes that satisfy the zone-of-dependence constraint.

A few common difference schemes for 3-D boundary layers will be briefly described. In the following discussion, the indices  $n, j, k$  will be associated with the coordinate directions  $x_1, x_2, x_3$  (or  $x, \eta, z$ ). The solution is being advanced from the  $n$ th marching plane to the  $n + 1$  plane. The solution at the  $n + 1$  level will start at  $k = 1$  (usually on the plane of symmetry), where the equations will be solved for the unknowns for all values of  $j$ . That is, fixing  $n$  and  $k$ , we obtain the solution along a line normal to the wall. Then the  $k$  index is advanced by 1, and the solution is obtained for another “column” of points along the surface normal. Thus the marching (or “sweeping”) at the  $n + 1$  level is in the crossflow direction. In difference representations below, the unknowns will be variables at the  $n + 1, k$  levels.

**Crank-Nicolson scheme.** The 3-D extension of the Crank-Nicolson scheme has been used by several investigators. Its use is restricted to flows in which the crossflow component of velocity does not change sign owing to zone-of-dependence and stability considerations. The difference molecule is centered at  $n + \frac{1}{2}, j, k - \frac{1}{2}$ . Figure 7.24(a) illustrates the molecule as we look down on the flow (i.e., only points in the  $x$ - $z$  plane are shown). The shaded area indicates the approximate maximum zone of dependence permitted by the molecule. The circled point indicates the location of the unknowns, and the  $x$  indicates the center of the molecule. The presence of negative crossflow components of velocity causes this scheme to violate the zone-of-dependence principle because no information is contained in the molecule that would reflect flow conditions in

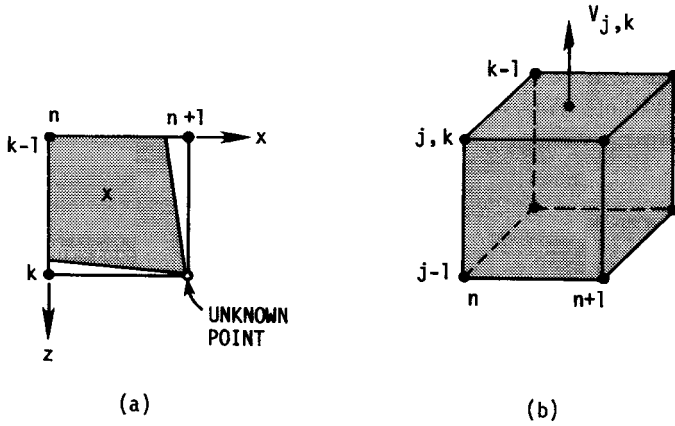


**Figure 7.24** The Crank-Nicolson scheme. (a) The difference molecule projected on the  $x$ - $z$  plane. (b) The control volume for the continuity equation.

the negative coordinate direction as the solution is advanced to the  $n + 1, k$  level. On the other hand, the zone-of-dependence principle imposes no restriction on the size of  $\Delta x$  as long as  $G \geq 0$ , since the molecule spans all possible flow angles for which  $F > 0, G \geq 0$ .

More than one variation of the Crank-Nicolson scheme has been proposed. In the most frequently used version, terms of the form  $\partial/\partial\eta(a \partial\phi/\partial\eta)$  are differenced as for the 2-D Crank-Nicolson scheme but *averaged* between  $k - 1$  and  $k$ . Likewise,  $\partial\phi/\partial x$  and  $\partial\phi/\partial\eta$  terms are represented as for the 2-D Crank-Nicolson scheme but averaged over  $k$  and  $k - 1$ . Derivatives in the crossflow direction [as for example in the term labeled (1) in Eq. (7.107)] are represented by

$$\left. \frac{\partial\phi}{\partial z} \right)_{j, k-1/2}^{n+1/2} \cong \frac{\phi_{j, k}^{n+1} + \phi_{j, k}^n - \phi_{j, k-1}^{n+1} - \phi_{j, k-1}^n}{2 \Delta z}$$

For flows over curved surfaces for which the curvature parameters  $K_1$  and  $K_3$  are nonzero, new terms of the form represented by terms labeled (2) and (3) in Eq. (7.107) must be represented. Similar terms appear in the untransformed equations in orthogonal curvilinear coordinates given in Chapter 5. Terms of this general form, not involving derivatives of the dependent variables, are considered source terms according to the definition given in Section 7.3.1. The terms labeled (4) and (5) in Eq. (7.107) are two additional source terms that arise due to the introduction of the  $F$  and  $G$  variables. These terms, (2)-(5) in Eq. (7.107), require linearization in the difference representations as do the convective terms. Any of the linearization techniques suggested in Section 7.3.3 can be used, although coupling of the equations is not commonly used. The source terms are represented at the center of the difference molecule

$(n + \frac{1}{2}, j, k - \frac{1}{2})$  by appropriate averages of variables at neighboring grid points. As an example, the term labeled (2) in Eq. (7.107) can be represented as

$$(FGxK_1)_{j,k-1/2}^{n+1} \approx x^{n+1/2}(K_1)_{k-1/2}^{n+1/2}(F_{j,k}^n + F_{j,k-1}^n + F_{j,k}^{n-1} + F_{j,k-1}^{n-1}) \times (G_{j,k}^n + G_{j,k-1}^n + G_{j,k-1}^{n+1} + \hat{G}_{j,k}^{n+1})/16 \quad (7.114)$$

The only quantity treated algebraically as an unknown in Eq. (7.114) is  $F_{j,k}^{n-1}$ . The linearization is implemented by treating  $\hat{G}_{j,k}^{n+1}$  algebraically as a known. The value of  $\hat{G}_{j,k}^{n+1}$  can be determined by extrapolation, updated iteratively, or simply lagged, although lagging is not often used for the 3-D boundary-layer equations. Considerable flexibility exists in the way in which the various terms can be linearized. Other source terms appear on the right-hand side of Eq. (7.107), but these do not require linearization. The algebraic formulation for each momentum equation results in a simultaneous system of equations for the unknowns along the  $n + 1, k$  column of points. The coefficient matrix is tridiagonal, so that the Thomas algorithm can be used.

Most current procedures for the 3-D boundary-layer equations solve the continuity equation separately for  $V_{j,k}^{n+1}$  after  $F$  and  $G$  have been determined from the solution to the momentum equations. The difference representation for the continuity equation is usually established by considering a control volume centered about  $(n + \frac{1}{2}, j - \frac{1}{2}, k - \frac{1}{2})$ . Such a control volume is illustrated in Fig. 7.24(b). For  $F$  and  $G$  the average value of these quantities over a face of the control volume is established by taking the average of the quantities at the four corners of the face. Values of  $V$  are only needed at locations  $n + \frac{1}{2}, j, k - \frac{1}{2}$  in the momentum equations. Thus, computational effort is normally saved by simply letting the value of  $V$  determined from the continuity equation be the value at the center of the  $x-z$  planes of the control volume. For computer storage the  $V$  physically considered to be located at  $n + \frac{1}{2}, j, k - \frac{1}{2}$  is usually assigned the subscript  $n + 1, j, k$ . The location of  $V_{j,k}^{n+1}$  is indicated in Fig. 7.24(b), where the labeling usually used for computer storage is employed. Grid schemes in which the dependent variables are evaluated at different locations in the computational domain are usually referred to as "staggered" grids. In this staggered grid, all variables except  $V$  are evaluated at regular grid points. Further examples of staggered grids arise in Chapter 8. The Crank-Nicolson scheme has the potential of being formally second-order accurate  $\{(T. E. = O[(\Delta x)^2, (\Delta \eta)^2, (\Delta z)^2])\}$ . The T.E. may be less favorable, depending on how linearizations and unequal mesh sizes are handled.

**Krause zig-zag scheme.** The Krause (1969) scheme has been widely used for flows in which the crossflow velocity component changes sign. The difference molecule is centered at  $n + \frac{1}{2}, j, k$ , and its projection on the  $x-z$  plane is given in Fig. 7.25(a). The shaded area again denotes the approximate maximum zone of dependence permitted by the molecule. We note that the molecule includes information in both  $z$  directions from point  $n + 1, j, k$  so that, within limits,

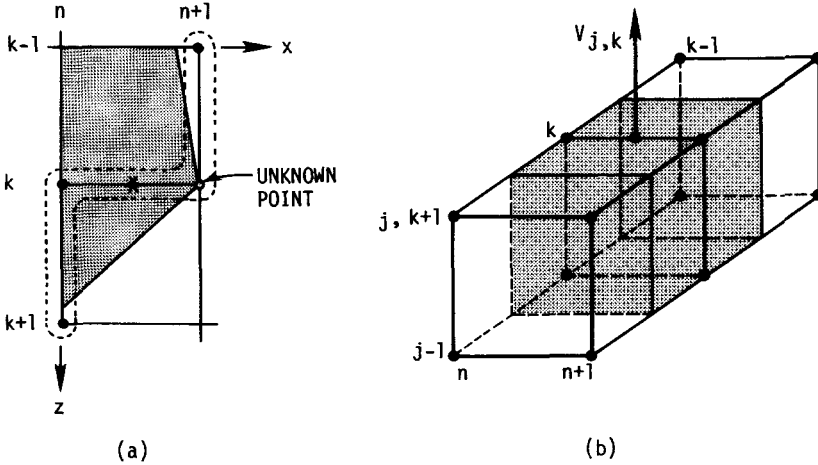


**Figure 7.25** The Krause zig-zag scheme. (a) The difference molecule projected on the x-z plane. (b) The control volume for the continuity equation.

cross flow in both directions is permitted as long as the flow direction remains within the zone of dependence of the molecule. As for the Crank-Nicolson scheme, we observe that no mesh size constraint occurs when  $F > 0$ ,  $G \geq 0$ . However, a constraint is observed when cross flow in the negative z direction occurs. The zone of dependence and the stability constraint for the Krause scheme can be stated as

$$F > 0 \quad \frac{\Delta x h_1 G}{\Delta z h_3 F} \geq -1$$

It should be noted that the permitted flow direction can be altered by changing the aspect ratio,  $\Delta z / \Delta x$ , of the molecule.

The Krause difference representation is somewhat simpler algebraically than the Crank-Nicolson scheme, primarily because most difference representations are only averaged between  $n + 1$  and  $n$ , but *not* between two  $k$  levels. For the Krause scheme, terms of the form  $\partial / \partial \eta (a \partial \phi / \partial \eta)$  and  $\partial \phi / \partial x$  are differenced in the same manner as in the 2-D Crank-Nicolson scheme. Derivatives in the crossflow direction in the momentum equations are differenced using points in the zig-zag pattern denoted by the dashed lines in Fig. 7.25(a). For equal  $\Delta z$  increments this representation can be written

$$\left. \frac{\partial \phi}{\partial z} \right)_{j,k}^{n+1/2} \approx \frac{\phi_{j,k+1}^n - \phi_{j,k}^n + \phi_{j,k}^{n+1} - \phi_{j,k-1}^{n+1}}{2 \Delta z} \tag{7.115}$$

Since the sweep in the z direction is from columns  $(n + 1, k - 1)$  to  $(n + 1, k)$ ,  $\phi_{j,k}^{n+1}$  is the only unknown in Eq. (7.115). The problem of linearization of the algebraic representation is much the same as for the Crank-Nicolson scheme

except that the molecule is more compact because quantities generally only need to be averaged between two grid points instead of four. For example, the term labeled (2) in Eq. (7.107) can be represented as

$$(FGxK_1)_{j,k}^{n+1/2} = \frac{x^{n+1/2} K_{1k}^{n+1/2} (F_{j,k}^n + F_{j,k}^{n+1})(G_{j,k}^n + \hat{G}_{j,k}^{n+1})}{4} \quad (7.116)$$

A tridiagonal system of algebraic equations results from the Krause formulation, which can be solved by the Thomas algorithm.

The difference representation for the continuity equation is established by considering a control volume centered about  $(n + \frac{1}{2}, j - \frac{1}{2}, k)$  as indicated in Fig. 7.25(b). The average value of  $F$  on an  $\eta$ - $z$  face of the control volume can be determined from averaging only in the  $\eta$  direction, since the middle of the plane coincides with a  $k$  level. A zig-zag (or diagonal) average is used to represent  $G$  on an  $x$ - $\eta$  plane. To illustrate this for equal  $\Delta z$  increments, we would represent a term of the form  $\partial(aG)/\partial z$  in the Krause continuity equation as

$$\begin{aligned} \left. \frac{\partial(aG)}{\partial z} \right)_{j-1/2,k}^{n+1/2} \simeq & \left\{ [(aG)_{j,k+1}^n + (aG)_{j-1,k+1}^n + (aG)_{j,k+1}^{n+1} + (aG)_{j-1,k}^{n+1}] \right. \\ & \left. - [(aG)_{j,k}^n + (aG)_{j-1,k}^n + (aG)_{j,k-1}^{n+1} + (aG)_{j-1,k-1}^{n+1}] \right\} / 4 \Delta z \end{aligned} \quad (7.117)$$

The  $V$  determined from the Krause continuity equation is located at the center of the upper  $x$ - $z$  plane of the control volume (at  $n + \frac{1}{2}, j, k$ , but usually stored as  $n + 1, j, k$ ). The storage index is the one indicated in the labeling of Fig. 7.25(b). The truncation error for the Krause scheme is the same as for the Crank-Nicolson scheme. Further details on the Crank-Nicolson and Krause schemes can be found in the work by Blottner and Ellis (1973).

**Some variations.** Two variations on the Krause scheme that have proven to be suitable for both positive and negative crossflow velocity components will be mentioned briefly. Wang (1973) has developed a second-order accurate two-step method that eliminates the need to linearize terms in the momentum equations. As with all multilevel methods, initial data must be provided at two marching levels. This is usually accomplished through the use of some other scheme for one or more steps. The projection of the two-step molecule on the  $x$ - $z$  plane is shown in Fig. 7.26. The shaded area again indicates the approximate zone of dependence permitted by the molecule. Known data on the  $n - 1$  and  $n$  levels are used to advance the solution. The method is implicit and centered at the point  $(n, j, k)$ . Derivatives in the  $x$  and  $z$  direction are represented centrally about  $(n, j, k)$ . Derivatives of the form

$$\frac{\partial}{\partial \eta} \left( a \frac{\partial \phi}{\partial \eta} \right)$$

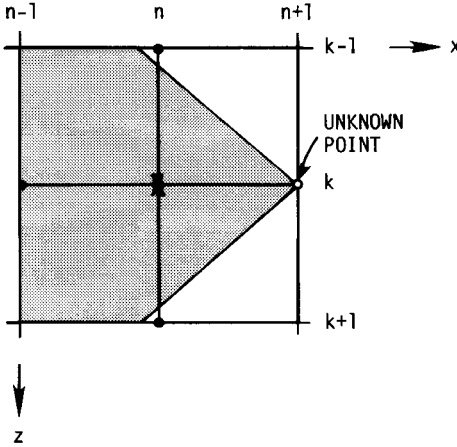


Figure 7.26 The two-step scheme.

are represented at  $(n + 1, j, k)$  and  $(n - 1, j, k)$  and averaged. The zone-of-dependence constraint is given by

$$F > 0 \quad \left| \frac{\Delta x h_1 G}{\Delta z h_3 F} \right| \leq 1$$

No formal stability constraint is observed so long as  $F > 0$ .

Kitchens et al. (1975) compared the properties of four schemes for 3-D boundary layers and found that their scheme D had quite favorable error growth and stability properties. In addition, the results seemed relatively insensitive to violations in the zone-of-dependence constraint. The projection of this difference molecule on the  $x$ - $z$  plane is shown in Fig. 7.27. The shaded area indicates the approximate zone of dependence for the method. The method is implicit. Derivatives in the  $x$  direction are represented centrally about  $(n + \frac{1}{2}, j, k)$  with one very unique twist that converts an otherwise unstable scheme into a stable one. In the representation for  $\partial\phi/\partial x$ , values needed at  $n, j, k$  are replaced by the average of  $\phi_{j,k+1}^n$  and  $\phi_{j,k-1}^n$ . Thus for equal increments we would use

$$\frac{\partial\phi}{\partial x} \approx \frac{\phi_{j,k}^{n+1} - 0.5(\phi_{j,k+1}^n + \phi_{j,k-1}^n)}{\Delta x}$$

Derivatives in the crossflow direction are represented centrally about  $(n, j, k)$ . Derivatives of the form  $\partial/\partial\eta(a \partial\phi/\partial\eta)$  are represented at  $(n + 1, j, k)$  and  $(n, j, k)$  and averaged. The T.E. stated by Kitchens et al. (1975) is  $O[\Delta x, (\Delta z)^2/\Delta x, (\Delta\eta)^2, (\Delta z)^2]$ . The zone-of-dependence constraint for this method is the same as for the two-step method. In this case, the stability restriction is the same as the zone-of-dependence constraint.

**Inverse methods and viscous-inviscid interaction.** McLean and Randall (1979) reported the use of a viscous-inviscid interaction in 3-D for computing flows

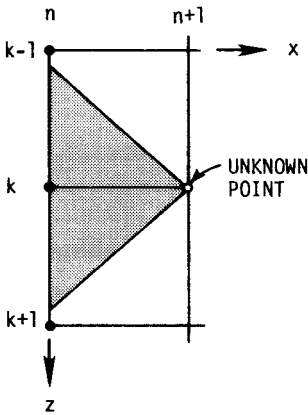


Figure 7.27 Scheme D (Kitchens et al., 1975).

over wings. The boundary-layer equations were solved in a direct manner in their work. The computation of the displacement surface needed to interface with the inviscid solution is somewhat more complex in 3-D. The simple Hilbert integral small-disturbance correction [Eq. (7.76)] for an inviscid flow has been extended to 3-D (Edwards, 1986), although the inviscid flow may also be recomputed in its entirety for each iterative pass. However, rather than recomputing the inviscid flow for the body modified by the displacement surface, it is frequently advantageous to maintain the same body in the inviscid calculation and represent the effects of the viscous flow by a distribution of sources and sinks (Lighthill, 1958). In the full inviscid potential flow solution, the sources and sinks (related to space derivatives of the displacement thicknesses) are represented as normal velocity boundary conditions (blowing or suction) at the body surface. This formulation offers an advantage when direct methods are used to solve the elliptic PDEs for the subsonic flow, in that the influence matrix and its inverse need not be recomputed for each interaction iteration.

A number of investigators (for example, Delery and Formery, 1983; Edwards and Carter, 1985; Edwards, 1986) have reported success in using an inverse procedure for solving the 3-D incompressible boundary-layer equations. Such a capability is the first step toward the development of 3-D viscous-inviscid interaction procedures that could permit computation of separated flows.

As in two dimensions, the 3-D inverse procedure treats the pressure as unknown. Since the direct solution of the 3-D boundary-layer system requires specification of two components of the pressure gradient, it is not surprising that an inverse solution method requires specification of two alternative functions. Edwards and Carter (1985) evaluated the suitability of specifying four different combinations of parameters and found that three of them worked satisfactorily but a fourth led to the formulation of an elliptic system that allowed departure (exponentially growing) solutions when solved in a forward marching manner. Examples of boundary condition combinations that worked included the specifi-

cation of both integral parameters,

$$\delta_1 = \int_0^\infty \left(1 - \frac{u}{u_e}\right) dy \quad \delta_2 = \int_0^\infty \left(\frac{w_e - w}{u_e}\right) dy$$

and  $\delta_1$  and the crossflow component of the edge velocity  $w_e$ . Three-dimensional viscous-inviscid interaction schemes based on an inverse treatment of the boundary-layer equations apparently have not been widely used in applications, although Edwards (1986) demonstrated that such a strategy is workable. This may be partly due to the inherent complexity of the two-solver approach and partly due to advances in methods based on the solution of a single set of governing equations, which have been enabled by rapid progress in computer technology.

### 7.7.4 Example Calculations

Here we briefly present some example computational results for the sample 3-D flow illustrated in Fig. 7.24. The results were obtained by application of the Krause scheme to Eqs. (7.106)–(7.108) for an incompressible laminar flow. The Crank-Nicolson scheme was used at the last  $z$  station to permit the calculation to end without requiring information from the  $k + 1$  level. Computed results for this flow have been reported in the literature by several investigators (see, for example, Cebeci, 1975). For this flow, the inviscid velocity distribution is given by

$$u_{1,e} = u_\infty \left(1 + a^2 \frac{\gamma_2}{\gamma_1^2}\right) \quad u_{3,e} = -2u_\infty a^2 \frac{\gamma_3}{\gamma_1^2}$$

where  $u_\infty$  is the reference free stream velocity and  $\gamma_1 = (x - x_0)^2 + z^2$ ,  $\gamma_2 = -(x - x_0)^2 + z^2$ , and  $\gamma_3 = (x - x_0)z$ . The parameter  $x_0$  is the distance of the cylinder axis from the leading edge,  $a$  is the cylinder radius, and  $x$  and  $z$  denote the distance measured from the leading edge and plane of symmetry, respectively. It is also useful to know  $\partial u_{3,e} / \partial z$  along the plane of symmetry:

$$\left. \frac{\partial u_{3,e}}{\partial z} \right)_{z=0} = \frac{-2u_\infty a^2}{(x - x_0)^3}$$

Calculations were made for  $u_\infty = 30.5$  m/s,  $a = 0.061$  m,  $x_0 = 0.457$  m using  $\Delta x = 0.0061$  m,  $\Delta \eta = 0.28$ , and  $\Delta z = 0.0061$  m. Typical velocity profiles for this flow are shown in Fig. 7.28. In particular, we note that the crossflow velocity component reaches a maximum within the inner one-third of the boundary layer. The variation in the flow angle (in  $x$ - $z$  plane) with distance from the wall is shown in Fig. 7.29(a). The maximum skewing is observed to occur close to the wall. The velocity vector is seen to rotate through an angle of about  $13^\circ$  along the surface normal. This corresponds to the included angle made by the zone of dependence at this location (see Fig. 7.23). The variation in the skin-friction coefficient is shown in Fig. 7.29(b). The presence of the cylinder causes the flow

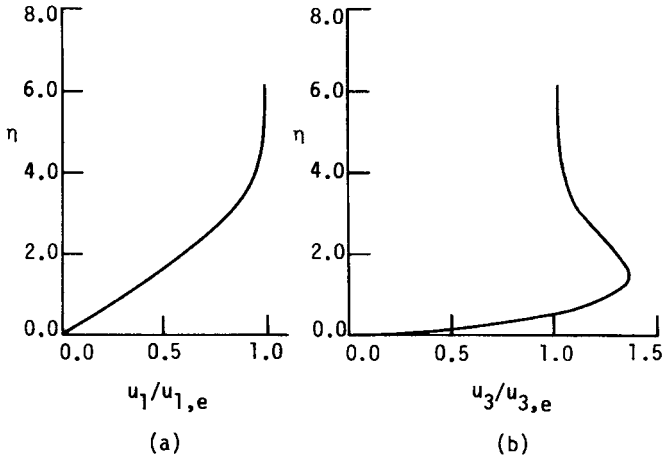


**Figure 7.28** Velocity profiles at  $x = 0.219$  m,  $z = 0.079$  m, for an example three-dimensional flow over a flat plate with an attached cylinder. (a) Streamwise velocity distribution. (b) Crossflow velocity distribution.

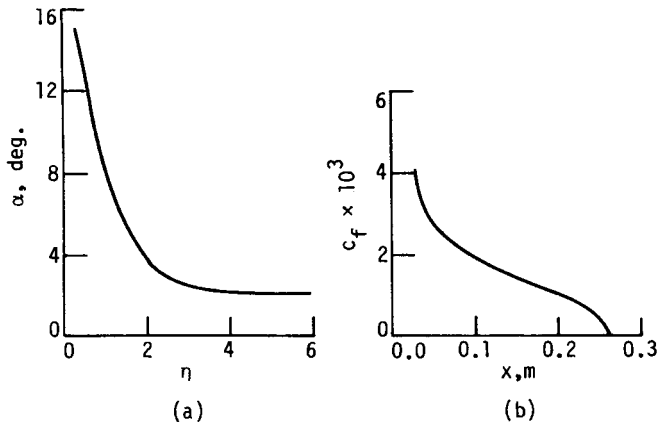


**Figure 7.29** Example of three-dimensional boundary-layer flow over a flat plate with an attached cylinder. (a) Variation of flow angle (measured from  $x$ - $\eta$  plane) along the surface normal at  $x = 0.219$  m,  $z = 0.079$  m. (b) Variation of skin-friction coefficient along plane of symmetry.

on the plane of symmetry to separate at  $x \approx 0.26$  m. Conventional boundary-layer calculation methods can proceed no farther along the plane of symmetry because both the  $x$  and  $z$  components of velocity have vanished.

### 7.7.5 Additional Remarks

Only a few representative difference schemes for 3-D boundary layers have been discussed in this chapter. Many other useful procedures have been suggested. Several of these are discussed by Wang (1974), Kitchens et al. (1975), and Blottner (1975b). Cebeci (1975) has extended the box scheme to 3-D flows, and Cebeci et al. (1979a) have implemented a zig-zag feature that permits the calculation of 3-D flows in which the crossflow velocity component changes sign. No single scheme has emerged to date as being superior for all flows. Several investigators have found the need to employ more than one scheme in order to cover all regions efficiently in some flows. The Krause zig-zag scheme is recommended as a reasonable starting point for the development of a 3-D boundary-layer finite-difference procedure. After the Krause procedure is well in hand, the user should be encouraged to explore the possible advantages offered by the several variations that have been suggested.

Turbulence modeling is certainly an important concern in 3-D flows. Most 3-D turbulent calculations to date have assumed that the turbulent viscosity is a scalar. Measurements tend to support the view that in the outer portion of the flow the apparent viscosity in a Boussinesq evaluation of the stress in the crossflow direction may be substantially less (by a factor  $\sim 0.4-0.7$ ) than the viscosity for the apparent stress in the streamwise direction. Further research on turbulence modeling for 3-D flows would seem desirable.

The most successful application of 3-D boundary-layer theory has probably been for flows over wings. Reasonably refined computer programs have been documented for this application (Cebeci et al., 1977; McLean and Randall, 1979). Several papers and reports in the literature of a review or general nature should prove useful in obtaining a broad view of the status of predictions in 3-D boundary layers. The list includes Wang (1974, 1975), Bushnell et al. (1976), Blottner (1975b), and Kitchens et al. (1975).

## 7.8 UNSTEADY BOUNDARY LAYERS

It is frequently desirable to predict unsteady boundary-layer behavior, especially in the design of flight vehicles. Numerical aspects of this problem are reasonably well understood; however, challenging aspects of turbulence modeling remain. We will limit our discussion to 2-D unsteady boundary layers, although many of the concepts carry over to the 3-D case.

The unsteady 2-D boundary-layer equations appear as Eqs. (5.116)-(5.118) in Chapter 5. They differ from their steady flow counterparts only through the appearance of the term  $\rho \partial u / \partial t$  in the momentum equation and  $\partial \rho / \partial t$  in the

continuity equation. The unsteady equations are also parabolic but with time as the marching parameter. Values of  $u$ ,  $v$ ,  $H$ , and fluid properties must be stored at grid points throughout the flow domain. Initial values of  $u$ ,  $v$ , and  $H$  must be specified for all  $x$  and  $y$ . Boundary conditions may vary with time. The usual boundary conditions are as follows:

1. At  $x = x_0$ ,  $u(t, x_0, y)$  and  $H(t, x_0, y)$  are prescribed for all  $y$  and  $t$ .
2. At  $y = 0$ ,  $u(t, x, 0) = v(t, x, 0) = 0$ .
3. The  $\lim_{y \rightarrow \infty} u(t, x, y) = u_e(t, x)$ .

The main objective is to develop computational procedures that will provide accurate and stable solutions when flow reversal ( $u < 0$ ) occurs. In this respect, the unsteady 2-D boundary-layer problem is similar to the 3-D steady problem, where the concern was to identify methods that would permit flow reversal in the crossflow direction. When flow reversal occurs in the unsteady problem, it is crucial to employ a difference representation that permits upstream influence. This principle has not been formulated in terms of a zone-of-dependence concept for the 2-D unsteady boundary-layer equations, but to ignore the possibility of information being convected in the flow direction is unacceptable. Furthermore, the steady boundary-layer equations are parabolic in the  $x$  direction, which again requires that information move in the direction of the  $x$  component of velocity; otherwise it would not be possible to achieve the correct steady-state solution from the transient formulation.

An adaptation of the zig-zag representation introduced by Krause for the 3-D boundary-layer equations has been frequently used to represent  $\partial u / \partial x$  when flow reversal is present. This representation is illustrated in Fig. 7.30. Using the mesh notation introduced in the figure, the zig-zag representation of the streamwise derivative for equal  $\Delta x$  increments is

$$\frac{\partial u}{\partial x} \approx \frac{u_{i,j}^{n+1} - u_{i-1,j}^{n+1} + u_{i+1,j}^n - u_{i,j}^n}{2 \Delta x} \tag{7.118}$$

The  $j$  index is associated with the normal coordinate. The representation of Eq. (7.118) can be used with a difference scheme centered at  $n + \frac{1}{2}, i, j$ , which can

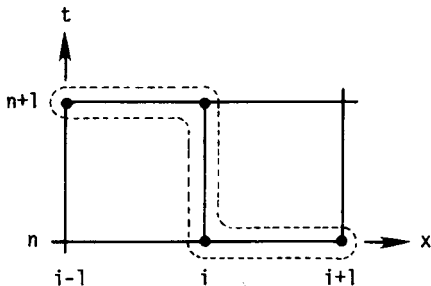


Figure 7.30 The zig-zag representation for streamwise derivatives in unsteady flows.

be thought of as the unsteady 2-D boundary-layer version of the Krause scheme for 3-D boundary layers.

Concepts from the zig-zag box scheme for 3-D boundary layers have also been used to develop a zig-zag box representation for unsteady boundary layers. This scheme also appears applicable when flow reversal is present (Cebeci et al., 1979a).

Other types of upwind differencing have been found to work satisfactorily with flow reversal by Telionis et al. (1973) and Murphy and Prenter (1981). The method of Murphy and Prenter (1981) also utilizes a fourth-order accurate discretization in the normal direction.

Blottner (1975a, 1975b) provides a helpful review of computational work on the unsteady boundary-layer equations. Other useful references include Telionis et al. (1973), Tsahalis and Telionis (1974), Telionis and Tsahalis (1976), Cebeci et al. (1979b), Phillips and Ackerberg (1973), Murphy and Prenter (1981), Telionis (1979), Kwon et al. (1988a, 1988b), and Ramin and Pletcher (1993).

## PROBLEMS

7.1 Verify the stability constraints given in Section 7.3.2 for the two versions of the simple explicit procedure for the boundary-layer equations.

7.2 The term  $(\partial u / \partial y)^2$  needs to be evaluated at the  $n + 1$  marching level, where  $u$  is an unknown. The marching coordinate is  $x$ , and  $y$  denotes the normal distance from the wall in a viscous flow problem. Utilize Newton linearization to obtain a difference representation for  $(\partial u / \partial y)^2$  that could be used iteratively with the Thomas algorithm and that would be linear in the unknowns at each application of the algorithm.

7.3 Verify Eq. (7.24).

7.4 Generalize Eq. (7.24) to provide a second-order accurate representation when the mesh increments  $\Delta x$  and  $\Delta y$  are not constant.

7.5 Consider the following proposed implicit representation for the boundary-layer momentum equation:

$$u_j^n \frac{u_j^{n+1} - u_j^n}{\Delta x} + v_j^n \frac{u_j^{n+1} - u_{j-1}^{n+1}}{\Delta y} = \frac{\nu}{(\Delta y)^2} (u_{j+1}^{n+1} - 2u_j^{n+1} + u_{j-1}^{n+1})$$

Would you expect to find any mesh Reynolds number restrictions on the use of this representation when employing the Thomas algorithm for  $u$  and  $\nu > 0$ ? Substantiate your answer.

7.6 Work Prob. 7.5 for the difference equation that results when the second term in the equation is replaced by

$$v_j^n \frac{u_{j+1}^{n+1} - u_j^{n+1}}{\Delta y}$$

7.7 Verify the stability constraint given by Eq. (7.30).

7.8 Establish that the algebraic system represented by Eqs. (7.38) and (7.39) is block tridiagonal with  $2 \times 2$  blocks. Verify that it fits the format required by the modified tridiagonal elimination scheme given in Section 7.3.3 for solving the momentum and continuity equations in a coupled manner.

7.9 Write a computer program using an implicit method (either fully implicit, Crank-Nicolson, or the modified box scheme) to solve the incompressible laminar boundary-layer equations for flat plate flow in both physical (scheme A) and transformed (scheme B) [Eqs. (7.42) and (7.43)] coordinates. Linearize the difference equations either by lagging or extrapolating the coefficients  $\nu$  and  $u$ . Solve the momentum and continuity equations in an uncoupled manner. Use the tridiagonal elimination scheme to solve the system of simultaneous equations. Use  $\Delta \eta = 0.3$  for scheme B and

$\rho u_x \Delta y / \mu = 60$  for scheme A. For scheme A the boundary layer will grow with increasing  $x$ , so that it will be necessary to add points to the computational domain as the calculation progresses. It will be possible to increase the marching step size in proportion to the boundary-layer thickness. It is suggested that the first step be established as  $\Delta x = \rho u_x (\Delta y)^2 / 2 \mu$  for scheme A.

Compare schemes A and B for ease of programming and accuracy. Consider the similarity solution tabulated by Schlichting (1979) as an "exact" solution for purposes of comparison. Calculate

$$C_f = \frac{\mu (\partial u / \partial y)_w}{\rho u_e^2 / 2}$$

from the solution. Determine  $(\partial u / \partial y)_w$  by fitting a second-degree polynomial through the solution near the wall. Limit the downstream extent of the calculation to 75 streamwise steps. Investigate the sensitivity of methods to the streamwise step size. Perform the calculations for  $\Delta x = 1\delta, 2\delta, 4\delta$ . For scheme B, study the influence of the starting procedure on accuracy by first performing a streamwise calculation sweep by using  $v = 0$  at  $x = 0$  in the momentum equation and then repeating the calculation determining  $v$  at  $x = 0$  iteratively through the use of the continuity equation.

**7.10** Work Prob. 7.9 with the following changes. Select an implicit scheme and choose either physical or transformed coordinates in which to express the boundary-layer equations. Scheme A linearizes the coefficients by lagging, and scheme B implements the linearization through the Newton procedure with coupling of the continuity equation.

**7.11** Work Prob. 7.9 using either physical or transformed coordinates. Let scheme A be an implicit scheme of your choice and scheme B be an explicit procedure such as DuFort-Frankel, hopscotch, or ADE.

**7.12** Modify a difference scheme used in working Probs. 7.9 through 7.11 to permit the calculation of a boundary-layer flow in a pressure gradient. Verify your difference scheme by comparing the predicted velocity profiles with the results from the similarity solutions to the Falkner-Skan equations (see Schlichting, 1979) for a potential flow given by  $u_e(x) = u_1 x^m$  where  $u_1$  and  $m$  are constants and  $x$  is the streamwise coordinate. Make your comparisons for  $m = \frac{1}{3}$  and  $-0.0654$ . You may choose any convenient value for  $u_1$ .

**7.13** Modify a difference scheme used in working Probs. 7.9 through 7.11 to permit the calculation of a boundary-layer flow with blowing or suction. Verify your difference scheme by comparing the predicted velocity profiles with the results obtained by Hartnett and Eckert (1957) for blowing and suction distributions given by

$$\frac{u_w(x)}{u_x} \sqrt{\text{Re}_x} = 0.25 \text{ and } -2.5$$

**7.14** Develop a computer program to solve the 2-D incompressible constant property boundary-layer equations in transformed coordinates using the analytical transformation given in Section 7.3.7. Use either the Crank-Nicolson or fully implicit scheme and the Newton-linearized scheme with coupling. Validate your code by solving for the zero pressure gradient laminar flow on a flat plate at a plate Reynolds number of 800. Compare your predicted skin-friction coefficient with the analytical result:  $C_f(\text{Re}_x)^{0.5} = 0.664$ . Use a second-degree polynomial through points near the wall to compute the wall shear stress from the velocity distribution. Tabulate  $C_f(\text{Re}_x)^{0.5}$  for at least 15 locations along the plate out to a location where the  $\text{Re} = 800$ . Use your scheme to estimate the separation point for a laminar flow where the free stream velocity distribution is given by  $u_e = 100 - 300x$ . Use at least 50 points across the boundary layer as separation is approached. Refine the  $\Delta \xi$  step near separation until the separation point no longer changes.

**7.15** Work Prob. 7.14 using the generalized coordinate approach instead of the analytical transformation. Establish the grid based on  $\xi = x/L$ ,  $\eta = (y/x)(\text{Re}_x)^{0.5}$ .

**7.16** Develop a finite-difference scheme for compressible laminar boundary-layer flow. Solve the energy equation in an uncoupled manner. Use the computer program to predict the skin-friction coefficient and Stanton number distributions for the flow of air over a flat plate at  $M_e = 4$  and  $T_w/T_\infty = 2$ . Use the Sutherland equation (Section 5.1.4) to evaluate the fluid viscosity as a function of temperature. Assume constant values of  $\text{Pr}$  and  $c_p$  [ $\text{Pr} = 0.75$ ,  $c_p = 1 \times 10^3 \text{ J/(kg K)}$ ]. Compare

your predictions with the analytical results of van Driest (1952) [heat transfer results can be found in the work by Kays and Crawford (1993)].

**7.17** Modify a difference scheme used in working Probs. 7.9 through 7.11 to permit calculation of an incompressible turbulent boundary layer on a flat plate. Use an algebraic turbulence model from Chapter 5. Use  $u_\infty = 33$  m/s and  $\nu = 1.51 \times 10^{-5}$  m<sup>2</sup>/s. Compare your velocity profiles in law-of-the-wall coordinates with Fig. 5.7. Compare your predicted values of  $C_f$  with the measurements of Wieghardt and Tillmann (1951) tabulated below:

$x, m$	$C_f$
0.087	0.00534
0.187	0.00424
0.287	0.00386
0.387	0.00364
0.487	0.00345
0.637	0.00337
0.787	0.00317
0.937	0.00317
1.087	0.00308

**7.18** Verify Eq. (7.72).

**7.19** An inverse boundary-layer method is to be applied to steady incompressible 2-D flow. Use  $\rho = 1$  kg/m<sup>3</sup>,  $\nu = 1$  m<sup>2</sup>/s, and  $\Delta y = \Delta x = 0.1$  m. The solution at the  $n$ th station is tabulated below. Use the simple explicit method to advance the solution to  $n + 1$  (see Fig. P7.1). Use the secant method to determine the pressure gradient required to maintain a constant value of the displacement thickness as the solution is advanced to  $n + 1$ . That is, find the pressure gradient required to give  $(\delta^*)^{n+1} = (\delta^*)^n$ .

$n$ th station		
$j$	$u$	$v$
1	0	0
2	6	0
3	10	0
4	10	0

**7.20** Work out the details of the terms  $Q_j^n$  and  $R_j^n$  in Eq. (7.90) for the DuFort-Frankel scheme for internal flows.

**7.21** Using the boundary-layer equations, develop a finite-difference scheme for the incompressible laminar developing flow in a channel. Use the nondimensionalization that removes the Reynolds number from the equations (Eq. 7.80). Because of symmetry, you need only solve the equations to the channel centerline. Solve out to  $x/(h Re_h) = 0.02$ , where  $h$  is the channel half-height. Suppose your friend needs the solution for  $Re = 500$  from the inlet to a distance of 25 channel heights

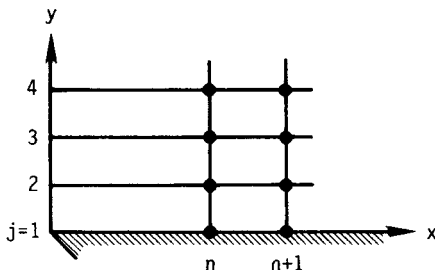


**Figure P7.1**

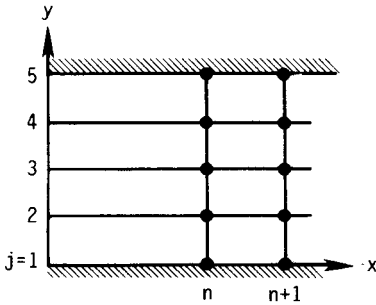


Figure P7.2

downstream. Explain how you would provide the information needed from your numerical solution. Is the flow fully developed after 25 channel heights? Compare the predicted centerline velocity development  $U_{CL}/U_{INLET}$  vs.  $x/(h Re_h)$  with the highest Reynolds number Navier-Stokes solutions reported by Chen and Pletcher (1991).

7.22 The steady viscous flow through a 2-D channel is to be determined by a solution to the boundary-layer equations. Use  $\rho = 1 \text{ kg/m}^3$ ,  $\nu = 1 \text{ m}^2/\text{s}$ ,  $\Delta y = 0.1 \text{ m}$ , and  $\Delta x = 0.025 \text{ m}$ . The solution at the  $n$ th station is tabulated below. Use the simple explicit method to advance the solution to the  $n + 1$  station (see Fig. P7.2). Determine the pressure and the velocities.

nth station		
$p = 100 \text{ N/m}^2$		
$j$	$u$	$v$
1	0	0
2	10	0
3	10	0
4	10	0
5	0	0

7.23 Work Prob. 7.22 using the fully implicit method with lagged coefficients.

7.24 Verify Eq. (7.93) for a fully implicit method.

7.25 Verify Eq. (7.96).

7.26 Verify Eq. (7.100).

7.27 Derive Eq. (7.112).

7.28 Specialize Eqs. (7.106)–(7.108) for an incompressible 3-D laminar flow in the Cartesian coordinate system. Write out the Crank-Nicolson representation for the equations. Explain your scheme for linearizing the algebraic equations.

7.29 Work Prob. 7.28 for the Krause zig-zag scheme.

7.30 Choose a suitable implicit finite-difference scheme to solve the 3-D laminar boundary-layer equations on the plane of symmetry for the example flow described in Section 7.7.4. Compare your predicted skin-friction coefficients with the results of Cebeci (1975) and/or Fig. 7.29(b).

7.31 Solve the example flow of Section 7.7.4 using the Crank-Nicolson scheme. Use the grid described in the example. Compare your results with those given by Cebeci (1975).

7.32 Write out a Krause-type difference scheme for the 2-D unsteady incompressible boundary-layer equations.